Cell Reports

Article

Opposing roles of p38α-mediated phosphorylation and PRMT1-mediated arginine methylation in driving TDP-43 proteinopathy

Graphical abstract

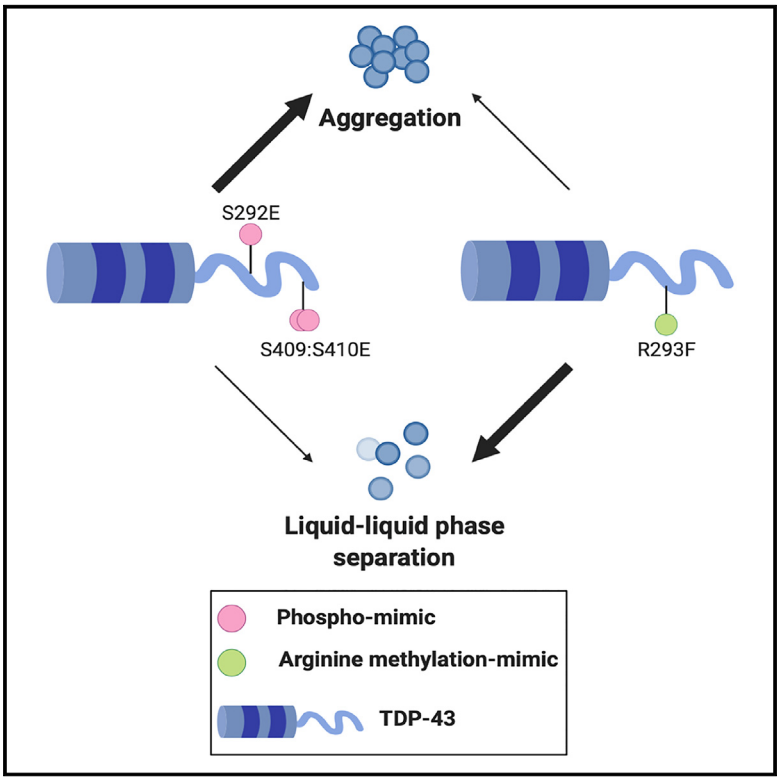

Authors

Mari Aikio, Hana M. Odeh, Heike J. Wobst, ..., Stephen J. Moss, Nicholas J. Brandon, James Shorter

Correspondence

jshorter@pennmedicine.upenn.edu

In brief

In this study, Aikio et al. establish opposing roles for p38α-mediated TDP-43 phosphorylation and PRMT1-mediated TDP-43 arginine methylation in driving TDP-43 proteinopathy. These findings suggest therapeutic strategies for ALS and related TDP-43 proteinopathies.

Highlights

- p38α inhibition reduces aberrant TDP-43 phenotypes in patient-derived motor neurons
- p38α phosphorylates TDP-43 at S292 and S409/S410, reducing LLPS but not aggregation
- PRMT1 methylates TDP-43 at R293, reducing TDP-43 aggregation but not LLPS
- Antagonistic TDP-43 methylation and phosphorylation suggest therapeutic strategies

Aikio et al., 2025, Cell Reports *44*, 115205
January 28, 2025
https://doi.org/10.1016/j.celrep.2024.115205

CellPress

Cell Reports

CellPress
OPEN ACCESS

Article

Opposing roles of p38α-mediated phosphorylation and PRMT1-mediated arginine methylation in driving TDP-43 proteinopathy

Mari Aikio,[1,2,17] Hana M. Odeh,[3,17] Heike J. Wobst,[4] Bo Lim Lee,[3] Úna Chan,[5] Jocelyn C. Mauna,[6,7,8] Korrie L. Mack,[2,3,9] Bradley Class,[4] Thomas A. Ollerhead,[1] Alice F. Ford,[3,10] Edward M. Barbieri,[3] Ryan R. Cupo,[3,11] Lauren E. Drake,[3] Joshua L. Smalley,[1] Yuan-Ta Lin,[2] Stephanie Lam,[5] Reuben Thomas,[12] Nicholas Castello,[5] Ashmita Baral,[5] Jenna N. Beyer,[3,9] Mohd A. Najar,[3] John Dunlop,[2,4] Aaron D. Gitler,[13] Ashkan Javaherian,[5] Julia A. Kaye,[5,14] George M. Burslem,[3,9,11] Dean G. Brown,[15] Christopher J. Donnelly,[6,7,8] Steven Finkbeiner,[5,14,16] Stephen J. Moss,[1,18] Nicholas J. Brandon,[1,2,4,18] and James Shorter[3,9,10,11,18,19,*]

[1]AstraZeneca-Tufts Laboratory for Basic and Translational Neuroscience, Department of Neuroscience, Tufts University, Boston, MA 02111, USA
[2]Neumora Therapeutics, Watertown, MA 02472, USA
[3]Department of Biochemistry and Biophysics, Perelman School of Medicine, University of Pennsylvania, Philadelphia, PA 19104, USA
[4]Neuroscience, BioPharmaceuticals R&D, AstraZeneca, Waltham, MA 02451, USA
[5]Center for Systems and Therapeutics, Gladstone Institutes, San Francisco, CA 94158, USA
[6]Department of Neurobiology, University of Pittsburgh School of Medicine, Pittsburgh, PA 15261, USA
[7]LiveLikeLou Center for ALS Research, University of Pittsburgh School of Medicine, Pittsburgh, PA 15261, USA
[8]University of Pittsburgh Brain Institute, University of Pittsburgh School of Medicine, Pittsburgh, PA 15261, USA
[9]Biochemistry and Molecular Biophysics Graduate Group, Perelman School of Medicine, University of Pennsylvania, Philadelphia, PA 19104, USA
[10]Neuroscience Graduate Group, Perelman School of Medicine, University of Pennsylvania, Philadelphia, PA 19104, USA
[11]Pharmacology Graduate Group, Perelman School of Medicine, University of Pennsylvania, Philadelphia, PA 19104, USA
[12]Gladstone Institute of Data Science and Biotechnology, Gladstone Institutes, San Francisco, CA 94158, USA
[13]Department of Genetics, Stanford University School of Medicine, Stanford, CA 94305, USA
[14]Taube/Koret Center for Neurodegenerative Disease Research, Gladstone Institutes, San Francisco, CA 94158, USA
[15]Hit Discovery, Discovery Sciences, BioPharmaceuticals R&D, AstraZeneca, Waltham, MA 02451, USA
[16]Deparments of Neurology and Physiology, Neuroscience Graduate Program and Biomedical Sciences Program, University of California, San Francisco, San Francisco, CA 94158, USA
[17]These authors contributed equally
[18]Senior author
[19]Lead contact
*Correspondence: jshorter@pennmedicine.upenn.edu
https://doi.org/10.1016/j.celrep.2024.115205

SUMMARY

Amyotrophic lateral sclerosis (ALS) is a devastating neurodegenerative disorder typically characterized by insoluble inclusions of hyperphosphorylated TDP-43. The mechanisms underlying toxic TDP-43 accumulation are not understood. Persistent activation of p38 mitogen-activated protein kinase (MAPK) is implicated in ALS. However, it is unclear how p38 MAPK affects TDP-43 proteinopathy. Here, we show that p38α MAPK inhibition reduces pathological TDP-43 phosphorylation, aggregation, cytoplasmic mislocalization, and neurotoxicity. Remarkably, p38α MAPK inhibition mitigates aberrant TDP-43 phenotypes in diverse ALS patient-derived motor neurons. p38α MAPK phosphorylates TDP-43 at pathological S409/S410 and S292, which reduces TDP-43 liquid-liquid phase separation (LLPS) but allows pathological TDP-43 aggregation. Moreover, we establish that PRMT1 methylates TDP-43 at R293. Importantly, S292 phosphorylation reduces R293 methylation, and R293 methylation reduces S409/S410 phosphorylation. Notably, R293 methylation permits TDP-43 LLPS and reduces pathological TDP-43 aggregation. Thus, strategies to reduce p38α-mediated TDP-43 phosphorylation and promote PRMT1-mediated R293 methylation could have therapeutic utility for ALS and related TDP-43 proteinopathies.

INTRODUCTION

Amyotrophic lateral sclerosis (ALS) is a fatal disorder caused by motor neuron degeneration.[1] While most ALS cases (approximately 90%–95%) are considered sporadic with unknown etiology, approximately 5%–10% of cases are familial in nature (fALS).[2,3] ALS is linked to mutations in more than 25 genes, with the *C9ORF72* hexanucleotide repeat expansion and mutations in SOD1 being the most common.[4] Although mutations in transactive response DNA binding protein 43 kDa (*TARDBP*),

the gene encoding TDP-43, are a rare cause of ALS, approximately 97% of ALS cases and approximately 45% of patients with frontotemporal dementia (FTD) present with TDP-43 proteinopathy characterized by nuclear and cytoplasmic TDP-43 inclusions in affected neurons.[5–12]

TDP-43 is a highly conserved, ubiquitously expressed, and predominantly nuclear RNA/DNA-binding protein.[7,13] TDP-43 functions in transcriptional repression, RNA transport, alternative splicing, microRNA biogenesis, and stress granule formation.[14–25] TDP-43 is composed of an N-terminal domain involved in dimerization, a nuclear localization sequence, two RNA-recognition motifs (RRM1 and RRM2), and a C-terminal prion-like domain (PrLD) that enables liquid-liquid phase separation (LLPS) and pathological aggregation (Figure 1A).[18,26–33] The PrLD harbors the majority of disease-linked mutations (Figure 1A).[34,35]

Phosphorylation at serine residues 409/410 (S409/S410) is a major pathological marker for TDP-43 inclusions in disease.[36,37] TDP-43 undergoes additional post-translational modifications (PTMs) in patients with ALS including ubiquitination, generation of C-terminal domain fragments (CTFs), cysteine oxidation, sumoylation, and acetylation.[38] However, the functional and pathological significance of TDP-43 PTMs remains largely unknown. A clear understanding of the effects of phosphorylation and other PTMs on the solubility, localization, and aggregation propensity of TDP-43 will enable mechanistic insights into ALS pathogenesis.

The mitogen-activated protein kinase (MAPK) signaling pathway regulates cell differentiation, motility, growth, and survival.[39] MAPKs, which include extracellular-signal-regulated kinases, Jun amino-terminal kinases, and p38 MAPKs, are activated by cytokines, growth factors, and environmental stress.[40–42] In mammals, p38 MAPKs comprise four isoforms (α, β, γ, and δ).[43] p38α and p38β are expressed in most tissues, including the brain,[44] whereas p38γ is most highly expressed in skeletal muscle, and p38δ in testis, pancreas, kidney, and small intestine.[45] Aberrant p38 signaling is linked to several neurodegenerative diseases, including ALS.[46–49] Specifically, p38 MAPK inhibition reduces motor neuron degeneration and restores physiological axonal retrograde transport in SOD1-ALS models.[46–48] Furthermore, genetic and pharmacological inhibition of p38β in a *Drosophila* model of TDP-43 toxicity mitigated premature lethality.[49]

Here, we establish a role for p38α MAPK in promoting TDP-43 proteinopathy. We show that the inhibition of p38α MAPK reduces ALS-associated TDP-43 phenotypes. Importantly, p38α inhibition mitigates aberrant TDP-43 phenotypes in motor neurons derived from patients with ALS. Furthermore, we establish that protein arginine methyltransferase 1 (PRMT1)-mediated methylation of TDP-43 at R293 opposes the effects of p38α in driving TDP-43 proteinopathy. Our results suggest that strategies to decrease p38α-mediated TDP-43 phosphorylation and promote PRMT1-mediated TDP-43 methylation could have therapeutic utility for ALS/FTD and related TDP-43 proteinopathies.

RESULTS

Inhibition of p38α reduces TDP-43 aggregation, phosphorylation, and toxicity

Several findings suggest a role for p38 MAPK in ALS.[48–52] Thus, we first assessed whether p38α modulates TDP-43 aggregation in human neuronal SH-SY5Y cells. Increased expression of wild-type (WT) or ALS-linked TDP-43 variants elicit ALS-like phenotypes *in vitro* and *in vivo*.[53–56] Indeed, elevated expression of TDP-43^{WT} is connected with FTD,[57] and disease-linked TDP-43 aggregation is proposed to increase TDP-43 expression due to the loss of TDP-43 autoregulation.[58,59] TDP-43^{M337V}, a pathological fALS-linked variant, is especially aggregation prone and becomes highly phosphorylated.[31,53,60] Thus, we used TDP-43^{M337V} in our initial experiments to detect more prominent changes in TDP-43 solubility and phosphorylation. Using small interfering RNA (siRNA)-mediated knockdown of p38α and TDP-43^{M337V} expression, we monitored accumulation of total and phosphorylated TDP-43 (pTDP-43) in RIPA or urea soluble fractions over time. p38α depletion significantly reduced accumulation of insoluble TDP-43^{M337V} in the urea fraction at all times (Figures 1B and 1C). Thus, p38α depletion reduces TDP-43^{M337V} aggregation in human neuronal cells.

Phosphorylation of S409 and S410 of TDP-43 is a consistent feature in all TDP-43 proteinopathies.[37] TDP-43 is phosphorylated at S409/S410 in pathological inclusions, but never under physiological conditions in the nucleus.[11,37] We observed a marked decrease in pTDP-43 in the urea fraction when p38α is knocked down (Figures 1B and 1D). Consistently, increased TDP-43^{WT} expression, in place of TDP-43^{M337V}, or using a different siRNA to knockdown p38α also decreased pTDP-43 in the urea fraction (Figures S1A–S1D). Moreover, p38α depletion reduced accumulation of insoluble TDP-43^{WT} in the urea fraction, particularly at early time points (Figure S1E). Thus, p38α depletion reduces TDP-43 aggregation and pathological S409/410 phosphorylation in human neuronal cells.

Next, we assessed whether pharmacological inhibition of p38α affects TDP-43 solubility and phosphorylation in a similar manner to genetic ablation. Indeed, treatment of SH-SY5Y cells with a p38α inhibitor, compound 1 (Figure 1E), significantly reduced TDP-43^{M337V} phosphorylation and aggregation, in a concentration- and time-dependent manner (Figures 1F–1I). Note that we only observe TDP-43 phosphorylation at S409/S410 in the insoluble urea fraction and not in the soluble RIPA fraction (Figure 1F), indicating the pathological nature of S409/S410 phosphorylation. We suggest that p38α inhibition is an effective strategy to reduce pathological TDP-43 aggregation and phosphorylation.

To test whether p38α pharmacological inhibition affects toxicity induced by increased TDP-43 expression, we performed a lactate dehydrogenase cytotoxicity assay in mouse motor-neuron-like NSC-34 cells. Expression of TDP-43^{WT} (Figure 1J) or TDP-43^{M337V} (data not shown) in NSC-34 cells induces cytotoxicity. Importantly, p38α inhibition by compound 1 significantly mitigated TDP-43^{WT}-induced cytotoxicity (Figure 1J). Thus, pharmacological inhibition of p38α mitigates TDP-43 toxicity in motor-neuron-like NSC-34 cells.

To determine whether p38α pharmacological inhibition mitigates TDP-43-induced neurodegeneration, we used longitudinal imaging to measure neuronal survival.[61] We cultured primary mouse cortical neurons, sparsely labeled them with a fluorescent protein (mApple), and also expressed

CellPress
OPEN ACCESS

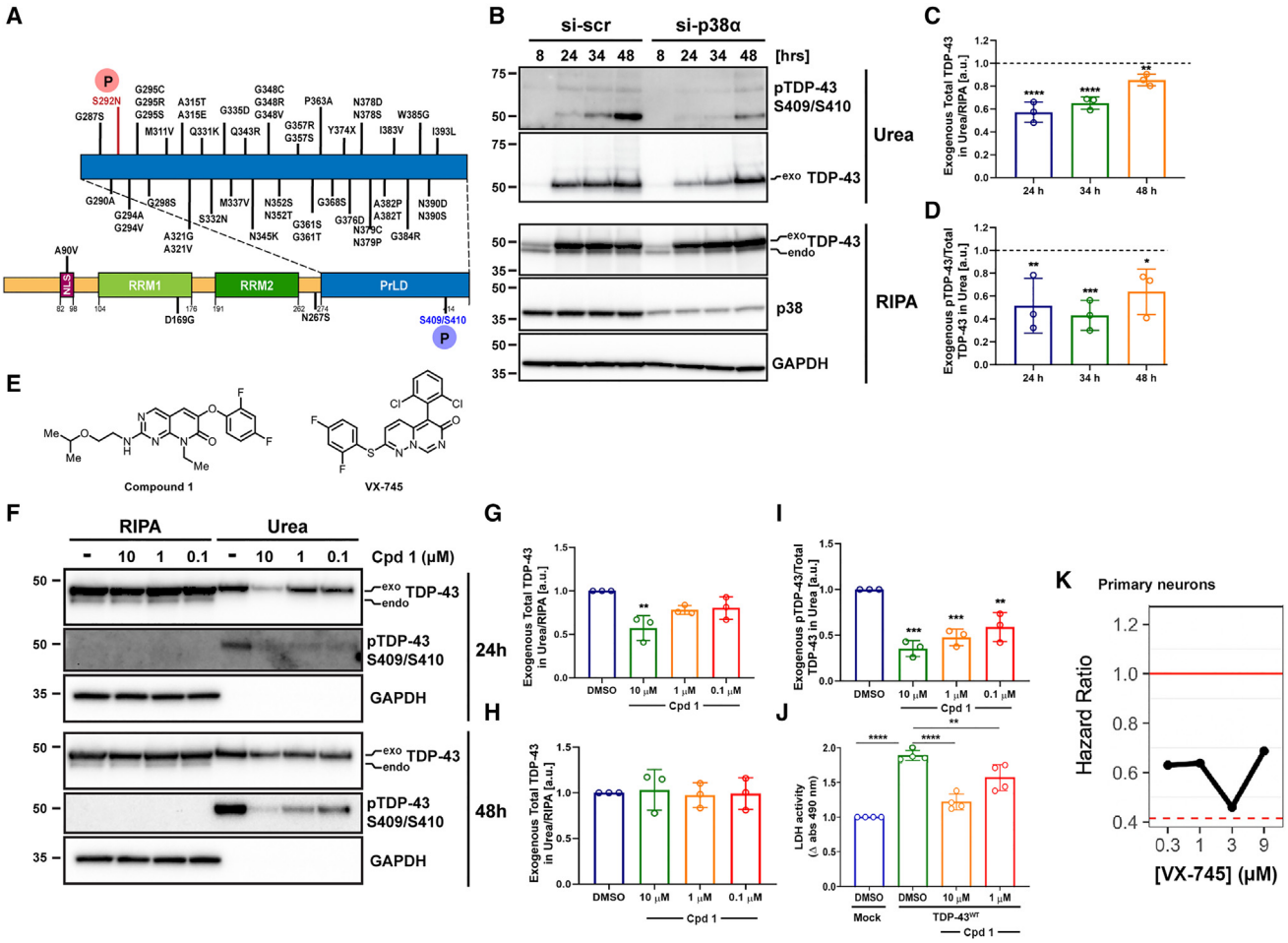

Figure 1. Genetic and pharmacological inhibition of p38α MAPK reduces TDP-43 aggregation, S409/S410 phosphorylation, and neurotoxicity

(A) TDP-43 domain architecture with location of ALS-linked mutations and phosphorylation sites (P) detected after p38α treatment *in vitro*.

(B) Western blot of total and pTDP-43^{M337V} in RIPA and urea fractions of SH-SY5Y cells with siRNA-induced p38α knockdown. GAPDH serves as a loading control. SH-SY5Y cells were treated with siRNA for 24 h and then transfected with TDP-43^{M337V} (myc tagged). Positions of myc-tagged TDP-43^{M337V} (exo) and endogenous TDP-43 (endo) are indicated.

(C) Quantification of urea/RIPA ratio of total TDP-43 (exogenously expressed) normalized to levels in scrambled siRNA (si-scr; mean ± SD, two-way ANOVA with Sidak's multiple comparison test, $n = 3$). $^{**}p < 0.01$, $^{****}p < 0.0001$.

(D) Quantification of pTDP-43/total TDP-43 ratio (exogenously expressed) in urea fraction normalized to levels in si-scr (mean ± SD, two-way ANOVA with Sidak's multiple comparison test, $n = 3$). $^{*}p < 0.05$, $^{**}p < 0.01$, $^{***}p < 0.001$.

(E) Chemical structures of compound 1 and VX-745 (neflamapimod).

(F) Western blot of total and pTDP-43^{M337V} in RIPA and urea fractions of SH-SY5Y cells with pharmacological p38α inhibition with compound 1. GAPDH serves as a loading control. Positions of myc-tagged TDP-43^{M337V} (exo) and endogenous TDP-43 (endo) are indicated.

(G and H) Quantification of urea/RIPA ratio of total TDP-43 at 24 h (G) and 48 h (H) after transfection (mean ± SD, one-way ANOVA with Dunnett's multiple comparison test, $n = 3$). $^{**}p < 0.01$.

(I) Quantification of pTDP-43/total TDP-43 ratio in urea fraction at 48 h after transfection normalized to levels in DMSO-treated cells (mean band signal ± SD, one-way ANOVA with Dunnett's multiple comparison test, $n = 3$). $^{**}p < 0.01$, $^{***}p < 0.001$.

(J) Quantification of lactate dehydrogenase (LDH) activity in conditioned medium normalized to levels in DMSO-treated TDP-43^{WT}-transfected NSC-34 cells (one-way ANOVA with Dunnett's multiple comparison test, $n = 4$ with 6 replicates in each). $^{**}p < 0.01$, $^{****}p < 0.0001$.

(K) Hazard ratios of primary neurons expressing mApple and TDP-43^{M337V}-EGFP treated with p38α inhibitor VX-745 at 0.3, 1, 3, and 9 μM compared with DMSO control (reference, set at 1.0) were 0.6296, 0.6378, 0.4596, and 0.6869, respectively. Reduction of hazard ratio was most significant at 3 μM (Cox proportional hazard, $p < 0.01$). The number of neurons tracked per treatment group were 82, 76, 54, and 58, for each concentration of the drug, respectively; and 246 for the DMSO control. For comparison, the hazard ratio for control neurons expressing only mApple and GFP (without TDP43^{M337V}) and treated with DMSO was 0.4149 ($N = 555$ neurons) ($p < 0.001$). See also Figures S1–S4.

TDP43^{M337V} in the mApple-labeled neurons. We imaged the neurons daily for 7 days and used Cox proportional hazards analysis to measure the cumulative risk of death and hazard ratios. This assay is very sensitive to detecting TDP-43-induced neurodegeneration.[61] Treatment of neurons with a brain-penetrant p38α pharmacological inhibitor, VX-745

(neflamapimod) (Figure 1E),[62] which has entered phase 2 clinical trials for Alzheimer's disease and dementia with Lewy bodies (DLB),[63–65] significantly reduced the hazard ratio of TDP-43^{M337V}-expressing neurons compared with neurons expressing TDP43^{M337V} and treated with DMSO (Figure 1K). Thus, a clinical stage, brain-penetrant p38α inhibitor can also mitigate TDP-43 neurotoxicity. Importantly, compound 1 and VX-745 are different chemotypes (Figure 1E), which along with p38α knockdown data (Figures 1B–1D), increases confidence that p38α is a *bona fide* target to mitigate aberrant TDP-43 phenotypes. Our results demonstrate that p38α inhibition reduces pathological TDP-43 aggregation, phosphorylation, and toxicity in multiple settings.

p38α inhibition reduces TDP-43 aggregation and phosphorylation in human induced pluripotent stem cell-derived motor neurons subjected to MG-132-induced stress

p38α inhibition can mitigate TDP-43 aggregation and toxicity under conditions where TDP-43 is overexpressed (Figures 1B–1K), which is relevant to various TDP-43 proteinopathies.[57–59] However, it is also important to determine whether p38α inhibition antagonizes TDP-43 aggregation, phosphorylation, and toxicity when TDP-43 is expressed at endogenous levels. Hence, we also studied the effects of p38α inhibition in human induced pluripotent stem cell (iPSC)-derived motor neurons (iMNs).

In iMNs, various transient, non-lethal stressors, such as oxidative stress and proteasome dysfunction, induce formation of cytoplasmic aggregates of pTDP-43, leading to reduced TDP-43 function.[60,66–68] We found that impairing proteasome activity with MG-132 induces cytoplasmic mislocalization and aggregation of pTDP-43 in iMNs (Figures S2A and S2B). Importantly, co-treatment of iMNs with MG-132 and the specific p38α inhibitor, VX-745, significantly reduced levels of insoluble, pTDP-43 (Figures S2A and S2B). Thus, specific inhibition of p38α reduces levels of insoluble, pTDP-43 elicited by proteotoxic stress at endogenous levels of TDP-43 expression in human motor neurons.

p38α inhibition reduces TDP-43^{A382T} toxicity in patient-derived iMNs

We next examined the survival of two patient-derived iMN lines that harbored the ALS-linked TDP-43^{A382T} variant using the GEDI biosensor,[69] a live cell marker that detects intracellular calcium levels at the point when a cell has irreversibly committed to death (Figure S3A). TDP-43^{A382T} iMNs displayed a significantly higher death rate than gene-corrected (GC) control iMNs (Figures S3A and S3B), indicating that the ALS-linked TDP-43^{A382T} variant is deleterious for motor neurons. Importantly, the specific p38α inhibitor VX-745 significantly reduced the death rate of TDP-43^{A382T} iMNs (Figure S3B). VX-745 also improved the survival of the GC controls, suggesting that VX-745 is beneficial to human iMNs in the absence of TDP-43 pathology (Figure S3B). Our findings establish that specific inhibition of p38α with VX-745 can mitigate neurodegeneration induced by the ALS-linked TDP-43 variant, TDP43^{A382T}, at endogenous levels of TDP-43 expression in patient-derived iMNs.

p38α inhibition restores nuclear TDP-43 in patient-derived iMNs that harbor a hexanucleotide repeat expansion in the *C9ORF72* gene

We next examined two different patient-derived iMN lines that harbor a hexanucleotide repeat expansion in the *C9ORF72* gene, which is the most common genetic cause of ALS/FTD, termed c9ALS/FTD.[70,71] We first treated control and c9 iMN lines with various doses of the specific p38α inhibitor, VX-745, and assessed cell viability after 24 h. We found that 1 μM VX-745 was not toxic under these conditions, and so we used this concentration for our experiments. The c9 iMNs present with a significantly decreased nuclear/cytoplasmic cytoplasmic ratio of TDP-43 compared with control iMNs (Figures S4A–S4D). Importantly, VX-745 significantly restored nuclear TDP-43 levels in c9 patient-derived iMN lines, and restored the ratio of nuclear:cytoplasmic TDP-43 back to levels observed in control iMNs (Figures S4A–S4D). VX-745 did not alter the nuclear:cytoplasmic TDP-43 ratio in control iMNs (Figures S4A–S4D). Thus, specific p38α inhibition with VX-745 can reduce aberrant TDP-43 phenotypes in several human iMN lines at endogenous levels of TDP-43 expression (Figures S2–S4).

Constitutively active p38α promotes TDP-43 aggregation, S409/S410 phosphorylation, and cytoplasmic accumulation

p38α depletion reduces TDP-43 aggregation and phosphorylation at S409 and S410 (Figure 1B). Therefore, we hypothesized that p38α overexpression would increase TDP-43 aggregation and phosphorylation. To test our hypothesis, we co-expressed TDP-43^{M337V} with WT, constitutively active (CA), or dominant negative (DN) forms of p38α in SH-SY5Y cells. First, we established that expression of CA-p38α, DN-p38α, or WT-p38α alone in the absence of TDP-43^{M337V} in SH-SY5Y cells did not elicit cell death (Figures S5A–S5D). Moreover, CA-p38α, DN-p38α, or WT-p38α were all expressed at similar levels (Figures S5B and S5D). The CA-p38α variant we used (D176A/F327S) exhibits approximately 25% of the activity of fully activated p38α,[72] which likely minimizes any toxicity at the time points studied. Co-expression of WT or DN-p38α with TDP-43^{M337V} did not have any significant effect on S409/S410 phosphorylation or accumulation of TDP-43 in the urea fraction (Figures 2A–2D). By contrast, CA-p38α promoted TDP-43^{M337V} aggregation and phosphorylation at S409/S410 (Figures 2A–2D). Thus, p38α activation promotes pathological TDP-43 phosphorylation and aggregation in human neuronal cells.

Next, we assessed whether TDP-43^{M337V} co-localizes with p38α. Previously, TDP-43^{M337V} and p38α have been detected in ubiquitinated inclusions.[50,53] Interestingly, we found a significant increase in the number of cells displaying intranuclear TDP-43^{M337V} inclusions specifically when CA-p38α was co-expressed (Figures 2E and 2F). Furthermore, these intranuclear TDP-43 inclusions harbored p38α (Figure 2E). Intranuclear TDP-43 inclusions are a more common feature of TDP-43 proteinopathies than previously appreciated[11] and may even be initial sites of TDP-43 aggregation.[73] Expression of CA-p38α also promoted the cytoplasmic accumulation of TDP-43 (Figures 2G and 2H). Our data demonstrate that aberrant activation of p38α promotes several hallmarks of ALS pathology, including TDP-43

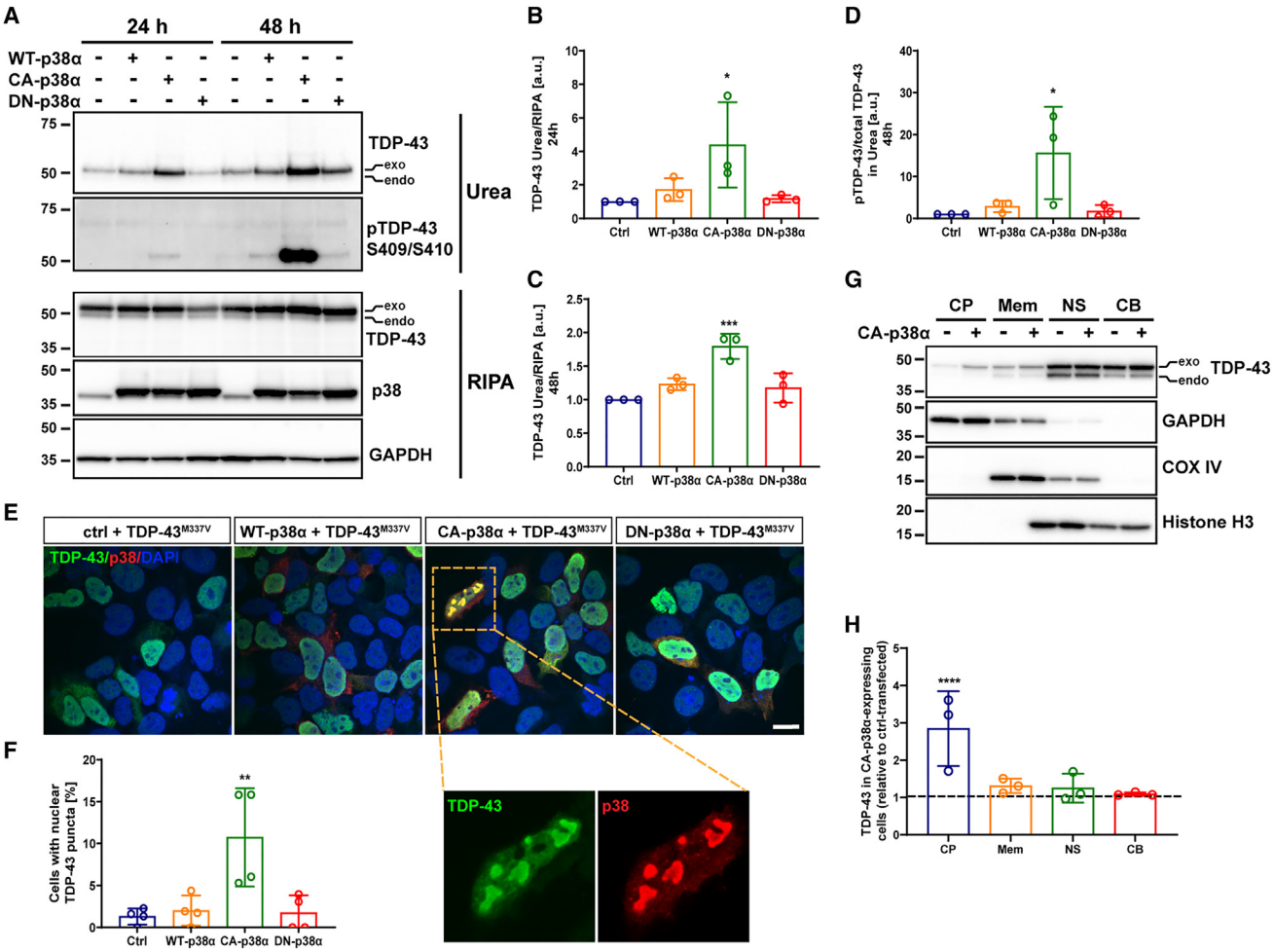

Figure 2. CA-p38α induces aggregation, phosphorylation, and cytoplasmic accumulation of TDP-43

(A) Western blot of total and pTDP-43 in RIPA and urea fractions of SH-SY5Y cells co-transfected with TDP-43^{M337V} and empty control plasmid (ctrl), WT-p38α, CA-p38α or DN-p38α. GAPDH serves as a loading control. The positions of myc-tagged TDP-43^{M337V} (exo) and endogenous TDP-43 (endo) are indicated. Quantification of urea/RIPA ratio of total TDP-43 at time points 24 h (B) or 48 h (C) after transfection, and pTDP-43/total TDP-43 ratio in urea fraction at time point 48 h after transfection (D), normalized to levels in ctrl-plasmid transfected cells (mean ± SD, one-way ANOVA with Dunnett's multiple comparison test, $n = 3$). $^{*}p < 0.05$, $^{***}p < 0.001$.

(E) Representative confocal images of SH-SY5Y cells co-expressing TDP-43^{M337V} (green, detected using an anti-TDP-43 antibody) and WT-p38α, CA-p38α or DN-p38α (red, detected using an anti-FLAG antibody) with quantification of the number of cells with nuclear TDP-43 puncta/granules (F) (one-way ANOVA with Dunnett's multiple comparison test, $n = 4$ and 10 fields each; scale bar, 20 μm). $^{**}p < 0.01$.

(G) Western blot of TDP-43 in different cellular compartments of SH-SY5Y cells co-transfected with TDP-43^{M337V} and ctrl-plasmid or CA-p38α. Exo denotes exogenous TDP-43 and endo denotes endogenous TDP-43. GAPDH serves as a loading control for cytoplasmic fraction (CP), COX IV for the membrane fraction (Mem), and histone H3 for the soluble nuclear (NS) and chromatin-bound (CB) fractions. The positions of myc-tagged TDP-43^{M337V} (exo) and endogenous TDP-43 (endo) are indicated.

(H) Quantification of total TDP-43 in cytoplasmic, membrane, soluble nuclear and chromatin-bound fractions (mean ± SD, two-way ANOVA with Sidak's multiple comparison test, $n = 3$). $^{****}p < 0.0001$. See also Figure S5.

aggregation, phosphorylation at S409/410, and cytoplasmic accumulation.

p38α can directly phosphorylate TDP-43 at residues S292, S409, and S410 *in vitro*

Co-localization of TDP-43 and CA-p38α in intranuclear aggregates might indicate direct physical interaction between TDP-43 and p38α (Figure 2E). To explore this possibility, we transfected and immunoprecipitated TDP-43^{WT} and p38α from SH-SY5Y cells and then probed for p38α or TDP-43, respectively (Figure 3A). TDP-43^{WT} and p38α co-immunoprecipitated in both reciprocal experiments, suggesting a robust interaction between TDP-43 and p38α (Figure 3A). Consistently, siRNA-mediated knockdown of p38α reduced the amount of immunoprecipitated pTDP-43, and also diminished the amount of endogenous p38α that co-immunoprecipitated with TDP-43^{M337V} (Figure S5E), further validating an interaction between p38α and TDP-43.

Next, we asked whether TDP-43 is directly phosphorylated by p38α. Thus, we performed *in vitro* kinase assays. Samples

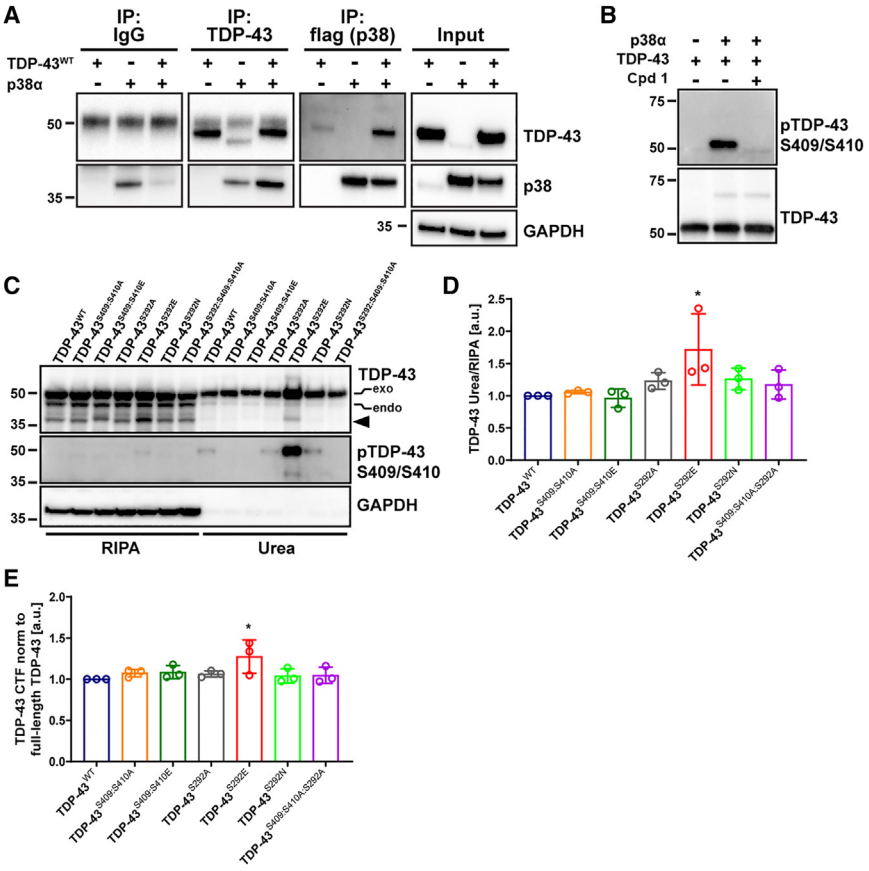

Figure 3. TDP-43 directly interacts with and is phosphorylated by p38α at S292 and S409/S410, with S292 regulating phosphorylation at S409/S410

(A) Western blot of immunoprecipitated TDP-43^{WT} and co-immunoprecipitated WT-p38α and immunoprecipitated WT-p38α (FLAG tagged) and co-immunoprecipitated TDP-43^{WT} in SH-SY5Y cells. Inputs are shown on the right. GAPDH serves as a loading control.

(B) Western blot of *in vitro* kinase assay (30°C for 30 min) of recombinant human TDP-43^{WT} (750ng) and recombinant active p38α (300 ng) with and without the p38α inhibitor compound 1.

(C) Western blot of total and pTDP-43 in RIPA and urea fractions of SH-SY5Y cells transfected with TDP-43^{WT} and with S292 and S409/S410 mutant constructs. The positions of myc-tagged TDP-43 variants (exo) and endogenous TDP-43 (endo) are indicated. An arrowhead shows the position of TDP-43 CTF.

(D and E) Quantification of urea/RIPA ratio of total TDP-43 (D), and CTF/full-length ratio of TDP-43 in RIPA fraction (E) at time point 24 h after transfection normalized to levels in TDP-43^{WT} (mean ± SD, one-way ANOVA with Dunnett's multiple comparison test, $n = 3$). *$p < 0.05$. See also Figure S5.

containing recombinant TDP-43 with or without active p38α were analyzed. In the absence of p38α, no phosphorylation was detected at S409/S410. However, in the presence of active kinase, TDP-43 was directly phosphorylated by p38α at S409/S410 (Figure 3B). As expected, the phosphorylation of TDP-43 was prevented by pharmacological inhibition of p38α with compound 1 (Figure 3B).

We also investigated whether p38α phosphorylates TDP-43 at additional serine or threonine residues. Therefore, we performed liquid chromatography tandem mass spectrometry (LC-MS/MS) analysis of trypsin-digested TDP-43 after incubation with p38α. Our LC-MS/MS approach yielded approximately 71% coverage of the TDP-43 sequence, which encompassed residues 1–293 (Figure S5F). This region of TDP-43 contains 20 serine residues and 15 threonine residues, which could potentially be phosphorylated by p38α. However, we only detected phosphorylation at serine residue 292 (S292) with high certainty (Figures S5G and S5H). The fact that we only detected 1 phosphoserine in residues 1–293 of TDP-43 indicates that, under our conditions, p38α phosphorylates TDP-43 at a specific position and does not indiscriminately phosphorylate any serine or threonine. Thus, p38α can specifically phosphorylate TDP-43 at S292 (Figures 1A and S5F–S5H). In fact, TDP-43 is phosphorylated at S292 in the brains of patients with ALS.[74] Furthermore, a serine-to-asparagine mutation at this site (S292N) is genetically linked to ALS.[35,75,76]

TDP-43 aggregation may be enhanced by phosphorylation at S292

To investigate the potential effects of phosphorylation at S292 on the aggregation propensity of TDP-43, we took a site-directed mutagenesis approach to generate phospho-mimetic (S292E; TDP-43^{S292E}), phospho-dead (S292A; TDP-43^{S292A}), and ALS-linked (S292N; TDP-43^{S292N}) TDP-43 mutants, which were transfected into human neuronal SH-SY5Y cells. Notably, the expression and localization of TDP-43^{S292E} was comparable with that of TDP-43^{WT} (Figures S6A and S6B). Interestingly, overexpressing the phospho-mimetic mutant TDP-43^{S292E} increased the aggregation propensity of TDP-43, evident by the accumulation of TDP-43 in the urea fraction and enhanced phosphorylation at S409/410 (Figures 3C and 3D). Moreover, TDP-43^{S292E} enhanced formation of 35kDa C-terminal fragments (CTFs) of TDP-43, which are associated with TDP-43 proteinopathy (Figures 3C and 3E).[38] Neither TDP-43^{S292A}, TDP-43^{S292N}, TDP-43$^{S409:S410A}$, TDP-43$^{S409:S410E}$, nor TDP-43$^{S292:S409:S410A}$ had any significant effect on TDP-43 aggregation propensity compared with TDP-43^{WT} (Figures 3C and 3D). Thus, TDP-43$^{S409:S410E}$ expression does not mimic the expression of CA-p38α, which likely generates a mixture of phosphoforms of TDP-43 phosphorylated at S292, S409, and/or S410. Our results suggest that the aggregation of TDP-43 may be enhanced by S292 phosphorylation. Moreover, S292 phosphorylation likely stimulates phosphorylation at S409/410. Of note, phosphorylation at S292 likely does not alter the localization of TDP-43 in SH-SY5Y cells. TDP-43 in cells expressing the phosphomimetic TDP-43^{S292E} had similar localization to TDP-43^{WT}-expressing cells (Figure S6A).

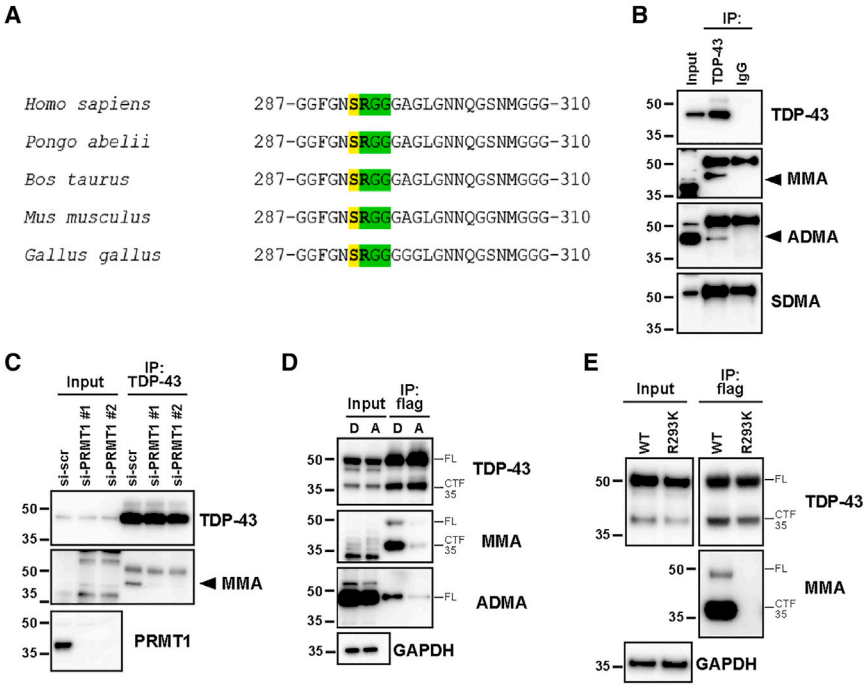

Figure 4. TDP-43 is methylated by PRMT1 at R293

(A) Sequence alignment of amino acids 287–307 of TDP-43 from diverse vertebrates. Conserved 292–293 sites are bolded. S292 phosphorylation site and R293-G295 RGG-motif are highlighted in yellow and green, respectively.

(B) Western blot of immunoprecipitated endogenous TDP-43 from SH-SY5Y-cells probed with antibodies against TDP-43, ADMA, MMA, and SDMA. TDP-43 with arginine methylation is marked by arrowheads.

(C) Western blot of immunoprecipitated endogenous TDP-43 from SH-SY5Y-cells with siRNA-induced PRMT1 knockdown probed with antibodies against TDP-43 or MMA. A PRMT1 blot was run separately to confirm siRNA-mediated knockdown of PRMT1.

(D) Western blot of expressed and immunoprecipitated TDP-43^{WT} using anti-FLAG antibody from SH-SY5Y-cells treated with DMSO (D) or with methyltransferase inhibitor AdOx (A) at a final concentration of 20 μM for 24 h. FL, full-length TDP-43; CTF35, C-terminal 35-kDa fragment of TDP-43.

(E) Western blot of expressed and immunoprecipitated TDP-43^{WT} and TDP-43^{R293K} using anti-FLAG antibody from SH-SY5Y cells probed with antibodies against TDP-43 and MMA. See also Figures S6 and S7.

TDP-43 undergoes arginine methylation catalyzed by PRMT1

Our findings suggest a role for S292 in regulating TDP-43 aggregation via p38α-mediated phosphorylation. A sequence alignment of TDP-43 revealed that S292 is highly conserved from *Homo sapiens* to *Gallus gallus* (Figure 4A). Intriguingly, an RGG motif directly follows S292 and is also highly conserved (Figure 4A). RGG/RG motifs are preferred substrates for methylation by PRMTs.[77] Given that several studies have shown that arginine methylation can attenuate phosphorylation at nearby residues on the same protein,[78–81] we hypothesized that R293 methylation could potentially interfere with p38α-mediated phosphorylation at the adjacent S292. Proteomic studies have found that TDP-43 is monomethylated at R293 in HCT116 and HEK293 cells, as well as in mouse embryos and human brain tissue.[82–85] Moreover, monomethylation of R293 has been reported as a rare modification in assembled TDP-43 fibrils isolated from type A FTD-TDP.[8] To assess TDP-43 arginine methylation in human neuronal SH-SY5Y cells, we immunoprecipitated endogenous TDP-43 and probed with antibodies against monomethyl-arginine (MMA), asymmetric dimethyl-arginine (ADMA), or symmetric dimethyl-arginine (SDMA). We found that immunoprecipitated TDP-43 was mono- and asymmetrically dimethylated and was recognized by the MMA and ADMA antibodies, but not an SDMA antibody (Figure 4B). The absence of SDMA indicates that TDP-43 is likely not dimethylated by type II PRMTs.[86] To the best of our knowledge, asymmetric arginine dimethylation of TDP-43 has not been reported before.

Next, we depleted PRMT1, the most abundant PRMT in mammalian cells,[87] using siRNA-mediated knockdown in SH-SY5Y cells, followed by TDP-43 immunoprecipitation and western blot analysis. We found a significant decrease in arginine monomethylation of endogenous TDP-43 (Figure 4C). Additionally, treating cells with adenosine dialdehyde (AdOx), a global methyltransferase inhibitor, significantly decreased the methylation of overexpressed TDP-43^{WT}, evident by a decrease in immunoprecipitated TDP-43 detected by anti-MMA and anti-ADMA (Figure 4D). Collectively, these data indicate that PRMT1 methylates TDP-43.

Next, we verified that R293 is the residue targeted for arginine methylation in this experimental setting. Using site-directed mutagenesis, we generated a methylation-dead mutant of TDP-43 by substituting R293 with lysine (TDP-43^{R293K}). Unlike TDP-43^{WT}, immunoprecipitating TDP-43^{R293K} and probing for monomethylated TDP-43 with an anti-MMA antibody revealed an absence of monomethylated TDP-43 (Figure 4E). Overall, our results suggest that TDP-43 undergoes arginine methylation by PRMT1 in human neuronal SH-SY5Y cells, and that residue R293 is the major site for methylation. Of note, methylation at R293 likely does not alter the localization of TDP-43 in human neuronal SH-SY5Y cells. The arginine methylation-mimic[88–90] TDP-43^{R293F} had similar localization and expression to TDP-43^{WT} human neuronal SH-SY5Y cells (Figures S6A and S6B).

PRMT1 can directly monomethylate TDP-43 at R293 *in vitro*

Next, we asked whether TDP-43 is directly methylated at R293 by PRMT1. Thus, we performed *in vitro* arginine methylation assays. Here, recombinant TDP-43 was incubated with *S*-adenosyl methionine in the presence or absence of PRMT1 (Figure S7A). Reactions were halted by the addition of formic acid and analyzed by bottom-up LC-MS/MS (Figure S7A), which yielded

approximately 92% coverage of the TDP-43 sequence (Figure S7B). Monomethylated R293 peptides were only observed in the PRMT1-treated samples (Figures S7C and S7D), ruling out non-enzymatic methylation. Thus, PRMT1 can directly monomethylate TDP-43 at R293 *in vitro*. Interestingly, under our *in vitro* conditions (with excess substrate and cofactor), we predominantly observed monomethylation at R293 (Figure S7), whereas dimethylation was very low abundance, despite ample time and opportunity for PRMT1 to catalyze asymmetric dimethylation at R293. In accordance with our results, monomethylation of TDP-43 at R293 but not dimethylation has been reported in proteomics studies[82–85] and as a rare modification in assembled TDP-43 fibrils isolated from type A FTD-TDP.[8] Overall, our findings and prior proteomics studies suggest that monomethylation of R293 of TDP-43 by PRMT1 is the major modification at this position, and that asymmetric dimethylation of R293 is comparatively rare.

TDP-43 arginine methylation favors physiological LLPS over aberrant aggregation

Arginine methylation of TDP-43 is largely unexplored. Thus, little is known about R293 methylation and whether it affects TDP-43 LLPS or aggregation propensity at the pure protein level. Likewise, a precise understanding of how specific phosphorylation events might affect TDP-43 LLPS and aggregation at the pure protein level is also lacking. To address how phosphorylation and methylation can alter TDP-43 LLPS behavior, we performed *in vitro* droplet formation assays. Purified recombinant maltose-binding protein (MBP)-tagged TDP-43^{WT}, the phospho-mimicking mutants TDP-43^{S292E}, TDP-43$^{S409:S410E}$, TDP-43$^{S292:S409:S410E}$, and the arginine methylation-mimic TDP-43^{R293F},[88–90] were separately incubated at physiological concentration (10 μM)[91] with phase separation buffer containing a physiological salt concentration and 10% (w/v) dextran to mimic the crowded cellular environment.[92–94] Formation of TDP-43 droplets was visualized using differential interference contrast (DIC) microscopy. TDP-43^{WT} formed spherical droplets that were relatively large in size (average area of approximately 12.6 ± 1.3 μm^2), and capable of fusion events, indicating liquid-like properties (Figure 5A). In contrast, all three phosphomimetic TDP-43 mutants partitioned into droplets that were smaller in size (TDP-43^{S292E}, approximately 5.8 ± 0.6 μm^2; TDP-43$^{S409:S410E}$, approximately 3.9 ± 0.3 μm^2; and TDP-43$^{S292:S409:S410E}$, approximately 3.2 ± 0.2 μm^2) compared with those of TDP-43^{WT} (Figures 5A–5C). There was no change in the number of droplets between mutants and TDP-43^{WT}. These reductions in droplet sizes suggest that phosphorylation of S292, S409, and S410 may limit the LLPS propensity of TDP-43. Interestingly, the arginine-methylation mimic, TDP-43^{R293F}, exhibited the formation of large droplets that were comparable with TDP-43^{WT} (approximately 12.6 ± 1.9 μm^2) (Figures 5A–5C). Thus, phosphorylation and methylation likely have contrasting effects on LLPS of TDP-43. R293 methylation likely permits WT levels of TDP-43 LLPS, whereas S292, S409, and S410 phosphorylation likely reduce TDP-43 LLPS. Therefore, aberrant phosphorylation of TDP-43 likely reduces physiological functions of TDP-43, including various RNA-processing events, that depend on TDP-43 LLPS.[94]

Given these outcomes, we next compared the effects of phosphorylation and methylation mimics on TDP-43 aggregation propensity *in vitro*. Recombinant TDP-43-MBP protein constructs were incubated with Tobacco Etch Virus (TEV) protease and their aggregation was monitored over time. Under these conditions, selective cleavage of the MBP tag by TEV protease results in the formation of solid-phase TDP-43 aggregates and fibrils,[95,96] indicated by an increase in turbidity measurements. Here, we found that there were only minor differences in aggregation between TDP-43^{WT} and the phosphomimics TDP-43^{S292E} and TDP-43$^{S409E:S410E}$ (Figure 5D). However, the phosphomimic TDP-43$^{S292E:S409E:S410E}$ and the arginine methylation mimic, TDP-43^{R293F}, exhibited modestly reduced aggregation (Figure 5D). However, compared with TDP-43^{WT}, this reduced aggregation was only significant for TDP-43^{R293F} (Figure 5E). Notably, R293 monomethylation is predicted to be incompatible with a specific fibril polymorph of TDP-43, which assembles in type A FTD-TDP.[8] Thus, R293 monomethylation may prevent TDP-43 from accessing specific aggregated states.

Next, we plotted the normalized aggregation against the LLPS propensities of TDP-43^{WT} and its mutant forms. Strikingly, phosphomimetic mutants have a relatively greater tendency for aggregation over LLPS (Figure 5F). By contrast, TDP-43^{R293F} has a relatively greater tendency to undergo LLPS over aggregation (Figure 5F). Our results imply that TDP-43 phosphorylation and methylation may have opposing effects on TDP-43 (Figure 5F). Phosphorylation at S292, S409, and S410 reduces the propensity for TDP-43 to undergo LLPS but has limited effects on TDP-43 aggregation (Figure 5G). Thus, S292, S409, and S410 phosphorylation may divert TDP-43 toward aggregation and away from LLPS (Figure 5G). This finding helps to explain why pTDP-43 exhibits a greater propensity to aggregate and enter the urea fraction in cells. In contrast, R293 methylation allows TDP-43 to undergo normal LLPS, but reduces TDP-43 aggregation (Figure 5G). Thus, R293 methylation may reduce the propensity of TDP-43 to aggregate and enter the urea fraction in cells.

Arginine methylation regulates TDP-43 aggregation in cells

We next investigated the impact of arginine methylation on TDP-43 in a cellular context. SH-SY5Y cells were treated with AdOx, an arginine methyltransferase inhibitor, followed by fractionation and western blot analysis. We found that global methyltransferase inhibition promoted the accumulation of total TDP-43 in the urea fraction (Figures 6A and 6B). AdOx did not significantly alter the levels of pTDP-43 in the urea fraction (Figure 6C). These findings suggest that protein arginine methylation antagonizes TDP-43 proteinopathy.

We next assessed the effect of PRMT1 overexpression on TDP-43 proteinpathy. Remarkably, overexpression of PRMT1 markedly decreased TDP-43 aggregation (Figures 6D and 6E), evident by a decrease of total TDP-43 in the urea fraction (Figures 6D and 6E). Importantly, the levels of pTDP-43 in the urea fraction were drastically reduced by PRMT1 overexpression (Figures 6D and 6F). These findings suggest that PRMT1 exerts a protective role on TDP-43, likely by decreasing its aggregation propensity via monomethylation of R293 and reducing pathological phosphorylation.

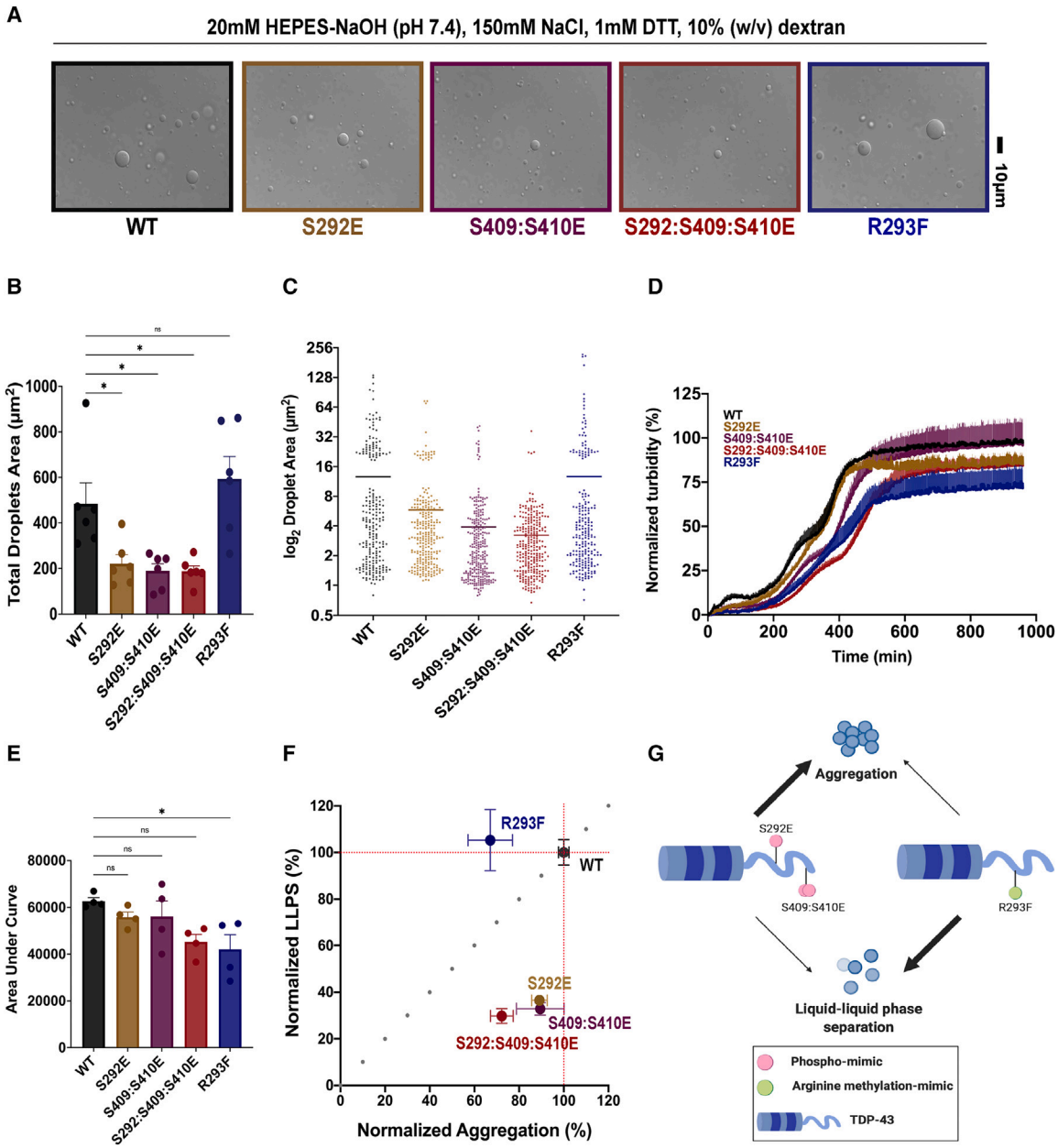

Figure 5. TDP-43 phosphorylation favors aggregation, whereas arginine methylation favors LLPS

(A) Representative DIC microscopy images of liquid-like droplets of 10μM TDP-43-MBP WT and variants. Purified recombinant proteins were incubated for 30min with phase separation buffer prior to imaging. Scale bar, 10 μm.

(B) Bar graph showing the total droplet area for each protein. Mean ± SEM, one-way ANOVA with Dunnett's multiple comparison test ($n = 6$, $^*p < 0.05$).

(C) Vertical scatterplot displaying the size distribution of droplets for each protein. Each data point corresponds with a single droplet. Bolded bars represent the average droplet area for each variant.

(D) Turbidity measurements of 5 μM TDP-43-MBP co-incubated with TEV protease (1 μg/mL). Turbidity was measured at an absorbance of 395 nm. Values represent the normalized mean ± SEM ($n = 4$).

(E) Aggregation data from (D) was quantified by calculating the area under the curve. Values represent means ± SEM ($n = 4$). One-way ANOVA with Dunnett's multiple comparison test was performed ($^*p < 0.05$).

(F) Aggregation versus LLPS plot shows the phospho-mimetics cluster below the dotted line, which represents the behavior of TDP-43^{WT}, while methylation-mimic appears above the line. The y axis represents normalized LLPS propensity relative to WT based on the average area of droplets from analysis in (C). The x axis represents normalized aggregation relative to WT from (D). Error bars represent SEM with n = 4–6.

(G) Schematic diagram describing the dichotomy in outcomes between TDP-43 phosphorylation and arginine methylation. Phospho-mimicking mutants favor aberrant aggregation over LLPS, whereas the arginine methylation-mimic favors LLPS over aberrant aggregation. See also Figures S6 and S7.

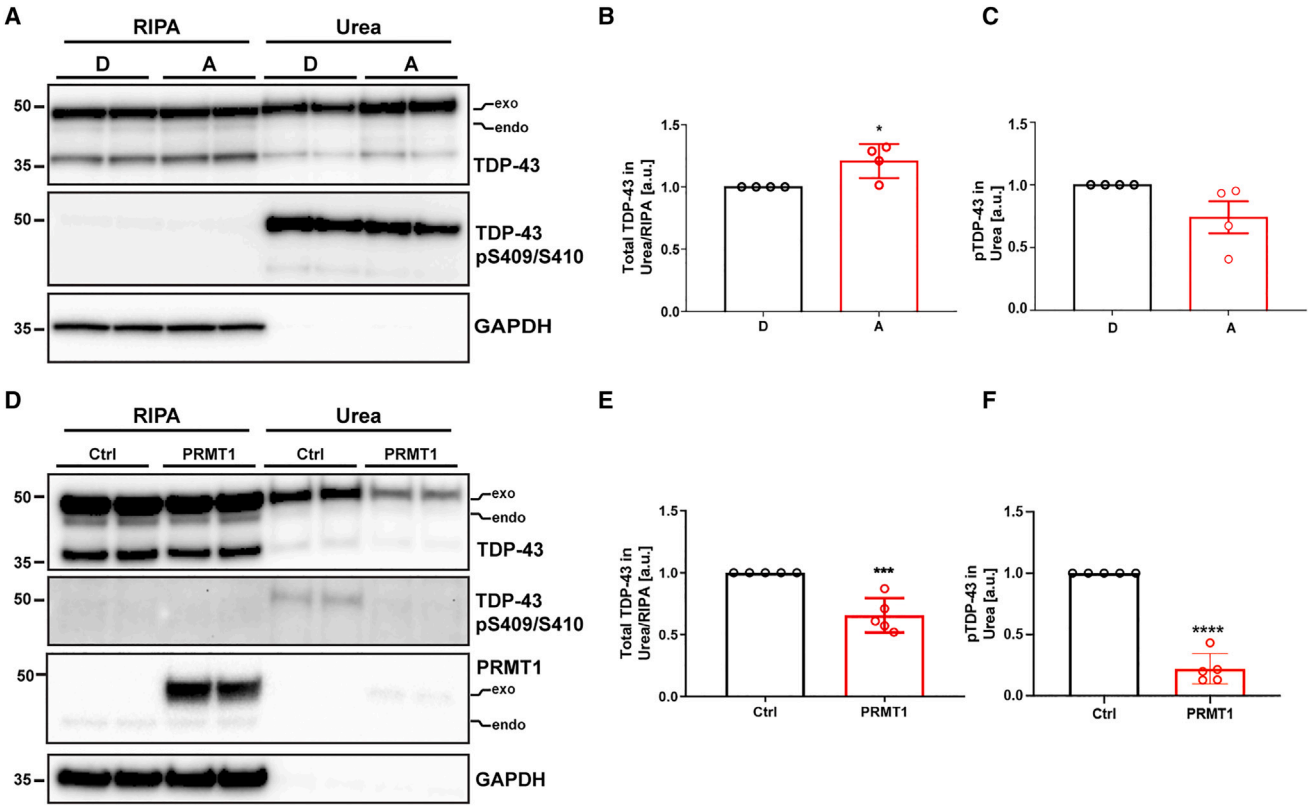

Figure 6. Arginine methylation of TDP-43 regulates its aggregation

(A) Western blot of total and pTDP-43 in RIPA and urea fractions of TDP-43^{WT}-transfected SH-SY5Y-cells treated with DMSO (D) or with methyltransferase inhibitor AdOx (A) at a final concentration of 20 μM for 24 h. The positions of FLAG-tagged TDP-43 (exo) and endogenous TDP-43 (endo) are indicated.

(B) Quantification of urea/RIPA ratio of total TDP-43 normalized to levels in DMSO-treated cells (mean ± SD, unpaired t test, $n = 4$). *$p < 0.05$.

(C) Quantification of pTDP-43 in the urea fraction normalized to levels in DMSO-treated cells (mean ± SD, unpaired t test, $n = 4$).

(D) Western blot of total and pTDP-43 in RIPA and urea fractions of TDP-43^{WT}-transfected SH-SY5Y-cells co-transfected with empty control plasmid (Ctrl) or PRMT1. The positions of FLAG-tagged TDP-43 (exo) and endogenous TDP-43 (endo) are indicated. The positions of Myc-tagged PRMT1 (exo) and endogenous PRMT1 (endo) are also indicated.

(E) Quantification of urea/RIPA ratio of total TDP-43 normalized to levels in Ctrl-plasmid co-transfected cells (mean ± SD, unpaired t test, $n = 5$). ***$p < 0.001$.

(F) Quantification of pTDP-43 in the urea fraction normalized to levels in control cells (mean ± SD, unpaired t test, $n = 5$). ****$p < 0.0001$. See also Figure S7.

Crosstalk between TDP-43 arginine methylation and p38α-mediated phosphorylation

The observation that TDP-43 undergoes PRMT1-mediated methylation at R293, coupled with our purified protein data suggesting contrasting outcomes between TDP-43 phosphorylation and methylation, led us to ask whether phosphorylation at S292 interferes with arginine methylation at the adjacent residue, R293, or vice versa (Figure 4A). Thus, we expressed FLAG-tagged TDP-43^{WT} as well as TDP-43^{S292E}, TDP-43^{S292N}, and TDP-43^{S292A} mutants in human neuronal SH-SY5Y cells and analyzed their methylation status. Immunoprecipitation followed by immunoblotting revealed a striking reduction in the MMA-signal in the phospho-mimicking TDP-43^{S292E} variant (Figure 7A). Interestingly, when compared with TDP-43^{WT}, the ALS-linked TDP-43^{S292N} variant showed a modest decrease in MMA-levels, which was more apparent for the approximately 35 kDa TDP-43-CTF (Figure 7A). By contrast, the TDP-43^{S292A} variant did not show any difference (Figure 7A). As shown previously (Figures 3C and 3D), the TDP-43^{S292E} mutant also promoted phosphorylation of TDP-43 at S409/S410, further underlining the anti-correlative relationship between TDP-43 arginine methylation and S409/S410 phosphorylation (Figure 7A). Thus, phosphorylation at S292, possibly combined with increased phosphorylation at S409/S410, could interfere with TDP-43 arginine methylation. However, these findings do not rule out that a reduction in TDP-43 methylation could be due to steric hindrance caused by the glutamic acid residue at position 292.

To further connect these two PTMs, we studied the methylation status of TDP-43 after genetic depletion of p38α. As shown previously (Figures S1A and S1C), we found that p38α downregulation reduced the phosphorylation of TDP-43^{WT} at S409/S410 (Figure 7B). Interestingly, western blot analysis also revealed that p38α depletion significantly decreased the formation of the approximately 35-kDa TDP-43-CTF (Figures 7B and 7C) and resulted in elevated levels of mono-methylated TDP-43-CTF (Figures 7B and 7D). By contrast, the effect of p38α depletion on monomethylation of full-length TDP-43 was less pronounced (Figure 7B). We also did not detect any ADMA signal

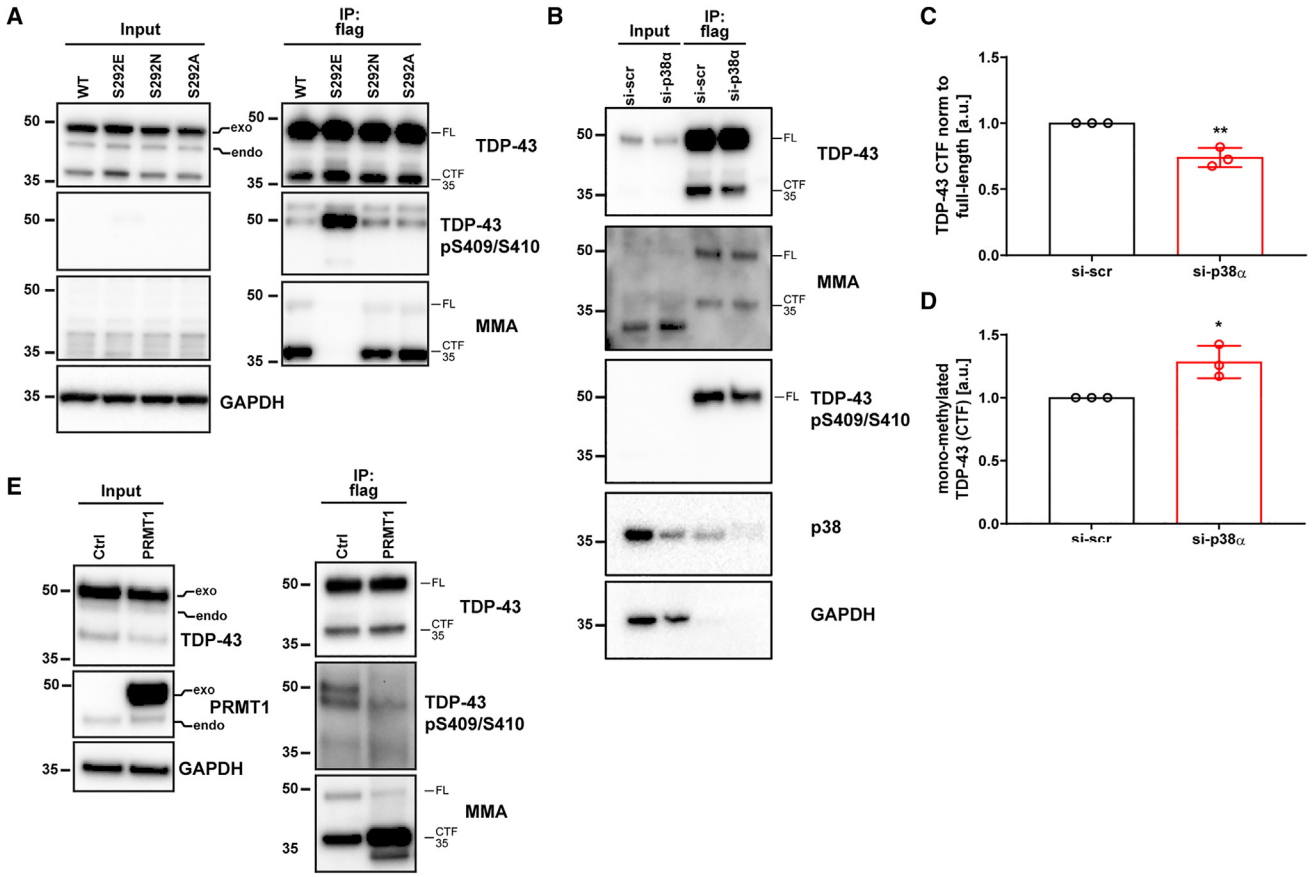

Figure 7. Crosstalk between PRMT1-catalyzed arginine methylation and p38α-mediated phosphorylation of TDP-43

(A) Western blot of immunoprecipitated FLAG-tagged TDP-43 from SH-SY5Y cells probed with antibodies against TDP-43, pTDP-43, and MMA. GAPDH serves as a loading control. The positions of FLAG-tagged TDP-43 (exo) and endogenous TDP-43 (endo) are indicated.

(B) Western blot of immunoprecipitated FLAG-tagged TDP-43^{WT} from SH-SY5Y cells with or without siRNA-induced p38α knockdown probed with antibodies against TDP-43, p38α, pTDP-43, and MMA. GAPDH serves as a loading control.

(C) Quantification of TDP-43-CTF/full length-ratio (mean ± SD, unpaired t test, $n = 3$). $^{**}p < 0.01$.

(D) Quantification of mono-methylated TDP-43-CTF normalized to total TDP-43-CTF (mean ± SD, unpaired t test, $n = 3$). $^{*}p < 0.05$.

(E) Western blot of immunoprecipitated FLAG-tagged TDP-43^{WT} from SH-SY5Y cells with or without PRMT1 overexpression probed with antibodies against TDP-43, pTDP-43, and MMA. GAPDH serves as a loading control. The positions of FLAG-tagged TDP-43 (exo) and endogenous TDP-43 (endo) are indicated. The positions of Myc-tagged PRMT1 (exo) and endogenous PRMT1 (endo) are also indicated. See also Figure S7.

via western blot, indicating that TDP-43 was predominantly arginine monomethylated under these conditions. Nonetheless, these observations suggest that there is an interplay between arginine methylation, p38α-mediated phosphorylation, and the formation of TDP-43 CTFs, indicating that reduced p38α activity could increase TDP-43 arginine methylation. We also found that PRMT1 overexpression led to a strong increase in mono-methylated TDP-43-CTF, but not full-length TDP-43, and a striking reduction in TDP-43 phosphorylation at S409/S410 (Figure 7E). These findings provide further support for our hypothesis that there is crosstalk between TDP-43 arginine methylation and phosphorylation at disease-relevant residues.

DISCUSSION

Since the discovery that approximately 97% of ALS cases and approximately 45% of FTD cases present with TDP-43 proteinopathy,[5,6] TDP-43 has been subject to intense investigation. However, the mechanisms underlying accumulation of TDP-43 aggregates are not yet understood. Aberrant TDP-43 phosphorylation is one of the major distinguishing pathological features of TDP-43 inclusions in human brains.[36,37] Although the consequences of these phosphorylation events have not been unequivocally established, aberrant phosphorylation of TDP-43 is associated with cytoplasmic mislocalization, decreased solubility, aberrant cleavage, and toxicity.[61,97–101] Several kinases including CK1, CK2, CDC7, and TTBK1/2 can phosphorylate TDP-43 and can promote pathological TDP-43 aggregation and neurotoxicity.[102–112] However, extensive hyperphosphorylation of TDP-43 by CK1δ can also reduce TDP-43 LLPS and aggregation.[113] Importantly, increased activation of p38 has been detected in human post-mortem ALS tissue, which is further substantiated by the findings that persistent activation of p38 signaling pathways induce neurodegeneration.[47,50,52]

Here, we elucidated the impact of p38α on TDP-43 proteinopathy. Genetic depletion and pharmacological inhibition of p38α suppressed TDP-43 phosphorylation, aggregation, and toxicity in neuronal systems. Importantly, p38α inhibition mitigated aberrant TDP-43 phenotypes in patient-derived motor neurons. A strength of our study is that we demonstrate therapeutic effects of p38α inhibition in multiple disease models, both in contexts where TDP-43 is overexpressed and in others where TDP-43 expression is at endogenous levels.

We have established that p38α can directly phosphorylate TDP-43 at residues S292 and S409/S410. In fact, mutations at S292 have been linked to pathogenicity in both sporadic and fALS.[35] However, no biochemical mechanistic data have been reported.[75,76] Here, we demonstrate that the phospho-mimetic mutant TDP-43^{S292E} promoted phosphorylation of TDP-43 at S409/S410 and enhanced the accumulation of TDP-43 aggregates. These findings identified S292 as a major site for TDP-43 phospho-regulation. The mechanism by which S292 phosphorylation promotes phosphorylation of S409/10 is not yet delineated. All these residues lie in the TDP-43 PrLD (residues 274–414),[35,114–116] which is predominantly unstructured except for a transient alpha-helical region approximately at residues 316–346.[117] However, we note that a similar interdependence of sites phosphorylated by p38α has been described for tau, another disease-linked, intrinsically disordered protein.[118] Thus, phosphorylation of an initial site in tau by p38α increases p38α-mediated phosphorylation of other sites across tau with specific sites showing strong interdependence.[118] Indeed, initial phosphorylation can alter the site-specific activity of p38α toward tau and site interdependence is a specific feature of p38α compared with other kinases.[118] A similar mechanism of phosphosite interdependence may occur in the p38α-mediated phosphorylation of TDP-43.

Interestingly, we found that S292, and the RGG-motif immediately following this residue, are highly conserved. The RGG-motif presents a major site for methylation by PRMTs.[77,119–121] Recent studies further support a role for arginine methylation and PRMT function in neurodegeneration.[122,123] For example, PRMT1 is a significant modulator of toxicity in C9-ALS.[124] Moreover, PRMT1 immunoreactivity and arginine dimethylation are increased in patients with ALS.[125] Methylation of specific arginines in FUS are also connected to ALS/FTD.[126–129] Here, we identified R293 as a major site for TDP-43 arginine methylation by PRMT1 in human neuronal SH-SY5Y cells, which is supported by earlier proteomic studies of mouse embryonic and brain tissue.[82,85]

There is increasing evidence suggesting that phosphorylation and arginine methylation co-exist on the same protein, and that these PTMs can have opposing or potentiating effects on protein function.[80,130] For example, p16 functions are regulated by antagonistic crosstalk between R138 methylation and S140 phosphorylation.[80] Here, we provide similar evidence for crosstalk between PRMT1-catalyzed methylation of R293 and p38α-mediated phosphorylation of S292 in the regulation of TDP-43 LLPS and aggregation. Our *in vitro* and *in vivo* data elucidate a dichotomous relationship between methylation and phosphorylation of TDP-43. Perhaps as a protective mechanism, TDP-43 methylation at R293 reduces phosphorylation at S292 and S409/S410, which in turn reduces TDP-43 aggregation. Indeed, R293 monomethylation is incompatible with a specific TDP-43 fibril polymorph connected with type A FTD-TDP,[8] and an arginine-methylation mimetic mutation at R293 significantly reduces TDP-43 aggregation at the pure protein level. Moreover, elevating PRMT1 expression reduces TDP-43 aggregation and phosphorylation at S409/S410. We note, however, that this effect could involve additional PRMT1 substrates beyond TDP-43.

Our studies suggest that S292 and S409/S410 phosphorylation render TDP-43 less prone to undergo LLPS, which may divert TDP-43 along pathological aggregation trajectories.[117] A reduced propensity for LLPS is predicted to dysregulate a subset of RNA clients of TDP-43, which could exacerbate TDP-43 loss of function in disease.[94] Whether TDP-43 methylation at R293 inhibits phosphorylation at S292, or vice versa, due to steric hindrance has yet to be determined. Regardless, our study suggests intricate interplay between protein phosphorylation and arginine methylation in the regulation of TDP-43. How S292 phosphorylation or R293 methylation might affect additional TDP-43 PTMs, such as neuroprotective SUMOylation of K408,[131] remains unclear and warrants further investigation. While additional studies will be necessary to further clarify the dynamics of these regulatory processes, especially in the context of more complex, clinically relevant models, our study provides a platform for developing therapeutics to inhibit p38α activity, promote PRMT1 activity, or both to rescue TDP-43 pathologies associated with ALS/FTD.

Importantly, we have shown that VX-745 mitigates aberrant TDP-43 phenotypes in c9ALS/FTD-patient derived motor neurons. Likewise, it has recently been shown that VX-745 reduces poly-GR-induced toxicity and enhances survival of iPSC-derived neurons from patients with c9ALS/FTD.[132] These two studies complement each other as Sun and coworkers[132] demonstrated that poly-GR induces p38α activation without providing a mechanism by which activation would lead to decreased neuronal survival, whereas we have elucidated a mechanism by which p38α aggravates TDP-43 toxicity, the primary pathology associated with c9ALS/FTD. We suggest that p38α inhibitors may find important applications in c9ALS/FTD.

In closing, we note that p38α has multiple cellular targets, which might complicate the development of p38α inhibitors as therapeutics.[39] However, the expression of p38α is actively repressed in healthy neurons, but is upregulated during neuronal stress or disease.[133] Indeed, inhibition or depletion of p38α reduces neurodegeneration in several mouse models of disease.[63,64,134,135] Moreover, VX-745 exhibits several important attributes as a clinical candidate, including potent and selective p38α inhibition, favorable pharmacokinetic profile, ability to cross the blood-brain barrier, and mitigation of neurodegeneration in mouse models of disease.[62,64,136,137] VX-745 has reached phase 2 clinical trials for Alzheimer's disease, Huntington's disease, and DLB.[63–65] Moreover, VX-745 has received orphan drug designation by the U.S. Food and Drug Administration to treat FTD and a fast-track designation for DLB. Indeed, VX-745 improved functional mobility and reduced dementia severity, and was well tolerated, in patients with DLB in a phase 2a trial.[64,138] These results are encouraging. However, a confirmatory phase 2b trial to assess VX-745 in DLB (ClinicalTrials.gov

ID: NCT05869669)[139] did not meet primary endpoints, perhaps due to target plasma drug concentrations not being achieved. We suggest that strategies to reduce p38α-mediated TDP-43 phosphorylation and promote R293 methylation could have therapeutic utility for ALS/FTD and related TDP-43 proteinopathies, including Alzheimer's disease, chronic traumatic encephalopathy, multisystem proteinopathy, and limbic-predominant age-related TDP-43 encephalopathy.[140–148]

Limitations of the study

We used phosphomimetic serine to glutamate mutations to explore how serine phosphorylation at specific positions of TDP-43 might affect TDP-43 behavior at the pure protein level and in human neuronal cells. Phosphomimetic mutations can accurately phenocopy serine phosphorylation events and have been extremely informative.[149–151] Moreover, phosphorylation sites often evolve from ancestral glutamate residues.[150] However, it is important to note phosphoserine creates a distinctive chemical microenvironment that is imperfectly mimicked by glutamate.[149,150,152] Indeed, the size of the ionic shell and the negative charge of the phosphate group is different than glutamate.[149,150,152] Hence, it will be important to assess TDP-43 behavior with phosphoserine at positions 292, 409, and 410. Advances in genetically encoding phosphoserine may enable these studies.[149,153] Likewise, we have used the methylation-mimetic arginine to phenylalanine mutation to explore how R293 methylation might affect TDP-43 behavior.[88] Although phenylalanine mimics the increased hydrophobicity of a methylated arginine,[88–90] it is an imperfect mimic because it lacks positive charge. Thus, it will be important to assess TDP-43 behavior with monomethylarginine or asymmetric dimethylarginine at position 293. Here, advances in site-specific installation or genetically encoding methylarginine may enable these studies.[154–157] Finally, it will be important to determine whether VX-745 mitigates neurotoxic effects of TDP-43 proteinopathy in mouse models of disease.

RESOURCE AVAILABILITY

Lead contact

Further information and requests for resources and reagents should be directed to and will be fulfilled by the lead contact, James Shorter (jshorter@pennmedicine.upenn.edu).

Materials availability

Plasmids newly generated in this study will be made readily available to the scientific community. We will honor requests in a timely fashion. Material transfers will be made with no more restrictive terms than in the Simple Letter Agreement or the Uniform Biological Materials Transfer Agreement and without reach through requirements.

Data and code availability

- The data supporting the findings of this study are available within the article and source data are available from the corresponding author upon request.
- Custom-written code in MATLAB to analyze DIC images of TDP-43 droplets has been deposited at Zenodo (https://doi.org/10.5281/zenodo.13963929).
- Any additional information required to reanalyze the data reported in this paper is available from the lead contact upon request.

ACKNOWLEDGMENTS

We thank Charlotte Fare, Katie Copley, Rebecca Jarvis, and John Alam for feedback. M.A. and H.M.O. were supported by the AstraZeneca postdoctoral program. H.M.O. was also supported by an Alzheimer's Association Research Fellowship and a Johnson Foundation Fellowship. B.C. was part of the AstraZeneca graduate program. K.L.M. and J.N.B. were supported by NSF graduate research fellowships. This work was supported by NIH grants T32AG00255 (A.F.F.), F31NS087676 (A.F.F.), F32NS108598 (E.M.B.), K99AG075242 (E.M.B), T32GM008275 (R.R.C.), F31AG060672 (R.R.C.), R35GM142505 (G.M.B.), R01LM013617 (S.F.), R01GM099836 (J.S.), and R21AG065854 (J.S.). E.M.B. was also supported by a Milton Safenowitz Post-Doctoral Fellowship from the ALS Association. R.R.C. was also supported by a Blavatnik Family Fellowship in Biomedical Research. J.A.K. and S.F. were supported by Target ALS IL-2023-C4-L2, U.S. Army Medical Research Acquisition Activity (USAMRAA) W81XWH-22-1-0721 CIRM (DISC0-13914), Answer ALS, and the ALS association. J.S. was supported by Target ALS, The Robert Packard Foundation for ALS research at Johns Hopkins, ALS Association, the G. Harold and Leila Y. Mathers Charitable Foundation, and the Office of the Assistant Secretary of Defense for Health Affairs (U.S.A.) through the Amyotrophic Lateral Sclerosis Research Program (W81XWH-20-1-0242). This work was supported by a grant to N.J.B., D.G.B., J.S., A.D.G., and S.F. from Target ALS Foundation and ALS Finding a Cure.

AUTHOR CONTRIBUTIONS

Conceptualization: M.A., H.M.O., H.J.W., J.D., A.D.G., A.J., J.A.K., G.M.B., D.G.B., C.J.D., S.F., S.J.M., N.J.B., and J.S.; methodology: M.A., H.M.O., H.J.W., B.L.L., Y-T.L., U.C., J.C.M., A.J., J.A.K., G.M.B., D.G.B., C.J.D., S.F., S.J.M., N.J.B., and J.S.; validation: M.A., H.M.O., H.J.W., B.L.L., B.C., T.A.O., J.L.S., Y-T.L., U.C., J.C.M., S.L., R.T., N.C., A.B., J.N.B., and M.A.N.; formal analysis: M.A., H.M.O., H.J.W., B.L.L., T.A.O., L.E.D., U.C., J.C.M., S.L., R.T., N.C., A.B., J.N.B., M.A.N, A.J., J.A.K., G.M.B., D.G.B., C.J.D., and S.F.; investigation: M.A., H.M.O., H.J.W., B.L.L., B.C., T.A.O., K.L.M., A.F.F., E.M.B., R.R.C., L.E.D., J.L.S., Y-T.L., U.C., J.C.M., S.L., R.T., N.C., A.B., J.N.B., M.A.N, A.J., J.A.K., and G.M.B.; resources: M.A., H.M.O., H.J.W., B.L.L., L.E.D., A.J., J.A.K., G.M.B., D.G.B., C.J.D., S.F., S.J.M., N.J.B., and J.S.; data curation: M.A., H.M.O., H.J.W., B.L.L., T.A.O., U.C., J.C.M., A.J., G.M.B., D.G.B., C.J.D., S.F., and J.S.; writing—original draft: M.A., H.M.O., H.J.W., B.L.L., J.C.M., A.J., J.A.K., G.M.B., D.G.B., C.J.D., S.F., N.J.B., and J.S.; writing—review and editing: M.A., H.M.O., H.J.W., B.L.L., B.C., T.A.O., K.L.M., A.F.F., E.M.B., R.R.C., L.E.D., J.L.S., Y-T.L., U.C., J.C.M., S.L., R.T., N.C., A.B., J.N.B., M.A.N, J.D., A.D.G., A.J., J.A.K., G.M.B., D.G.B., C.J.D., S.F., S.J.M., N.J.B., and J.S.; visualization: M.A., H.M.O., H.J.W., B.L.L., J.C.M., A.J., J.A.K., G.M.B., D.G.B., C.J.D., S.F., N.J.B., and J.S.; supervision: J.D., A.D.G., A.J., J.A.K., G.M.B., D.G.B., C.J.D., S.F., S.J.M., N.J.B., and J.S.; project administration: J.D., A.D.G., A.J., J.A.K., G.M.B., D.G.B., C.J.D., S.F., S.J.M., N.J.B., and J.S.; funding acquisition: M.A., H.M.O., K.L.M., A.F.F., E.M.B., R.R.C., J.D., A.D.G., A.J., J.A.K., G.M.B., D.G.B., C.J.D., S.F., S.J.M., N.J.B., and J.S.

DECLARATION OF INTERESTS

H.J.W., D.G.B., and N.J.B. were full-time employees and shareholders of AstraZeneca at the time these studies were conducted. S.J.M. is a consultant for SAGE Therapeutics and AstraZeneca, relationships that are regulated by Tufts University.

STAR★METHODS

Detailed methods are provided in the online version of this paper and include the following:

- KEY RESOURCES TABLE
- EXPERIMENTAL MODEL AND STUDY PARTICIPANT DETAILS
  - *E. coli* cultures
  - Human neuroblastoma cell line SH-SY5Y cultures

SUPPLEMENTAL INFORMATION

Supplemental information can be found online at https://doi.org/10.1016/j.celrep.2024.115205.

Received: August 4, 2021
Revised: October 21, 2024
Accepted: December 23, 2024
Published: January 14, 2025; corrected online: February 18, 2025

REFERENCES

1. Wobst, H.J., Mack, K.L., Brown, D.G., Brandon, N.J., and Shorter, J. (2020). The clinical trial landscape in amyotrophic lateral sclerosis-Past, present, and future. Med. Res. Rev. *40*, 1352–1384. https://doi.org/10.1002/med.21661.
2. Rowland, L.P., and Shneider, N.A. (2001). Amyotrophic lateral sclerosis. N. Engl. J. Med. *344*, 1688–1700. https://doi.org/10.1056/NEJM200105313442207.
3. Valdmanis, P.N., and Rouleau, G.A. (2008). Genetics of familial amyotrophic lateral sclerosis. Neurology *70*, 144–152. https://doi.org/10.1212/01.wnl.0000296811.19811.db.
4. Nguyen, H.P., Van Broeckhoven, C., and van der Zee, J. (2018). ALS Genes in the Genomic Era and their Implications for FTD. Trends Genet. *34*, 404–423. https://doi.org/10.1016/j.tig.2018.03.001.
5. Arai, T., Hasegawa, M., Akiyama, H., Ikeda, K., Nonaka, T., Mori, H., Mann, D., Tsuchiya, K., Yoshida, M., Hashizume, Y., and Oda, T. (2006). TDP-43 is a component of ubiquitin-positive tau-negative inclusions in frontotemporal lobar degeneration and amyotrophic lateral sclerosis. Biochem. Biophys. Res. Commun. *351*, 602–611. https://doi.org/10.1016/j.bbrc.2006.10.093.
6. Neumann, M., Sampathu, D.M., Kwong, L.K., Truax, A.C., Micsenyi, M.C., Chou, T.T., Bruce, J., Schuck, T., Grossman, M., Clark, C.M., et al. (2006). Ubiquitinated TDP-43 in frontotemporal lobar degeneration and amyotrophic lateral sclerosis. Science *314*, 130–133. https://doi.org/10.1126/science.1134108.
7. Guo, L., and Shorter, J. (2017). Biology and Pathobiology of TDP-43 and Emergent Therapeutic Strategies. Cold Spring Harbor Perspect. Med. *7*, a024554. https://doi.org/10.1101/cshperspect.a024554.
8. Arseni, D., Chen, R., Murzin, A.G., Peak-Chew, S.Y., Garringer, H.J., Newell, K.L., Kametani, F., Robinson, A.C., Vidal, R., Ghetti, B., et al. (2023). TDP-43 forms amyloid filaments with a distinct fold in type A FTLD-TDP. Nature *620*, 898–903. https://doi.org/10.1038/s41586-023-06405-w.
9. Arseni, D., Hasegawa, M., Murzin, A.G., Kametani, F., Arai, M., Yoshida, M., and Ryskeldi-Falcon, B. (2022). Structure of pathological TDP-43 filaments from ALS with FTLD. Nature *601*, 139–143. https://doi.org/10.1038/s41586-021-04199-3.
10. Odeh, H.M., and Shorter, J. (2022). Aggregates of TDP-43 protein spiral into view. Nature *601*, 29–30. https://doi.org/10.1038/d41586-021-03605-0.
11. Spence, H., Waldron, F.M., Saleeb, R.S., Brown, A.L., Rifai, O.M., Gilodi, M., Read, F., Roberts, K., Milne, G., Wilkinson, D., et al. (2024). RNA aptamer reveals nuclear TDP-43 pathology is an early aggregation event that coincides with STMN-2 cryptic splicing and precedes clinical manifestation in ALS. Acta Neuropathol. *147*, 50. https://doi.org/10.1007/s00401-024-02705-1.
12. Arseni, D., Nonaka, T., Jacobsen, M.H., Murzin, A.G., Cracco, L., Peak-Chew, S.Y., Garringer, H.J., Kawakami, I., Suzuki, H., Onaya, M., et al. (2024). Heteromeric amyloid filaments of ANXA11 and TDP-43 in FTLD-TDP Type C. Nature *634*, 662–668. https://doi.org/10.1038/s41586-024-08024-5.
13. Portz, B., Lee, B.L., and Shorter, J. (2021). FUS and TDP-43 Phases in Health and Disease. Trends Biochem. Sci. *46*, 550–563. https://doi.org/10.1016/j.tibs.2020.12.005.
14. Alami, N.H., Smith, R.B., Carrasco, M.A., Williams, L.A., Winborn, C.S., Han, S.S.W., Kiskinis, E., Winborn, B., Freibaum, B.D., Kanagaraj, A., et al. (2014). Axonal transport of TDP-43 mRNA granules is impaired by ALS-causing mutations. Neuron *81*, 536–543. https://doi.org/10.1016/j.neuron.2013.12.018.
15. Buratti, E., and Baralle, F.E. (2008). Multiple roles of TDP-43 in gene expression, splicing regulation, and human disease. Front. Biosci. *13*, 867–878. https://doi.org/10.2741/2727.
16. Kawahara, Y., and Mieda-Sato, A. (2012). TDP-43 promotes microRNA biogenesis as a component of the Drosha and Dicer complexes. Proc. Natl. Acad. Sci. USA *109*, 3347–3352. https://doi.org/10.1073/pnas.1112427109.
17. Lalmansingh, A.S., Urekar, C.J., and Reddi, P.P. (2011). TDP-43 is a transcriptional repressor: the testis-specific mouse acrv1 gene is a TDP-43 target in vivo. J. Biol. Chem. *286*, 10970–10982. https://doi.org/10.1074/jbc.M110.166587.
18. Li, H.R., Chen, T.C., Hsiao, C.L., Shi, L., Chou, C.Y., and Huang, J.R. (2018). The physical forces mediating self-association and phase-separation in the C-terminal domain of TDP-43. Biochim. Biophys. Acta, Proteins Proteomics *1866*, 214–223. https://doi.org/10.1016/j.bbapap.2017.10.001.
19. McDonald, K.K., Aulas, A., Destroismaisons, L., Pickles, S., Beleac, E., Camu, W., Rouleau, G.A., and Vande Velde, C. (2011). TAR DNA-binding protein 43 (TDP-43) regulates stress granule dynamics via differential

regulation of G3BP and TIA-1. Hum. Mol. Genet. *20*, 1400–1410. https://doi.org/10.1093/hmg/ddr021.

20. Tollervey, J.R., Curk, T., Rogelj, B., Briese, M., Cereda, M., Kayikci, M., König, J., Hortobágyi, T., Nishimura, A.L., Zupunski, V., et al. (2011). Characterizing the RNA targets and position-dependent splicing regulation by TDP-43. Nat. Neurosci. *14*, 452–458. https://doi.org/10.1038/nn.2778.
21. Ling, J.P., Pletnikova, O., Troncoso, J.C., and Wong, P.C. (2015). TDP-43 repression of nonconserved cryptic exons is compromised in ALS-FTD. Science *349*, 650–655. https://doi.org/10.1126/science.aab0983.
22. Ma, X.R., Prudencio, M., Koike, Y., Vatsavayai, S.C., Kim, G., Harbinski, F., Briner, A., Rodriguez, C.M., Guo, C., Akiyama, T., et al. (2022). TDP-43 represses cryptic exon inclusion in the FTD-ALS gene UNC13A. Nature *603*, 124–130. https://doi.org/10.1038/s41586-022-04424-7.
23. Brown, A.L., Wilkins, O.G., Keuss, M.J., Hill, S.E., Zanovello, M., Lee, W.C., Bampton, A., Lee, F.C.Y., Masino, L., Qi, Y.A., et al. (2022). TDP-43 loss and ALS-risk SNPs drive mis-splicing and depletion of UNC13A. Nature *603*, 131–137. https://doi.org/10.1038/s41586-022-04436-3.
24. Baughn, M.W., Melamed, Z., López-Erauskin, J., Beccari, M.S., Ling, K., Zuberi, A., Presa, M., Gonzalo-Gil, E., Maimon, R., Vazquez-Sanchez, S., et al. (2023). Mechanism of STMN2 cryptic splice-polyadenylation and its correction for TDP-43 proteinopathies. Science *379*, 1140–1149. https://doi.org/10.1126/science.abq5622.
25. Melamed, Z., López-Erauskin, J., Baughn, M.W., Zhang, O., Drenner, K., Sun, Y., Freyermuth, F., McMahon, M.A., Beccari, M.S., Artates, J.W., et al. (2019). Premature polyadenylation-mediated loss of stathmin-2 is a hallmark of TDP-43-dependent neurodegeneration. Nat. Neurosci. *22*, 180–190. https://doi.org/10.1038/s41593-018-0293-z.
26. Ayala, Y.M., Zago, P., D'Ambrogio, A., Xu, Y.F., Petrucelli, L., Buratti, E., and Baralle, F.E. (2008). Structural determinants of the cellular localization and shuttling of TDP-43. J. Cell Sci. *121*, 3778–3785. https://doi.org/10.1242/jcs.038950.
27. Buratti, E., Brindisi, A., Giombi, M., Tisminetzky, S., Ayala, Y.M., and Baralle, F.E. (2005). TDP-43 binds heterogeneous nuclear ribonucleoprotein A/B through its C-terminal tail: an important region for the inhibition of cystic fibrosis transmembrane conductance regulator exon 9 splicing. J. Biol. Chem. *280*, 37572–37584. https://doi.org/10.1074/jbc.M505557200.
28. Chang, C.K., Wu, T.H., Wu, C.Y., Chiang, M.H., Toh, E.K.W., Hsu, Y.C., Lin, K.F., Liao, Y.H., Huang, T.H., and Huang, J.J.T. (2012). The N-terminus of TDP-43 promotes its oligomerization and enhances DNA binding affinity. Biochem. Biophys. Res. Commun. *425*, 219–224. https://doi.org/10.1016/j.bbrc.2012.07.071.
29. Freibaum, B.D., Chitta, R.K., High, A.A., and Taylor, J.P. (2010). Global analysis of TDP-43 interacting proteins reveals strong association with RNA splicing and translation machinery. J. Proteome Res. *9*, 1104–1120. https://doi.org/10.1021/pr901076y.
30. Jiang, L.L., Xue, W., Hong, J.Y., Zhang, J.T., Li, M.J., Yu, S.N., He, J.H., and Hu, H.Y. (2017). The N-terminal dimerization is required for TDP-43 splicing activity. Sci. Rep. *7*, 6196. https://doi.org/10.1038/s41598-017-06263-3.
31. Johnson, B.S., Snead, D., Lee, J.J., McCaffery, J.M., Shorter, J., and Gitler, A.D. (2009). TDP-43 is intrinsically aggregation-prone, and amyotrophic lateral sclerosis-linked mutations accelerate aggregation and increase toxicity. J. Biol. Chem. *284*, 20329–20339. https://doi.org/10.1074/jbc.M109.010264.
32. Molliex, A., Temirov, J., Lee, J., Coughlin, M., Kanagaraj, A.P., Kim, H.J., Mittag, T., and Taylor, J.P. (2015). Phase separation by low complexity domains promotes stress granule assembly and drives pathological fibrillization. Cell *163*, 123–133. https://doi.org/10.1016/j.cell.2015.09.015.
33. Winton, M.J., Igaz, L.M., Wong, M.M., Kwong, L.K., Trojanowski, J.Q., and Lee, V.M.Y. (2008). Disturbance of nuclear and cytoplasmic TAR DNA-binding protein (TDP-43) induces disease-like redistribution, sequestration, and aggregate formation. J. Biol. Chem. *283*, 13302–13309. https://doi.org/10.1074/jbc.M800342200.
34. Prasad, A., Bharathi, V., Sivalingam, V., Girdhar, A., and Patel, B.K. (2019). Molecular Mechanisms of TDP-43 Misfolding and Pathology in Amyotrophic Lateral Sclerosis. Front. Mol. Neurosci. *12*, 25. https://doi.org/10.3389/fnmol.2019.00025.
35. Harrison, A.F., and Shorter, J. (2017). RNA-binding proteins with prion-like domains in health and disease. Biochem. J. *474*, 1417–1438. https://doi.org/10.1042/BCJ20160499.
36. Hasegawa, M., Arai, T., Nonaka, T., Kametani, F., Yoshida, M., Hashizume, Y., Beach, T.G., Buratti, E., Baralle, F., Morita, M., et al. (2008). Phosphorylated TDP-43 in frontotemporal lobar degeneration and amyotrophic lateral sclerosis. Ann. Neurol. *64*, 60–70. https://doi.org/10.1002/ana.21425.
37. Neumann, M., Kwong, L.K., Lee, E.B., Kremmer, E., Flatley, A., Xu, Y., Forman, M.S., Troost, D., Kretzschmar, H.A., Trojanowski, J.Q., and Lee, V.M.Y. (2009). Phosphorylation of S409/410 of TDP-43 is a consistent feature in all sporadic and familial forms of TDP-43 proteinopathies. Acta Neuropathol. *117*, 137–149. https://doi.org/10.1007/s00401-008-0477-9.
38. Buratti, E. (2018). TDP-43 post-translational modifications in health and disease. Expert Opin. Ther. Targets *22*, 279–293. https://doi.org/10.1080/14728222.2018.1439923.
39. Canovas, B., and Nebreda, A.R. (2021). Diversity and versatility of p38 kinase signalling in health and disease. Nat. Rev. Mol. Cell Biol. *22*, 346–366. https://doi.org/10.1038/s41580-020-00322-w.
40. Cuadrado, A., and Nebreda, A.R. (2010). Mechanisms and functions of p38 MAPK signalling. Biochem. J. *429*, 403–417. https://doi.org/10.1042/BJ20100323.
41. Morrison, D.K. (2012). MAP kinase pathways. Cold Spring Harbor Perspect. Biol. *4*, a011254. https://doi.org/10.1101/cshperspect.a011254.
42. Brennan, C.M., Emerson, C.P., Jr., Owens, J., and Christoforou, N. (2021). p38 MAPKs - roles in skeletal muscle physiology, disease mechanisms, and as potential therapeutic targets. JCI Insight *6*, e149915. https://doi.org/10.1172/jci.insight.149915.
43. Zarubin, T., and Han, J. (2005). Activation and signaling of the p38 MAP kinase pathway. Cell Res. *15*, 11–18. https://doi.org/10.1038/sj.cr.7290257.
44. Yasuda, S., Sugiura, H., Tanaka, H., Takigami, S., and Yamagata, K. (2011). p38 MAP kinase inhibitors as potential therapeutic drugs for neural diseases. Cent. Nerv. Syst. Agents Med. Chem. *11*, 45–59. https://doi.org/10.2174/187152411794961040.
45. Cuenda, A., Cohen, P., Buée-Scherrer, V., and Goedert, M. (1997). Activation of stress-activated protein kinase-3 (SAPK3) by cytokines and cellular stresses is mediated via SAPKK3 (MKK6); comparison of the specificities of SAPK3 and SAPK2 (RK/p38). EMBO J. *16*, 295–305. https://doi.org/10.1093/emboj/16.2.295.
46. Pickhardt, M., Tassoni, M., Denner, P., Kurkowsky, B., Kitanovic, A., Möhl, C., Fava, E., and Mandelkow, E. (2019). Screening of a neuronal cell model of tau pathology for therapeutic compounds. Neurobiol. Aging *76*, 24–34. https://doi.org/10.1016/j.neurobiolaging.2018.11.026.
47. Dewil, M., dela Cruz, V.F., Van Den Bosch, L., and Robberecht, W. (2007). Inhibition of p38 mitogen activated protein kinase activation and mutant SOD1(G93A)-induced motor neuron death. Neurobiol. Dis. *26*, 332–341. https://doi.org/10.1016/j.nbd.2006.12.023.
48. Gibbs, K.L., Kalmar, B., Rhymes, E.R., Fellows, A.D., Ahmed, M., Whiting, P., Davies, C.H., Greensmith, L., and Schiavo, G. (2018). Inhibiting p38 MAPK alpha rescues axonal retrograde transport defects in a mouse model of ALS. Cell Death Dis. *9*, 596. https://doi.org/10.1038/s41419-018-0624-8.
49. Zhan, L., Xie, Q., and Tibbetts, R.S. (2015). Opposing roles of p38 and JNK in a Drosophila model of TDP-43 proteinopathy reveal oxidative

stress and innate immunity as pathogenic components of neurodegeneration. Hum. Mol. Genet. *24*, 757–772. https://doi.org/10.1093/hmg/ddu493.

50. Bendotti, C., Atzori, C., Piva, R., Tortarolo, M., Strong, M.J., DeBiasi, S., and Migheli, A. (2004). Activated p38MAPK is a novel component of the intracellular inclusions found in human amyotrophic lateral sclerosis and mutant SOD1 transgenic mice. J. Neuropathol. Exp. Neurol. *63*, 113–119. https://doi.org/10.1093/jnen/63.2.113.

51. Correa, S.A., and Eales, K.L. (2012). The Role of p38 MAPK and Its Substrates in Neuronal Plasticity and Neurodegenerative Disease. J. Signal Transduct. *2012*, 649079. https://doi.org/10.1155/2012/649079.

52. Tortarolo, M., Veglianese, P., Calvaresi, N., Botturi, A., Rossi, C., Giorgini, A., Migheli, A., and Bendotti, C. (2003). Persistent activation of p38 mitogen-activated protein kinase in a mouse model of familial amyotrophic lateral sclerosis correlates with disease progression. Mol. Cell. Neurosci. *23*, 180–192. https://doi.org/10.1016/s1044-7431(03)00022-8.

53. Wobst, H.J., Wesolowski, S.S., Chadchankar, J., Delsing, L., Jacobsen, S., Mukherjee, J., Deeb, T.Z., Dunlop, J., Brandon, N.J., and Moss, S.J. (2017). Cytoplasmic Relocalization of TAR DNA-Binding Protein 43 Is Not Sufficient to Reproduce Cellular Pathologies Associated with ALS In vitro. Front. Mol. Neurosci. *10*, 46. https://doi.org/10.3389/fnmol.2017.00046.

54. Xu, Y.F., Zhang, Y.J., Lin, W.L., Cao, X., Stetler, C., Dickson, D.W., Lewis, J., and Petrucelli, L. (2011). Expression of mutant TDP-43 induces neuronal dysfunction in transgenic mice. Mol. Neurodegener. *6*, 73. https://doi.org/10.1186/1750-1326-6-73.

55. Watkins, J., Ghosh, A., Keerie, A.F.A., Alix, J.J.P., Mead, R.J., and Sreedharan, J. (2020). Female sex mitigates motor and behavioural phenotypes in TDP-43(Q331K) knock-in mice. Sci. Rep. *10*, 19220. https://doi.org/10.1038/s41598-020-76070-w.

56. Arnold, E.S., Ling, S.C., Huelga, S.C., Lagier-Tourenne, C., Polymenidou, M., Ditsworth, D., Kordasiewicz, H.B., McAlonis-Downes, M., Platoshyn, O., Parone, P.A., et al. (2013). ALS-linked TDP-43 mutations produce aberrant RNA splicing and adult-onset motor neuron disease without aggregation or loss of nuclear TDP-43. Proc. Natl. Acad. Sci. USA *110*, E736–E745. https://doi.org/10.1073/pnas.1222809110.

57. Gitcho, M.A., Bigio, E.H., Mishra, M., Johnson, N., Weintraub, S., Mesulam, M., Rademakers, R., Chakraverty, S., Cruchaga, C., Morris, J.C., et al. (2009). TARDBP 3'-UTR variant in autopsy-confirmed frontotemporal lobar degeneration with TDP-43 proteinopathy. Acta Neuropathol. *118*, 633–645. https://doi.org/10.1007/s00401-009-0571-7.

58. Gasset-Rosa, F., Lu, S., Yu, H., Chen, C., Melamed, Z., Guo, L., Shorter, J., Da Cruz, S., and Cleveland, D.W. (2019). Cytoplasmic TDP-43 Demixing Independent of Stress Granules Drives Inhibition of Nuclear Import, Loss of Nuclear TDP-43, and Cell Death. Neuron *102*, 339–357. https://doi.org/10.1016/j.neuron.2019.02.038.

59. Polymenidou, M., Lagier-Tourenne, C., Hutt, K.R., Huelga, S.C., Moran, J., Liang, T.Y., Ling, S.C., Sun, E., Wancewicz, E., Mazur, C., et al. (2011). Long pre-mRNA depletion and RNA missplicing contribute to neuronal vulnerability from loss of TDP-43. Nat. Neurosci. *14*, 459–468. https://doi.org/10.1038/nn.2779.

60. Sreedharan, J., Blair, I.P., Tripathi, V.B., Hu, X., Vance, C., Rogelj, B., Ackerley, S., Durnall, J.C., Williams, K.L., Buratti, E., et al. (2008). TDP-43 mutations in familial and sporadic amyotrophic lateral sclerosis. Science *319*, 1668–1672. https://doi.org/10.1126/science.1154584.

61. Barmada, S.J., Skibinski, G., Korb, E., Rao, E.J., Wu, J.Y., and Finkbeiner, S. (2010). Cytoplasmic mislocalization of TDP-43 is toxic to neurons and enhanced by a mutation associated with familial amyotrophic lateral sclerosis. J. Neurosci. *30*, 639–649. https://doi.org/10.1523/JNEUROSCI.4988-09.2010.

62. Duffy, J.P., Harrington, E.M., Salituro, F.G., Cochran, J.E., Green, J., Gao, H., Bemis, G.W., Evindar, G., Galullo, V.P., Ford, P.J., et al. (2011). The Discovery of VX-745: A Novel and Selective p38alpha Kinase Inhibitor. ACS Med. Chem. Lett. *2*, 758–763. https://doi.org/10.1021/ml2001455.

63. Germann, U.A., and Alam, J.J. (2020). P38alpha MAPK Signaling-A Robust Therapeutic Target for Rab5-Mediated Neurodegenerative Disease. Int. J. Mol. Sci. *21*, 5485. https://doi.org/10.3390/ijms21155485.

64. Jiang, Y., Alam, J.J., Gomperts, S.N., Maruff, P., Lemstra, A.W., Germann, U.A., Stavrides, P.H., Darji, S., Malampati, S., Peddy, J., et al. (2022). Preclinical and randomized clinical evaluation of the p38alpha kinase inhibitor neflamapimod for basal forebrain cholinergic degeneration. Nat. Commun. *13*, 5308. https://doi.org/10.1038/s41467-022-32944-3.

65. Prins, N.D., Harrison, J.E., Chu, H.M., Blackburn, K., Alam, J.J., and Scheltens, P.; REVERSE-SD Study Investigators (2021). A phase 2 double-blind placebo-controlled 24-week treatment clinical study of the p38 alpha kinase inhibitor neflamapimod in mild Alzheimer's disease. Alzheimer's Res. Ther. *13*, 106. https://doi.org/10.1186/s13195-021-00843-2.

66. Hicks, D.A., Cross, L.L., Williamson, R., and Rattray, M. (2020). Endoplasmic Reticulum Stress Signalling Induces Casein Kinase 1-Dependent Formation of Cytosolic TDP-43 Inclusions in Motor Neuron-Like Cells. Neurochem. Res. *45*, 1354–1364. https://doi.org/10.1007/s11064-019-02832-2.

67. Klim, J.R., Williams, L.A., Limone, F., Guerra San Juan, I., Davis-Dusenbery, B.N., Mordes, D.A., Burberry, A., Steinbaugh, M.J., Gamage, K.K., Kirchner, R., et al. (2019). ALS-implicated protein TDP-43 sustains levels of STMN2, a mediator of motor neuron growth and repair. Nat. Neurosci. *22*, 167–179. https://doi.org/10.1038/s41593-018-0300-4.

68. Streit, L., Kuhn, T., Vomhof, T., Bopp, V., Ludolph, A.C., Weishaupt, J.H., Gebhardt, J.C.M., Michaelis, J., and Danzer, K.M. (2022). Stress induced TDP-43 mobility loss independent of stress granules. Nat. Commun. *13*, 5480. https://doi.org/10.1038/s41467-022-32939-0.

69. Linsley, J.W., Shah, K., Castello, N., Chan, M., Haddad, D., Doric, Z., Wang, S., Leks, W., Mancini, J., Oza, V., et al. (2021). Genetically encoded cell-death indicators (GEDI) to detect an early irreversible commitment to neurodegeneration. Nat. Commun. *12*, 5284. https://doi.org/10.1038/s41467-021-25549-9.

70. DeJesus-Hernandez, M., Mackenzie, I.R., Boeve, B.F., Boxer, A.L., Baker, M., Rutherford, N.J., Nicholson, A.M., Finch, N.A., Flynn, H., Adamson, J., et al. (2011). Expanded GGGGCC hexanucleotide repeat in noncoding region of C9ORF72 causes chromosome 9p-linked FTD and ALS. Neuron *72*, 245–256. https://doi.org/10.1016/j.neuron.2011.09.011.

71. Renton, A.E., Majounie, E., Waite, A., Simón-Sánchez, J., Rollinson, S., Gibbs, J.R., Schymick, J.C., Laaksovirta, H., van Swieten, J.C., Myllykangas, L., et al. (2011). A hexanucleotide repeat expansion in C9ORF72 is the cause of chromosome 9p21-linked ALS-FTD. Neuron *72*, 257–268. https://doi.org/10.1016/j.neuron.2011.09.010.

72. Diskin, R., Askari, N., Capone, R., Engelberg, D., and Livnah, O. (2004). Active mutants of the human p38alpha mitogen-activated protein kinase. J. Biol. Chem. *279*, 47040–47049. https://doi.org/10.1074/jbc.M404595200.

73. Yu, H., Lu, S., Gasior, K., Singh, D., Vazquez-Sanchez, S., Tapia, O., Toprani, D., Beccari, M.S., Yates, J.R., 3rd, Da Cruz, S., et al. (2021). HSP70 chaperones RNA-free TDP-43 into anisotropic intranuclear liquid spherical shells. Science *371*, eabb4309. https://doi.org/10.1126/science.abb4309.

74. Kametani, F., Obi, T., Shishido, T., Akatsu, H., Murayama, S., Saito, Y., Yoshida, M., and Hasegawa, M. (2016). Mass spectrometric analysis of accumulated TDP-43 in amyotrophic lateral sclerosis brains. Sci. Rep. *6*, 23281. https://doi.org/10.1038/srep23281.

75. Xiong, H.L., Wang, J.Y., Sun, Y.M., Wu, J.J., Chen, Y., Qiao, K., Zheng, Q.J., Zhao, G.X., and Wu, Z.Y. (2010). Association between novel TARDBP mutations and Chinese patients with amyotrophic lateral sclerosis. BMC Med. Genet. *11*, 8. https://doi.org/10.1186/1471-2350-11-8.

76. Zou, Z.Y., Peng, Y., Wang, X.N., Liu, M.S., Li, X.G., and Cui, L.Y. (2012). Screening of the TARDBP gene in familial and sporadic amyotrophic lateral sclerosis patients of Chinese origin. Neurobiol. Aging *33*, 2229. https://doi.org/10.1016/j.neurobiolaging.2012.03.014.

77. Thandapani, P., O'Connor, T.R., Bailey, T.L., and Richard, S. (2013). Defining the RGG/RG motif. Mol. Cell *50*, 613–623. https://doi.org/10.1016/j.molcel.2013.05.021.

78. Guo, Z., Zheng, L., Xu, H., Dai, H., Zhou, M., Pascua, M.R., Chen, Q.M., and Shen, B. (2010). Methylation of FEN1 suppresses nearby phosphorylation and facilitates PCNA binding. Nat. Chem. Biol. *6*, 766–773. https://doi.org/10.1038/nchembio.422.

79. Hsu, J.M., Chen, C.T., Chou, C.K., Kuo, H.P., Li, L.Y., Lin, C.Y., Lee, H.J., Wang, Y.N., Liu, M., Liao, H.W., et al. (2011). Crosstalk between Arg 1175 methylation and Tyr 1173 phosphorylation negatively modulates EGFR-mediated ERK activation. Nat. Cell Biol. *13*, 174–181. https://doi.org/10.1038/ncb2158.

80. Lu, Y., Ma, W., Li, Z., Lu, J., and Wang, X. (2017). The interplay between p16 serine phosphorylation and arginine methylation determines its function in modulating cellular apoptosis and senescence. Sci. Rep. *7*, 41390. https://doi.org/10.1038/srep41390.

81. Yamagata, K., Daitoku, H., Takahashi, Y., Namiki, K., Hisatake, K., Kako, K., Mukai, H., Kasuya, Y., and Fukamizu, A. (2008). Arginine methylation of FOXO transcription factors inhibits their phosphorylation by Akt. Mol. Cell *32*, 221–231. https://doi.org/10.1016/j.molcel.2008.09.013.

82. Larsen, S.C., Sylvestersen, K.B., Mund, A., Lyon, D., Mullari, M., Madsen, M.V., Daniel, J.A., Jensen, L.J., and Nielsen, M.L. (2016). Proteome-wide analysis of arginine monomethylation reveals widespread occurrence in human cells. Sci. Signal. *9*, rs9. https://doi.org/10.1126/scisignal.aaf7329.

83. Geoghegan, V., Guo, A., Trudgian, D., Thomas, B., and Acuto, O. (2015). Comprehensive identification of arginine methylation in primary T cells reveals regulatory roles in cell signalling. Nat. Commun. *6*, 6758. https://doi.org/10.1038/ncomms7758.

84. Sylvestersen, K.B., Horn, H., Jungmichel, S., Jensen, L.J., and Nielsen, M.L. (2014). Proteomic analysis of arginine methylation sites in human cells reveals dynamic regulation during transcriptional arrest. Mol. Cell. Proteomics *13*, 2072–2088. https://doi.org/10.1074/mcp.O113.032748.

85. Guo, A., Gu, H., Zhou, J., Mulhern, D., Wang, Y., Lee, K.A., Yang, V., Aguiar, M., Kornhauser, J., Jia, X., et al. (2014). Immunoaffinity enrichment and mass spectrometry analysis of protein methylation. Mol. Cell. Proteomics *13*, 372–387. https://doi.org/10.1074/mcp.O113.027870.

86. Wu, Q., Schapira, M., Arrowsmith, C.H., and Barsyte-Lovejoy, D. (2021). Protein arginine methylation: from enigmatic functions to therapeutic targeting. Nat. Rev. Drug Discov. *20*, 509–530. https://doi.org/10.1038/s41573-021-00159-8.

87. Tang, J., Frankel, A., Cook, R.J., Kim, S., Paik, W.K., Williams, K.R., Clarke, S., and Herschman, H.R. (2000). PRMT1 is the predominant type I protein arginine methyltransferase in mammalian cells. J. Biol. Chem. *275*, 7723–7730. https://doi.org/10.1074/jbc.275.11.7723.

88. Mostaqul Huq, M.D., Gupta, P., Tsai, N.P., White, R., Parker, M.G., and Wei, L.N. (2006). Suppression of receptor interacting protein 140 repressive activity by protein arginine methylation. EMBO J. *25*, 5094–5104. https://doi.org/10.1038/sj.emboj.7601389.

89. Dillon, M.B.C., Rust, H.L., Thompson, P.R., and Mowen, K.A. (2013). Automethylation of protein arginine methyltransferase 8 (PRMT8) regulates activity by impeding S-adenosylmethionine sensitivity. J. Biol. Chem. *288*, 27872–27880. https://doi.org/10.1074/jbc.M113.491092.

90. Campbell, M., Chang, P.C., Huerta, S., Izumiya, C., Davis, R., Tepper, C.G., Kim, K.Y., Shevchenko, B., Wang, D.H., Jung, J.U., et al. (2012). Protein arginine methyltransferase 1-directed methylation of Kaposi sarcoma-associated herpesvirus latency-associated nuclear antigen. J. Biol. Chem. *287*, 5806–5818. https://doi.org/10.1074/jbc.M111.289496.

91. Ling, S.C., Albuquerque, C.P., Han, J.S., Lagier-Tourenne, C., Tokunaga, S., Zhou, H., and Cleveland, D.W. (2010). ALS-associated mutations in TDP-43 increase its stability and promote TDP-43 complexes with FUS/TLS. Proc. Natl. Acad. Sci. USA *107*, 13318–13323. https://doi.org/10.1073/pnas.1008227107.

92. McGurk, L., Gomes, E., Guo, L., Mojsilovic-Petrovic, J., Tran, V., Kalb, R.G., Shorter, J., and Bonini, N.M. (2018). Poly(ADP-Ribose) Prevents Pathological Phase Separation of TDP-43 by Promoting Liquid Demixing and Stress Granule Localization. Mol. Cell *71*, 703–717. https://doi.org/10.1016/j.molcel.2018.07.002.

93. Mann, J.R., Gleixner, A.M., Mauna, J.C., Gomes, E., DeChellis-Marks, M.R., Needham, P.G., Copley, K.E., Hurtle, B., Portz, B., Pyles, N.J., et al. (2019). RNA Binding Antagonizes Neurotoxic Phase Transitions of TDP-43. Neuron *102*, 321–338. https://doi.org/10.1016/j.neuron.2019.01.048.

94. Hallegger, M., Chakrabarti, A.M., Lee, F.C.Y., Lee, B.L., Amalietti, A.G., Odeh, H.M., Copley, K.E., Rubien, J.D., Portz, B., Kuret, K., et al. (2021). TDP-43 condensation properties specify its RNA-binding and regulatory repertoire. Cell *184*, 4680–4696. https://doi.org/10.1016/j.cell.2021.07.018.

95. Cook, C.N., Wu, Y., Odeh, H.M., Gendron, T.F., Jansen-West, K., Del Rosso, G., Yue, M., Jiang, P., Gomes, E., Tong, J., et al. (2020). C9orf72 poly(GR) aggregation induces TDP-43 proteinopathy. Sci. Transl. Med. *12*, eabb3774. https://doi.org/10.1126/scitranslmed.abb3774.

96. Guo, L., Mann, J.R., Mauna, J.C., Copley, K.E., Wang, H., Rubien, J.D., Odeh, H.M., Lin, J., Lee, B.L., Ganser, L., et al. (2023). Defining RNA oligonucleotides that reverse deleterious phase transitions of RNA-binding proteins with prion-like domains. Preprint at bioRxiv. https://doi.org/10.1101/2023.09.04.555754.

97. Brady, O.A., Meng, P., Zheng, Y., Mao, Y., and Hu, F. (2011). Regulation of TDP-43 aggregation by phosphorylation and p62/SQSTM1. J. Neurochem. *116*, 248–259. https://doi.org/10.1111/j.1471-4159.2010.07098.x.

98. Kim, K.Y., Lee, H.W., Shim, Y.M., Mook-Jung, I., Jeon, G.S., and Sung, J.J. (2015). A phosphomimetic mutant TDP-43 (S409/410E) induces Drosha instability and cytotoxicity in Neuro 2A cells. Biochem. Biophys. Res. Commun. *464*, 236–243. https://doi.org/10.1016/j.bbrc.2015.06.125.

99. Liachko, N.F., Guthrie, C.R., and Kraemer, B.C. (2010). Phosphorylation promotes neurotoxicity in a Caenorhabditis elegans model of TDP-43 proteinopathy. J. Neurosci. *30*, 16208–16219. https://doi.org/10.1523/JNEUROSCI.2911-10.2010.

100. Nonaka, T., Arai, T., Buratti, E., Baralle, F.E., Akiyama, H., and Hasegawa, M. (2009). Phosphorylated and ubiquitinated TDP-43 pathological inclusions in ALS and FTLD-U are recapitulated in SH-SY5Y cells. FEBS Lett. *583*, 394–400. https://doi.org/10.1016/j.febslet.2008.12.031.

101. Zhang, Y.J., Gendron, T.F., Xu, Y.F., Ko, L.W., Yen, S.H., and Petrucelli, L. (2010). Phosphorylation regulates proteasomal-mediated degradation and solubility of TAR DNA binding protein-43 C-terminal fragments. Mol. Neurodegener. *5*, 33. https://doi.org/10.1186/1750-1326-5-33.

102. Carlomagno, Y., Zhang, Y., Davis, M., Lin, W.L., Cook, C., Dunmore, J., Tay, W., Menkosky, K., Cao, X., Petrucelli, L., and Deture, M. (2014). Casein kinase II induced polymerization of soluble TDP-43 into filaments is inhibited by heat shock proteins. PLoS One *9*, e90452. https://doi.org/10.1371/journal.pone.0090452.

103. Choksi, D.K., Roy, B., Chatterjee, S., Yusuff, T., Bakhoum, M.F., Sengupta, U., Ambegaokar, S., Kayed, R., and Jackson, G.R. (2014). TDP-43 Phosphorylation by casein kinase Iepsilon promotes oligomerization and enhances toxicity in vivo. Hum. Mol. Genet. *23*, 1025–1035. https://doi.org/10.1093/hmg/ddt498.

104. Goh, C.W., Lee, I.C., Sundaram, J.R., George, S.E., Yusoff, P., Brush, M.H., Sze, N.S.K., and Shenolikar, S. (2018). Chronic oxidative stress promotes GADD34-mediated phosphorylation of the TAR DNA-binding

protein TDP-43, a modification linked to neurodegeneration. J. Biol. Chem. *293*, 163–176. https://doi.org/10.1074/jbc.M117.814111.

105. Kametani, F., Nonaka, T., Suzuki, T., Arai, T., Dohmae, N., Akiyama, H., and Hasegawa, M. (2009). Identification of casein kinase-1 phosphorylation sites on TDP-43. Biochem. Biophys. Res. Commun. *382*, 405–409. https://doi.org/10.1016/j.bbrc.2009.03.038.

106. Liachko, N.F., McMillan, P.J., Strovas, T.J., Loomis, E., Greenup, L., Murrell, J.R., Ghetti, B., Raskind, M.A., Montine, T.J., Bird, T.D., et al. (2014). The tau tubulin kinases TTBK1/2 promote accumulation of pathological TDP-43. PLoS Genet. *10*, e1004803. https://doi.org/10.1371/journal.pgen.1004803.

107. Liu, Y.J., Ju, T.C., Chen, H.M., Jang, Y.S., Lee, L.M., Lai, H.L., Tai, H.C., Fang, J.M., Lin, Y.L., Tu, P.H., and Chern, Y. (2015). Activation of AMP-activated protein kinase alpha1 mediates mislocalization of TDP-43 in amyotrophic lateral sclerosis. Hum. Mol. Genet. *24*, 787–801. https://doi.org/10.1093/hmg/ddu497.

108. Meyerowitz, J., Parker, S.J., Vella, L.J., Ng, D.C., Price, K.A., Liddell, J.R., Caragounis, A., Li, Q.X., Masters, C.L., Nonaka, T., et al. (2011). C-Jun N-terminal kinase controls TDP-43 accumulation in stress granules induced by oxidative stress. Mol. Neurodegener. *6*, 57. https://doi.org/10.1186/1750-1326-6-57.

109. Nonaka, T., Suzuki, G., Tanaka, Y., Kametani, F., Hirai, S., Okado, H., Miyashita, T., Saitoe, M., Akiyama, H., Masai, H., and Hasegawa, M. (2016). Phosphorylation of TAR DNA-binding Protein of 43 kDa (TDP-43) by Truncated Casein Kinase 1delta Triggers Mislocalization and Accumulation of TDP-43. J. Biol. Chem. *291*, 5473–5483. https://doi.org/10.1074/jbc.M115.695379.

110. Ko, V.I., Ong, K., Cleveland, D.W., Yu, H., and Ravits, J.M. (2024). CK1δ/ε kinases regulate TDP-43 phosphorylation and are therapeutic targets for ALS-related TDP-43 hyperphosphorylation. Neurobiol. Dis. *196*, 106516. https://doi.org/10.1016/j.nbd.2024.106516.

111. Tian, Y., Wang, Y., Jablonski, A.M., Hu, Y., Sugam, J.A., Koglin, M., Stachel, S.J., Zhou, H., Uslaner, J.M., and Parmentier-Batteur, S. (2021). Tau-tubulin kinase 1 phosphorylates TDP-43 at disease-relevant sites and exacerbates TDP-43 pathology. Neurobiol. Dis. *161*, 105548. https://doi.org/10.1016/j.nbd.2021.105548.

112. Ko, V.I., Ong, K., Kwon, D.Y., Li, X., Pietrasiewicz, A., Harvey, J.S., Lulla, M., Bhat, G., Cleveland, D.W., and Ravits, J.M. (2024). CK1δ/ε-mediated TDP-43 phosphorylation contributes to early motor neuron disease toxicity in amyotrophic lateral sclerosis. Acta Neuropathol. Commun. *12*, 187. https://doi.org/10.1186/s40478-024-01902-z.

113. Gruijs da Silva, L.A., Simonetti, F., Hutten, S., Riemenschneider, H., Sternburg, E.L., Pietrek, L.M., Gebel, J., Dötsch, V., Edbauer, D., Hummer, G., et al. (2022). Disease-linked TDP-43 hyperphosphorylation suppresses TDP-43 condensation and aggregation. EMBO J. *41*, e108443. https://doi.org/10.15252/embj.2021108443.

114. Cushman, M., Johnson, B.S., King, O.D., Gitler, A.D., and Shorter, J. (2010). Prion-like disorders: blurring the divide between transmissibility and infectivity. J. Cell Sci. *123*, 1191–1201. https://doi.org/10.1242/jcs.051672.

115. King, O.D., Gitler, A.D., and Shorter, J. (2012). The tip of the iceberg: RNA-binding proteins with prion-like domains in neurodegenerative disease. Brain Res. *1462*, 61–80. https://doi.org/10.1016/j.brainres.2012.01.016.

116. March, Z.M., King, O.D., and Shorter, J. (2016). Prion-like domains as epigenetic regulators, scaffolds for subcellular organization, and drivers of neurodegenerative disease. Brain Res. *1647*, 9–18. https://doi.org/10.1016/j.brainres.2016.02.037.

117. Conicella, A.E., Zerze, G.H., Mittal, J., and Fawzi, N.L. (2016). ALS Mutations Disrupt Phase Separation Mediated by alpha-Helical Structure in the TDP-43 Low-Complexity C-Terminal Domain. Structure *24*, 1537–1549. https://doi.org/10.1016/j.str.2016.07.007.

118. Stefanoska, K., Gajwani, M., Tan, A.R.P., Ahel, H.I., Asih, P.R., Volkerling, A., Poljak, A., and Ittner, A. (2022). Alzheimer's disease: Ablating single master site abolishes tau hyperphosphorylation. Sci. Adv. *8*, eabl8809. https://doi.org/10.1126/sciadv.abl8809.

119. Chang, Y.I., Hsu, S.C., Chau, G.Y., Huang, C.Y.F., Sung, J.S., Hua, W.K., and Lin, W.J. (2011). Identification of the methylation preference region in heterogeneous nuclear ribonucleoprotein K by protein arginine methyltransferase 1 and its implication in regulating nuclear/cytoplasmic distribution. Biochem. Biophys. Res. Commun. *404*, 865–869. https://doi.org/10.1016/j.bbrc.2010.12.076.

120. Huang, L., Wang, Z., Narayanan, N., and Yang, Y. (2018). Arginine methylation of the C-terminus RGG motif promotes TOP3B topoisomerase activity and stress granule localization. Nucleic Acids Res. *46*, 3061–3074. https://doi.org/10.1093/nar/gky103.

121. Wall, M.L., and Lewis, S.M. (2017). Methylarginines within the RGG-Motif Region of hnRNP A1 Affect Its IRES Trans-Acting Factor Activity and Are Required for hnRNP A1 Stress Granule Localization and Formation. J. Mol. Biol. *429*, 295–307. https://doi.org/10.1016/j.jmb.2016.12.011.

122. Ratovitski, T., Arbez, N., Stewart, J.C., Chighladze, E., and Ross, C.A. (2015). PRMT5- mediated symmetric arginine dimethylation is attenuated by mutant huntingtin and is impaired in Huntington's disease (HD). Cell Cycle *14*, 1716–1729. https://doi.org/10.1080/15384101.2015.1033595.

123. Simandi, Z., Pajer, K., Karolyi, K., Sieler, T., Jiang, L.L., Kolostyak, Z., Sari, Z., Fekecs, Z., Pap, A., Patsalos, A., et al. (2018). Arginine Methyltransferase PRMT8 Provides Cellular Stress Tolerance in Aging Motoneurons. J. Neurosci. *38*, 7683–7700. https://doi.org/10.1523/JNEUROSCI.3389-17.2018.

124. Ortega, J.A., Daley, E.L., Kour, S., Samani, M., Tellez, L., Smith, H.S., Hall, E.A., Esengul, Y.T., Tsai, Y.H., Gendron, T.F., et al. (2020). Nucleocytoplasmic Proteomic Analysis Uncovers eRF1 and Nonsense-Mediated Decay as Modifiers of ALS/FTD C9orf72 Toxicity. Neuron *106*, 90–107. https://doi.org/10.1016/j.neuron.2020.01.020.

125. Ikenaka, K., Atsuta, N., Maeda, Y., Hotta, Y., Nakamura, R., Kawai, K., Yokoi, D., Hirakawa, A., Taniguchi, A., Morita, M., et al. (2019). Increase of arginine dimethylation correlates with the progression and prognosis of ALS. Neurology *92*, e1868–e1877. https://doi.org/10.1212/WNL.0000000000007311.

126. Dormann, D., Madl, T., Valori, C.F., Bentmann, E., Tahirovic, S., Abou-Ajram, C., Kremmer, E., Ansorge, O., Mackenzie, I.R.A., Neumann, M., and Haass, C. (2012). Arginine methylation next to the PY-NLS modulates Transportin binding and nuclear import of FUS. EMBO J. *31*, 4258–4275. https://doi.org/10.1038/emboj.2012.261.

127. Hofweber, M., Hutten, S., Bourgeois, B., Spreitzer, E., Niedner-Boblenz, A., Schifferer, M., Ruepp, M.D., Simons, M., Niessing, D., Madl, T., and Dormann, D. (2018). Phase Separation of FUS Is Suppressed by Its Nuclear Import Receptor and Arginine Methylation. Cell *173*, 706–719. https://doi.org/10.1016/j.cell.2018.03.004.

128. Qamar, S., Wang, G., Randle, S.J., Ruggeri, F.S., Varela, J.A., Lin, J.Q., Phillips, E.C., Miyashita, A., Williams, D., Ströhl, F., et al. (2018). FUS Phase Separation Is Modulated by a Molecular Chaperone and Methylation of Arginine Cation-pi Interactions. Cell *173*, 720–734. https://doi.org/10.1016/j.cell.2018.03.056.

129. Suarez-Calvet, M., Neumann, M., Arzberger, T., Abou-Ajram, C., Funk, E., Hartmann, H., Edbauer, D., Kremmer, E., Gobl, C., Resch, M., et al. (2016). Monomethylated and unmethylated FUS exhibit increased binding to Transportin and distinguish FTLD-FUS from ALS-FUS. Acta Neuropathol. *131*, 587–604. https://doi.org/10.1007/s00401-016-1544-2.

130. Basso, M., and Pennuto, M. (2015). Serine phosphorylation and arginine methylation at the crossroads to neurodegeneration. Exp. Neurol. *271*, 77–83. https://doi.org/10.1016/j.expneurol.2015.05.003.

131. Suk, T.R., Part, C.E., Nguyen, T.T., Zhang, J.L., Heer, M.M., Caballero-Gómez, A., Grybas, V.S., McKeever, P.M., Nguyen, B., Callaghan, S.M., et al. (2024). A stress-dependent TDP-43 SUMOylation program preserves neuronal function. Preprint at bioRxiv. https://doi.org/10.1101/2024.04.12.589206.

132. Dong, D., Zhang, Z., Li, Y., Latallo, M.J., Wang, S., Nelson, B., Wu, R., Krishnan, G., Gao, F.B., Wu, B., and Sun, S. (2024). Poly-GR repeats associated with ALS/FTD gene C9ORF72 impair translation elongation and induce a ribotoxic stress response in neurons. Sci. Signal. *17*, eadl1030. https://doi.org/10.1126/scisignal.adl1030.

133. Lawson, S.K., Dobrikova, E.Y., Shveygert, M., and Gromeier, M. (2013). p38alpha mitogen-activated protein kinase depletion and repression of signal transduction to translation machinery by miR-124 and -128 in neurons. Mol. Cell Biol. *33*, 127–135. https://doi.org/10.1128/MCB.00695-12.

134. Schnoder, L., Gasparoni, G., Nordstrom, K., Schottek, A., Tomic, I., Christmann, A., Schafer, K.H., Menger, M.D., Walter, J., Fassbender, K., and Liu, Y. (2020). Neuronal deficiency of p38alpha-MAPK ameliorates symptoms and pathology of APP or Tau-transgenic Alzheimer's mouse models. Faseb. J. *34*, 9628–9649. https://doi.org/10.1096/fj.201902731RR.

135. Iba, M., Kim, C., Kwon, S., Szabo, M., Horan-Portelance, L., Peer, C.J., Figg, W.D., Reed, X., Ding, J., Lee, S.J., et al. (2023). Inhibition of p38alpha MAPK restores neuronal p38gamma MAPK and ameliorates synaptic degeneration in a mouse model of DLB/PD. Sci. Transl. Med. *15*, eabq6089. https://doi.org/10.1126/scitranslmed.abq6089.

136. Alam, J.J., and Nixon, R.A. (2023). Drug development targeting degeneration of the basal forebrain cholinergic system: its time has come. Mol. Neurodegener. *18*, 74. https://doi.org/10.1186/s13024-023-00663-y.

137. Alam, J.J. (2015). Selective Brain-Targeted Antagonism of p38 MAPKalpha Reduces Hippocampal IL-1beta Levels and Improves Morris Water Maze Performance in Aged Rats. J. Alzheimers Dis. *48*, 219–227. https://doi.org/10.3233/JAD-150277.

138. Alam, J.J., Maruff, P., Doctrow, S.R., Chu, H.M., Conway, J., Gomperts, S.N., and Teunissen, C. (2023). Association of Plasma Phosphorylated Tau With the Response to Neflamapimod Treatment in Patients With Dementia With Lewy Bodies. Neurology *101*, e1708–e1717. https://doi.org/10.1212/WNL.0000000000207755.

139. Prins, N.D., de Haan, W., Gardner, A., Blackburn, K., Chu, H.M., Galvin, J.E., and Alam, J.J. (2024). Phase 2A Learnings Incorporated into RewinD-LB, a Phase 2B Clinical Trial of Neflamapimod in Dementia with Lewy Bodies. J. Prev. Alzheimers Dis. *11*, 549–557. https://doi.org/10.14283/jpad.2024.36.

140. Taylor, J.P., Brown, R.H., Jr., and Cleveland, D.W. (2016). Decoding ALS: from genes to mechanism. Nature *539*, 197–206. https://doi.org/10.1038/nature20413.

141. Nelson, P.T., Dickson, D.W., Trojanowski, J.Q., Jack, C.R., Boyle, P.A., Arfanakis, K., Rademakers, R., Alafuzoff, I., Attems, J., Brayne, C., et al. (2019). Limbic-predominant age-related TDP-43 encephalopathy (LATE): consensus working group report. Brain *142*, 1503–1527. https://doi.org/10.1093/brain/awz099.

142. Ling, S.C., Polymenidou, M., and Cleveland, D.W. (2013). Converging mechanisms in ALS and FTD: disrupted RNA and protein homeostasis. Neuron *79*, 416–438. https://doi.org/10.1016/j.neuron.2013.07.033.

143. van Es, M.A., Hardiman, O., Chio, A., Al-Chalabi, A., Pasterkamp, R.J., Veldink, J.H., and van den Berg, L.H. (2017). Amyotrophic lateral sclerosis. Lancet *390*, 2084–2098. https://doi.org/10.1016/S0140-6736(17)31287-4.

144. Selkoe, D.J., and Hardy, J. (2016). The amyloid hypothesis of Alzheimer's disease at 25 years. EMBO Mol. Med. *8*, 595–608. https://doi.org/10.15252/emmm.201606210.

145. Karran, E., and De Strooper, B. (2022). The amyloid hypothesis in Alzheimer disease: new insights from new therapeutics. Nat. Rev. Drug Discov. *21*, 306–318. https://doi.org/10.1038/s41573-022-00391-w.

146. McKee, A.C., Gavett, B.E., Stern, R.A., Nowinski, C.J., Cantu, R.C., Kowall, N.W., Perl, D.P., Hedley-Whyte, E.T., Price, B., Sullivan, C., et al. (2010). TDP-43 proteinopathy and motor neuron disease in chronic traumatic encephalopathy. J. Neuropathol. Exp. Neurol. *69*, 918–929. https://doi.org/10.1097/NEN.0b013e3181ee7d85.

147. McKee, A.C., Stein, T.D., Kiernan, P.T., and Alvarez, V.E. (2015). The neuropathology of chronic traumatic encephalopathy. Brain Pathol. *25*, 350–364. https://doi.org/10.1111/bpa.12248.

148. Kim, H.J., Kim, N.C., Wang, Y.D., Scarborough, E.A., Moore, J., Diaz, Z., MacLea, K.S., Freibaum, B., Li, S., Molliex, A., et al. (2013). Mutations in prion-like domains in hnRNPA2B1 and hnRNPA1 cause multisystem proteinopathy and ALS. Nature *495*, 467–473. https://doi.org/10.1038/nature11922.

149. Allen, M.C., Karplus, P.A., Mehl, R.A., and Cooley, R.B. (2024). Genetic Encoding of Phosphorylated Amino Acids into Proteins. Chem. Rev. *124*, 6592–6642. https://doi.org/10.1021/acs.chemrev.4c00110.

150. Pearlman, S.M., Serber, Z., and Ferrell, J.E., Jr. (2011). A mechanism for the evolution of phosphorylation sites. Cell *147*, 934–946. https://doi.org/10.1016/j.cell.2011.08.052.

151. Kliche, J., Garvanska, D.H., Simonetti, L., Badgujar, D., Dobritzsch, D., Nilsson, J., Davey, N.E., and Ivarsson, Y. (2023). Large-scale phosphomimetic screening identifies phospho-modulated motif-based protein interactions. Mol. Syst. Biol. *19*, e11164. https://doi.org/10.15252/msb.202211164.

152. Hunter, T. (2012). Why nature chose phosphate to modify proteins. Philos. Trans. R. Soc. Lond. B Biol. Sci. *367*, 2513–2516. https://doi.org/10.1098/rstb.2012.0013.

153. Rogerson, D.T., Sachdeva, A., Wang, K., Haq, T., Kazlauskaite, A., Hancock, S.M., Huguenin-Dezot, N., Muqit, M.M.K., Fry, A.M., Bayliss, R., and Chin, J.W. (2015). Efficient genetic encoding of phosphoserine and its nonhydrolyzable analog. Nat. Chem. Biol. *11*, 496–503. https://doi.org/10.1038/nchembio.1823.

154. Gan, Q., and Fan, C. (2024). Orthogonal Translation for Site-Specific Installation of Post-translational Modifications. Chem. Rev. *124*, 2805–2838. https://doi.org/10.1021/acs.chemrev.3c00850.

155. Le, D.D., Cortesi, A.T., Myers, S.A., Burlingame, A.L., and Fujimori, D.G. (2013). Site-specific and regiospecific installation of methylarginine analogues into recombinant histones and insights into effector protein binding. J. Am. Chem. Soc. *135*, 2879–2882. https://doi.org/10.1021/ja3108214.

156. Wright, T.H., Bower, B.J., Chalker, J.M., Bernardes, G.J.L., Wiewiora, R., Ng, W.L., Raj, R., Faulkner, S., Vallée, M.R.J., Phanumartwiwath, A., et al. (2016). Posttranslational mutagenesis: A chemical strategy for exploring protein side-chain diversity. Science *354*, aag1465. https://doi.org/10.1126/science.aag1465.

157. Akahoshi, A., Suzue, Y., Kitamatsu, M., Sisido, M., and Ohtsuki, T. (2011). Site-specific incorporation of arginine analogs into proteins using arginyl-tRNA synthetase. Biochem. Biophys. Res. Commun. *414*, 625–630. https://doi.org/10.1016/j.bbrc.2011.09.137.

158. Cupo, R.R., and Shorter, J. (2020). Expression and Purification of Recombinant Skd3 (Human ClpB) Protein and Tobacco Etch Virus (TEV) Protease from Escherichia coli. Bio. Protoc. *10*, e3858. https://doi.org/10.21769/BioProtoc.3858.

159. Zhang, K., Daigle, J.G., Cunningham, K.M., Coyne, A.N., Ruan, K., Grima, J.C., Bowen, K.E., Wadhwa, H., Yang, P., Rigo, F., et al. (2018). Stress Granule Assembly Disrupts Nucleocytoplasmic Transport. Cell *173*, 958–971. https://doi.org/10.1016/j.cell.2018.03.025.

160. Schneider, C.A., Rasband, W.S., and Eliceiri, K.W. (2012). NIH Image to ImageJ: 25 years of image analysis. Nat. Methods *9*, 671–675. https://doi.org/10.1038/nmeth.2089.

161. Arrasate, M., and Finkbeiner, S. (2005). Automated microscope system for determining factors that predict neuronal fate. Proc. Natl. Acad. Sci. USA *102*, 3840–3845. https://doi.org/10.1073/pnas.0409777102.

162. Gatto, L., and Lilley, K.S. (2012). MSnbase-an R/Bioconductor package for isobaric tagged mass spectrometry data visualization, processing and quantitation. Bioinformatics *28*, 288–289. https://doi.org/10.1093/bioinformatics/btr645.

163. Gatto, L., Gibb, S., and Rainer, J. (2021). MSnbase, Efficient and Elegant R-Based Processing and Visualization of Raw Mass Spectrometry Data. J. Proteome Res. *20*, 1063–1069. https://doi.org/10.1021/acs.jproteome.0c00313.

164. Baxi, E.G., Thompson, T., Li, J., Kaye, J.A., Lim, R.G., Wu, J., Ramamoorthy, D., Lima, L., Vaibhav, V., Matlock, A., et al. (2022). Answer ALS, a large-scale resource for sporadic and familial ALS combining clinical and multi-omics data from induced pluripotent cell lines. Nat. Neurosci. *25*, 226–237. https://doi.org/10.1038/s41593-021-01006-0.

165. NeuroLINCS Consortium; Li, J., Lim, R.G., Kaye, J.A., Dardov, V., Coyne, A.N., Wu, J., Milani, P., Cheng, A., Thompson, T.G., et al. (2021). An integrated multi-omic analysis of iPSC-derived motor neurons from C9ORF72 ALS patients. iScience *24*, 103221. https://doi.org/10.1016/j.isci.2021.103221.

166. Ziller, M.J., Ortega, J.A., Quinlan, K.A., Santos, D.P., Gu, H., Martin, E.J., Galonska, C., Pop, R., Maidl, S., Di Pardo, A., et al. (2018). Dissecting the Functional Consequences of De Novo DNA Methylation Dynamics in Human Motor Neuron Differentiation and Physiology. Cell Stem Cell *22*, 559–574. https://doi.org/10.1016/j.stem.2018.02.012.

167. Winzen, R., Kracht, M., Ritter, B., Wilhelm, A., Chen, C.Y., Shyu, A.B., Müller, M., Gaestel, M., Resch, K., and Holtmann, H. (1999). The p38 MAP kinase pathway signals for cytokine-induced mRNA stabilization via MAP kinase-activated protein kinase 2 and an AU-rich region-targeted mechanism. EMBO J. *18*, 4969–4980. https://doi.org/10.1093/emboj/18.18.4969.

168. Goldstein, D.M., Soth, M., Gabriel, T., Dewdney, N., Kuglstatter, A., Arzeno, H., Chen, J., Bingenheimer, W., Dalrymple, S.A., Dunn, J., et al. (2011). Discovery of 6-(2,4-difluorophenoxy)-2-[3-hydroxy-1-(2-hydroxyethyl)propylamino]-8-methyl-8H-pyrido[2,3-d]pyrimidin-7-one (pamapimod) and 6-(2,4-difluorophenoxy)-8-methyl-2-(tetrahydro-2H-pyran-4-ylamino)pyrido[2,3-d]pyrimidin-7(8H)-one (R1487) as orally bioavailable and highly selective inhibitors of p38alpha mitogen-activated protein kinase. J. Med. Chem. *54*, 2255–2265. https://doi.org/10.1021/jm101423y.

169. Linsley, J.W., Shah, K., Castello, N., Chan, M., Haddad, D., Doric, Z., Wang, S., Leks, W., Mancini, J., Oza, V., et al. (2021). Genetically encoded cell-death indicators (GEDI) to detect an early irreversible commitment to neurodegeneration. Nat. Commun. *12*, 5284. https://doi.org/10.1038/s41467-021-25549-9.

170. Baxi, E.G., Thompson, T., Li, J., Kaye, J.A., Lim, R.G., Wu, J., Ramamoorthy, D., Lima, L., Vaibhav, V., Matlock, A., et al. (2022). Answer ALS, a large-scale resource for sporadic and familial ALS combining clinical and multi-omics data from induced pluripotent cell lines. Nat. Neurosci. *25*, 226–237. https://doi.org/10.1038/s41593-021-01006-0.

171. Nelder, J.A., and Wedderburn, R.W.M. (1972). Generalized linear models. Soc. Anim. *135*, 370–384. https://doi.org/10.2307/2344614.

172. R Core Team (2012). R: A language and environment for statistical computing.

173. Shevchenko, A., Wilm, M., Vorm, O., and Mann, M. (1996). Mass spectrometric sequencing of proteins silver-stained polyacrylamide gels. Anal. Chem. *68*, 850–858. https://doi.org/10.1021/ac950914h.

174. Peng, J., and Gygi, S.P. (2001). Proteomics: the move to mixtures. J. Mass Spectrom. *36*, 1083–1091. https://doi.org/10.1002/jms.229.

175. Eng, J.K., McCormack, A.L., and Yates, J.R. (1994). An approach to correlate tandem mass spectral data of peptides with amino acid sequences in a protein database. J. Am. Soc. Mass Spectrom. *5*, 976–989. https://doi.org/10.1016/1044-0305(94)80016-2.

176. Beausoleil, S.A., Villén, J., Gerber, S.A., Rush, J., and Gygi, S.P. (2006). A probability-based approach for high-throughput protein phosphorylation analysis and site localization. Nat. Biotechnol. *24*, 1285–1292. https://doi.org/10.1038/nbt1240.

177. Choi, C., Smalley, J.L., Lemons, A.H.S., Ren, Q., Bope, C.E., Dengler, J.S., Davies, P.A., and Moss, S.J. (2022). Analyzing the mechanisms that facilitate the subtype-specific assembly of gamma-aminobutyric acid type A receptors. Front. Mol. Neurosci. *15*, 1017404. https://doi.org/10.3389/fnmol.2022.1017404.

178. Smalley, J.L., Kontou, G., Choi, C., Ren, Q., Albrecht, D., Abiraman, K., Santos, M.A.R., Bope, C.E., Deeb, T.Z., Davies, P.A., et al. (2020). Isolation and Characterization of Multi-Protein Complexes Enriched in the K-Cl Co-transporter 2 From Brain Plasma Membranes. Front. Mol. Neurosci. *13*, 563091. https://doi.org/10.3389/fnmol.2020.563091.

179. Kim, S., and Pevzner, P.A. (2014). MS-GF+ makes progress towards a universal database search tool for proteomics. Nat. Commun. *5*, 5277. https://doi.org/10.1038/ncomms6277.

180. Wang, A., Conicella, A.E., Schmidt, H.B., Martin, E.W., Rhoads, S.N., Reeb, A.N., Nourse, A., Ramirez Montero, D., Ryan, V.H., Rohatgi, R., et al. (2018). A single N-terminal phosphomimic disrupts TDP-43 polymerization, phase separation, and RNA splicing. EMBO J. *37*, e97452. https://doi.org/10.15252/embj.201797452.

STAR★METHODS

KEY RESOURCES TABLE

REAGENT or RESOURCE	SOURCE	IDENTIFIER
Antibodies		
TDP-43 Polyclonal antibody	Proteintech	Cat # 10782-2-AP RRID: AB_615042
DYKDDDDK Tag Antibody, mAb, Mouse	GenScript	Cat # A00187 RRID: AB_1720813
Anti TAR DNA-Binding Protein 43 (TDP-43), phospho-Ser409/410 mAb (Clone 11-9)	Cosmo Bio LTD	Cat # CAC-TIP-PTD-M01 RRID: AB_1961900
p38 MAPK Antibody	Cell Signaling Technology	Cat # 9212 RRID: AB_330713
COX IV (3E11) Rabbit mAb	Cell Signaling Technology	Cat # 4850 RRID: AB_2085424
Histone H3 (96C10) Mouse mAb	Cell Signaling Technology	Cat # 3638 RRID: AB_1642229
Mono-Methyl Arginine (R*GG) (D5A12) Rabbit mAb	Cell Signaling Technology	Cat # 8711 RRID: AB_10896849
Asymmetric Di-Methyl Arginine Motif [adme-R] MultiMab™ Rabbit mAb mix	Cell Signaling Technology	Cat # 13522 RRID: AB_2665370
Symmetric Di-Methyl Arginine Motif [sdme-RG] MultiMab™ Rabbit mAb mix	Cell Signaling Technology	Cat # 13222 RRID: AB_2714013
PRMT1 (A33) Antibody	Cell Signaling Technology	Cat # 2449 RRID: AB_2237696
GAPDH Monoclonal antibody	Proteintech	Cat # 60004-1-Ig RRID: AB_2107436
Donkey anti-Mouse IgG (H + L) Highly Cross-Adsorbed Secondary Antibody, Alexa Fluor Plus 647	ThermoFisher Scientific	Cat # A32787 RRID: AB_2762830
Donkey anti-Rabbit IgG (H + L) Highly Cross-Adsorbed Secondary Antibody, Alexa Fluor Plus 488	ThermoFisher Scientific	Cat # A32790 RRID: AB_2762833
Goat Anti-Mouse IgG (H + L)-HRP	Jackson ImmunoResearch Laboratories	Cat # 115-035-003 RRID: AB_1001528
Goat Anti-Rabbit IgG (H + L)-HRP	Jackson ImmunoResearch Laboratories Cat # 115-035-003	Cat # 111-035-003 RRID: AB_2313567
DYKDDDDK Tag Antibody, mAb, Mouse	Sigma	F1804 RRID: AB_262044
Goat Anti-MAP2	Phosphosolutions	Cat # 1099;RRID:AB_2752241
Rabbit Anti-TDP-43 N-terminal	Proteintech	Cat # 10782-2-AP;RRID:AB_615042
Alexa Fluor® 647 AffiniPure™ Donkey Anti-Goat IgG	Jackson ImmunoResearch	Cat # 705-605-003;RRID:AB_2340436
Alexa Fluor® 488 AffiniPure™ Donkey Anti-Rabbit IgG	Jackson ImmunoResearch	Cat # 711-545-152;RRID:AB_2313584
Anti-rabbit IgG, HRP-linked Antibody	Cell Signaling Technology	Cat # 7074S;RRID:AB_2099233
Bacterial and virus strains		
Escherichia coli DH5α competent cells	ThermoFisher	Cat # 18265017
Escherichia coli BL21-CodonPlus (DE3) -RIL competent cells	Agilent	Cat # 230245
Chemicals, peptides, and recombinant proteins		
Compound 1	This paper	N/A

(*Continued on next page*)

Continued

REAGENT or RESOURCE	SOURCE	IDENTIFIER
VX-745	Tocris	Cat # 3915
VX-745	Selleck Chem	Cat #S1458
Minimum essential medium (MEM)	ThermoFisher Scientific	Cat # 11095080
Penicillin-streptomycin	ThermoFisher Scientific	Cat # 15140122
Poly-L-Lysine	Millipore Sigma	Cat #P2658
Dimethyl sulfoxide	ThermoFisher Scientific	Cat #J66650.AK
Adenosine-2′,3′-dialdehyde	Millipore Sigma	Cat # A7154
Opti-MEM I Reduced Serum Medium	ThermoFisher Scientific	Cat # 31985070
RIPA Buffer	Boston BioProducts	Cat # BP-115
cOmplete™, EDTA-free Protease Inhibitor Cocktail	Millipore Sigma	Cat # 11873580001
PhosSTOP	Millipore Sigma	Cat # 4906845001
4-12% NuPAGE Bis-Tris gels	ThermoFisher Scientific	Cat # NP0322BOX
Immobilon-P-PVDF membrane	Millipore Sigma	Cat # IPVH00005
NuPAGE LDS Sample Buffer (4X)	ThermoFisher Scientific	Cat # NP0007
NuPAGE Sample Reducing Agent (10X)	ThermoFisher Scientific	Cat # NP0009
NuPAGE MOPS SDS Running Buffer (20X)	ThermoFisher Scientific	Cat # NP000102
SuperSignal West Dura Extended Duration Substrate	ThermoFisher Scientific	Cat # 34075
Restore Western Blot Stripping Buffer	ThermoFisher Scientific	Cat # 21059
Dulbecco's Modified Eagle Medium (DMEM)	ThermoFisher Scientific	Cat # 10566016
Lipofectamine 3000 Transfection Reagent	ThermoFisher Scientific	Cat #L3000008
Lipofectamine RNAiMAX-reagent	ThermoFisher Scientific	Cat # 13778030
FuGENE HD Transfection Reagent	Promega	Cat #E2311
Subcellular Protein Fractionation Kit for Cultured Cells	ThermoFisher Scientific	Cat # 78840
Paraformaldehyde	Fisher Scientific	Cat # AA47377-9M
Triton X-100	ThermoFisher Scientific	Cat # A16046.AE
Normal Goat Serum	Abcam	Cat # Ab7481
Prolong Gold Antifade Mountant with DAPI	ThermoFisher Scientific	Cat #P36931
Kinase Buffer (10X)	Cell Signaling Technology	Cat # 9802
Adenosine-5′-triphosphate (ATP)	Cell Signaling Technology	Cat # 9804
Recombinant human TDP-43	Proteintech	Cat # Ag13119
Recombinant human p38 alpha, Active	SignalChem Biotech	Cat #M39-10BG
MG-132	Millipore Sigma	Cat #M7449
SimplyBlue SafeStain	ThermoFisher Scientific	Cat # LC6060
Nondenaturing cell Lysis Buffer (10X)	Cell Signaling Technology	Cat # 9803
Anti-FLAG M2 Magnetic Beads	Millipore Sigma	Cat #M8823
Dynabeads Protein A	ThermoFisher Scientific	Cat # 10001D
Ni-NTA agarose	Qiagen	Cat # 30210
Amylose Resin	New England BioLabs	Cat #E8021S
TEV protease	Cupo & Shorter[158]	
Dextran from Leuconostoc spp	Millipore Sigma	Cat # 31392
GeneXPlus Transfection Reagent	ATCC	ACS-4004
Formaldehyde solution (37%)	Sigma	252549
TDP-43^{WT}-MBP	Hallegger et al.[94]	N/A
TDP-43^{S292E}-MBP	This paper	N/A
TDP-43$^{S409:S410E}$-MBP	This paper	N/A
TDP-43$^{S292:S409:S410E}$-MBP	This paper	N/A
TDP-43^{R293F}-MBP	This paper	N/A

(*Continued on next page*)

Continued

REAGENT or RESOURCE	SOURCE	IDENTIFIER
Recombinant human PRMT1 protein	Abcam	ab89007
S-(5′-Adenosyl)-L-methionine chloride dihydrochloride	Sigma	A7007
mTESR media	StemCell Technologies	Cat # 05825
ROCK inhibitor	Selleck Chemicals	Cat #S1049
Growth factor-reduced matrigel	Corning	Cat # 356231
Versene	Gibco	Cat # 5040066
DBPS	Thermo Fisher	Cat # 21-031-CV
Accutase	Thermo Fisher	Cat # NC9839010
Poly-L-ornithine solution	Sigma	Cat # RNBK5888
Mouse laminin	Sigma	Cat #L2020
FGF	R@D	Cat # 233-FB
Stem-Cell Banker GMP Grade	CedarLane Labs	Cat # 11890
Fibronectin	Corning	Cat # CB40008A
Neurobasal media	Gibco	Cat # 12348017
NEAA	Gibco	Cat # 11-140-050
Glutamax	Gibco	Cat # 35050061
N2	Gibco	Cat # 17502048
B27	Gibco	Cat # 17504044
SB431542	StemCell Technologies	Cat # 72234
LDN193189	Sigma-Aldrich	Cat # SML0559
Retinoic Acid	Sigma-Aldrich	Cat #R2625
Smoothened-Agonist (SAG)	Cayman Chemical	Cat # 11914
DAPT	Cayman Chemical	Cat # 13197
BDNF	PeproTech	Cat # 450-02
GDNF	PeproTech	Cat # 450-10
CNTF	PeproTech	Cat # 450-13
Ascorbic acid	Sigma-Aldrich	Cat # A4403
DMSO	Sigma-Aldrich	Cat #D4540
OptiMEM	Gibco	Cat # 31985070
PBS	Gibco	Cat # 10010023
Paraformaldehyde	Electron Microscopy Sciences	Cat # 15714-S
Donkey Serum	Jackson ImmunoResearch	Cat # 017-000-121
Prolong Glass mounting media	Invitrogen	Cat #P36981
Trypan Blue Solution, 0.4%	Gibco	Cat # 15250061
cOmplete™, Mini, EDTA-free Protease Inhibitor Cocktail	Millipore Sigma	Cat # 4693159001
NuPAGE MES SDS Running Buffer (20X)	ThermoFisher Scientific	Cat # NP0002
NuPAGE Bis-Tris Mini Protein Gels, 4–12%, 1.5 mm	ThermoFisher Scientific	Cat # NP0335BOX
Pierce™ Reversible Protein Stain Kit for Nitrocellulose Membranes	Thermo Scientific	Cat # PI24580
Trans-Blot Turbo Mini 0.2 μm Nitrocellulose Transfer Packs	Bio-Rad	Cat # 1704158
SuperSignal™ West Pico PLUS Chemiluminescent Substrate	Thermo Scientific	Cat # PI34577
Critical commercial assays		
Pierce BCA Protein Assay Kit	ThermoFisher Scientific	Cat # 23225
Z'-Lyte kinase assay for p38α	ThermoFisher Scientific	Cat # PV3177
Pierce LDH Cytotoxicity Assay Kit	ThermoFisher Scientific	Cat # 88953

(*Continued on next page*)

Continued

REAGENT or RESOURCE	SOURCE	IDENTIFIER
QuikChange Site-Directed Mutagenesis Kit	Agilent	Cat # 200519
CellTiter-Glo kit	Promega	Cat #G9241
CyQUANT™ LDH Cytotoxicity Assay	ThermoFisher Scientific	Cat #C20300
Experimental models: Cell lines		
Human neuroblastoma cell line SH-SY5Y	ATCC	Cat # CRL-2266
Mouse Motor Neuron-Like Hybrid Cell Line (NSC-34)	TebuBio	Cat # CLU140-A
Mouse primary cortical neurons	This paper	N/A
Human male XCL-1 iPSCs	XCell Science	XCL-1 iPSC
NINDS human female iPSC line NH50305	NINDS	NH50305
NINDS human female iPSC line NH50306	NINDS	NH50306
Human female iPSC line CS06iCTR-n2	Cedars-Sinai iPSC Core	CS06iCTR-n2
Human male iPSC line CS15iCTR-5	Cedars-Sinai iPSC Core	CS15iCTR-5
Human male iPSC line CS52iALS-n6A	Cedars-Sinai iPSC Core	CS52iALS-n6A
Human female iPSC line JH034	Zhang et al.[159]	
Oligonucleotides		
siRNA targeting sequence: p38α	ThermoFisher Scientific	Cat #s3585
siRNA targeting sequence: p38α	ThermoFisher Scientific	Cat #s3586
siRNA targeting sequence: PRMT1	ThermoFisher Scientific	Cat #s6917
siRNA targeting sequence: PRMT1	ThermoFisher Scientific	Cat #s6919
siRNA targeting sequence: negative control	ThermoFisher Scientific	Cat # 4390846
siRNA targeting sequence: negative control	ThermoFisher Scientific	Cat # 4390843
Sequencing primer: T7 promoter Forward: TAATACGACTCACTATAGGG	Tufts university sequencing core	N/A
Sequencing primer: M13 Reverse: CAGGAAACAGCTATGAC	Tufts university sequencing core	N/A
Sequencing primer: TDP-43 1: TAATACGACTCACTATAGGGGAATTG	Eurofins Genomics	N/A
Sequencing primer: TDP-43 2: CGGTGAGGTGCTGATGGTCC	Eurofins Genomics	N/A
Sequencing primer: TDP-43 3: GGCTTTGGCAATTCGCGTGG	Eurofins Genomics	N/A
Recombinant DNA		
Myc- TDP-43^{M337V}	Wobst et al.[53]	N/A
Myc- TDP-43^{WT}	Wobst et al.[53]	N/A
TDP-43^{WT}-FLAG	GenScript	Clone ID: OHu19093
TDP-43$^{S409:S410A}$-FLAG	This paper	N/A
TDP-43$^{S409:S410E}$-FLAG	This paper	N/A
TDP-43^{S292A}-FLAG	This paper	N/A
TDP-43^{S292E}-FLAG	This paper	N/A
TDP-43^{S292N}-FLAG	This paper	N/A
TDP-43$^{S409:S410A:S292A}$-FLAG	This paper	N/A
TDP-43^{R293K}-FLAG	This paper	N/A
TDP-43^{G308R}-FLAG	This paper	N/A
TDP-43^{WT}-MBP	Addgene	Plasmid # 104480
TDP-43^{S292E}-MBP	This paper	N/A
TDP-43$^{S409:S410E}$-MBP	This paper	N/A
TDP-43$^{S292:S409:S410E}$-MBP	This paper	N/A
TDP-43^{R293F}-MBP	This paper	N/A

(*Continued on next page*)

Continued

REAGENT or RESOURCE	SOURCE	IDENTIFIER
p38α^{WT}-FLAG	GenScript	Clone ID: OHu17618
p38α$^{T180A:Y182F}$-FLAG	This paper	N/A
p38α$^{D176A:F327S}$-FLAG	This paper	N/A
PRMT1-Myc_DDK	Origene	Cat #: RC224239
TDP-43M337V-EGFP	This Paper	N/A
mApple	This Paper	N/A
TDP-43^{WT}-FLAG	GenScript	U7060HA050-3/X94677
TDP-43^{S292E}-FLAG	GenScript	U7060HA050-5/J80883
TDP-43^{R293F}-FLAG	GenScript	U7060HA050-4/X89530
Software and algorithms		
GraphPad Prism 7 and 8	GraphPad Software, Inc.	https://www.graphpad.com/
ImageJ	Schneider et al.[160]	https://imagej.nih.gov/ij/
NIS-Elements	Nikon	https://www.microscope.healthcare.nikon.com/products/software/nis-elements
Adobe Illustrator	Adobe	https://www.adobe.com/products/illustrator.html
Robotic imaging system	Arrasate & Finkbeiner[161] Barmada et al.[61]	N/A
MSnbase package in R	Gatto & Lilly[162] Gatto et al.[163]	https://lgatto.github.io/MSnbase/
Proteome Discoverer 3.0	ThermoFisher Scientific	N/A
Other		
Custom-written code in MATLAB to analyze DIC images of TDP-43 droplets	Zenodo	https://doi.org/10.5281/zenodo.13963929

EXPERIMENTAL MODEL AND STUDY PARTICIPANT DETAILS

E. coli cultures

E. coli BL21-CodonPlus (DE3)-RIL competent cells were transformed with antibiotic resistant plasmids and cultured in Lysogeny broth. Cultures (5mL) from individual colonies were grown overnight for use in protein purification (see below) or for generating frozen stocks by combining 1:1 with 50% (v/v) glycerol and storage at −80°C.

Human neuroblastoma cell line SH-SY5Y cultures

Female human SH-SY5Y neuroblastoma cells (ATCC) cells were cultured in minimum essential medium (MEM; Thermo Fisher Scientific) supplemented with L-glutamine, 10% fetal bovine serum and 1% penicillin/streptomycin in a humidified incubator at 37°C and 5% CO_2.

Mouse motor neuron-like hybrid cell line (NSC-34) cultures

Male mouse motor neuron-like hybrid NSC-34 cells (TebuBio) were cultured in Dulbecco's modified Eagle's medium (DMEM, Thermo Fisher Scientific), supplemented with 10% fetal bovine serum and 1% penicillin/streptomycin in a humidified incubator at 37°C and 5% CO_2.

Mouse primary cortical neuron cultures

All mouse work complied with UCSF Institutional Animal Care and Use Committee regulations. Mice (C57BL/6) were housed in approved facilities with humidity regulated between 30 and 70%, temperature between 68 and 79°F, and 12 h light/dark cycles. Primary mouse cortical neurons were harvested from E17 mouse embryos, cultured in Neurobasal medium with B27 and GlutaMAX in a humidified incubator at 37°C and 5% CO_2, and grown for 2 days in 384-well plates prior to transfection.

XCL-1 iPSC cultures

Human male XCL-1 iPSCs were differentiated into motor neurons using a directed differentiation protocol comprising 3 stages.[164] Briefly, in stage 1, iPSCs were plated in Matrigel-coated 6-well plates at a density of 5E + 05 cells/well in mTeSR1 media

supplemented with 10μM ROCK inhibitor (Y-27632) for 24 h, after which medium was switched to ST1 media (47.5% IMDM media, 47.5% Ham's F-12 Nutrient Mix, 1% MEM Non-Essential Amino Acids Solution, 2% B27 supplement, 1% N2 supplement, 1% Penicillin-Streptomycin, 0.2μM LDN193189, 3μM CHIR99021, and 10 μM SB431542). ST1 media was exchanged daily until Day 6.

In Stage 2, precursors were replated in fresh Matrigel-coated 6-well plates at a density of 7.5E + 05 cells per well in ST2 media (47.5% IMDM media, 47.5% Ham's F-12 Nutrient Mix, 1% MEM Non-Essential Amino Acids Solution, 2% B27 supplement, 1% N2 supplement, 1% Penicillin-Streptomycin, 0.1 μM all-trans retinoic acid, 1μM smoothened agonist (SAG), 0.2μM LDN193189, 3μM CHIR99021, and 10μM SB431542) supplemented with 10uM ROCK inhibitor for 24 h, after which ST2 media was full exchanged. ST2 media was exchanged every other day until Day 13.

Finally, in Stage 3 the precursors were replated in fresh Matrigel-coated 6-well plates at a density of 7.5E + 05 cells per well in ST3 media (47.5% IMDM media, 47.5% Ham's F-12 Nutrient Mix, 1% MEM Non-Essential Amino Acids Solution, 2% B27 supplement, 1% N2 supplement, 1% Penicillin-Streptomycin, 0.5μM all-trans retinoic acid, 0.1μM SAG, 0.1μM Dibutyryl-cAMP, 0.1μM compound E, 2.5μM DAPT, 200 ng/ml L-ascorbic acid, 10 ng/ml BDNF, and 10 ng/ml GDNF) supplemented with 10μM ROCK inhibitor for 24h, after which media was fully replaced with ST3 media with 0.5% Matrigel. Fresh ST3 media with 0.5% Matrigel was half exchanged every other day until day 20. On Day 20, ST3 media was replaced with ST3 media supplemented with 2 μM Cytosine β-D-arabinofuranoside (AraC). On day 24 AraC-containing media was replaced with SST3 media with 0.5% Matrigel, after which new media was half exchanged every other day until day 34.

NINDS iPSC lines culture

NINDS iPSC lines NH50305 (female) and NH50306 (female), referred to from here on as gene corrected (GC) control and TDP43^{A382T} lines, respectively, were thawed into mTESR media (StemCell Technologies) with ROCK inhibitor (Selleck Chemicals). iPSCs were cultured in a humidified incubator at 37°C and 5% CO_2 in mTESR and grown on growth factor-reduced matrigel (GFR, Corning). iPSCs were passaged ~1:5 using Versene (Gibco). To start the motor neuron differentiation, iPSCs were grown to ~80% confluency, washed once with DBPS 1X (Thermo Fisher) and disassociated with accutase (Thermo fisher) for ~10 min iPSCs were washed in mTESR and plated at 4 million cells per T25 flask (Omnilab) in mTESRPlus with ROCKi.

When the iPSCs reached ~90% confluency, (usually within 1–2 days after plating), they were differentiated in to motor neurons to methods based as described[164,165] but with various modifications. iPSCs were cultured in Stage 1 media[164,165] and fed daily until day 6. On day 5, T-25 flasks were coated with 2.5mL of a 1:4 dilution of 100μg/ml poly-L-ornithine solution (Sigma) to 25μg/ml using sterile cell culture water and left at room temperature overnight. The next day, the flasks were rinsed with cell culture water and 3mL of a 1:50 dilution of 1 mg/ml mouse laminin (Sigma) was added. The flasks were then stored in the incubator at 37°C for at least 30 min. Day 6 corresponds to the switch from Stage 1 to Stage 2 media, when the iPSCs are being patterned to motor neuron neural progenitors (MNPCs). The cells were passaged using a cell scraping tool (Corning) to lift the cells off the flask bottom and split 1:2 into a laminin-coated flask. Day 7, the media was switched to only Stage 2, and changed every other day until Day 13, at which point the MNPCs were cryopreserved. To freeze, the MNPCs were washed with DBPS and disassociated with accutase for 20 min at room temperature before washing with Stage 2 media with ROCKi. The MNPCs were frozen at 9 million cells per cryovial in freezing media, which consists of 4μg of FGF (R&D) for every 1mL of Stem-Cell Banker GMP Grade (CedarLane Labs).

Human iPSC line CS06iCTR-n2, CS15iCTR-5, CS52iALS-n6A, and JH034 cultures

Maintenance and differentiation of human iPSC line CS06iCTR-n2 (female, control line), CS15iCTR-5 (male, control line), CS52iALS-n6A (male, bearing a G_4C_2-repeat expansion [~6-8kb] in the C9ORF72 gene), and JH034 (female, bearing a G_4C_2-repeat expansion [>2.5kb] in the C9ORF72 gene[159]) in iMNs was performed as described previously.[124,166]

METHOD DETAILS

Plasmids

cDNA sequences were based on the accession number NM_007375.3 for human TARDBP, NM_001315 for human p38α (MAPK14) and NM_001536 for human PRMT1. The generation of plasmids harboring N-terminally myc-tagged wild-type or M337V-mutant TDP-43 sequences were as described.[53] Plasmids harboring C-terminally FLAG-tagged wild-type or mutant human TDP-43 and p38α sequences in pcDNA3.1+/C-(K)-DYK mammalian expression vector were purchased from Genscript and PRMT1 plasmid was purchased from Origene. TDP-43 bacterial expression vector harboring a C-terminal MBP tag (pJ4M TDP-43-TEV-MBP-6xHis) was purchased from Addgene (Plasmid # 104480). TDP-43 mutations were generated by site-directed mutagenesis using QuickChange (Agilent) and confirmed by DNA sequencing. The presence of the S409:S410E, S409:S410A, S292E, S292N, S292A, S292:S409:S410A, S292:S409:S410E, and R293F mutations in TDP-43, as well as dominant negative (DN) T180A/Y182F[167] and constitutively active (CA) D176A/F327S mutations[72] in p38α were confirmed by DNA sequencing performed by Tufts University Core Facilities (forward sequencing primer 5′-TAA-TAC-GAC-TCA-CTA-TAG-GG-3′, reverse sequencing primer 5′-CAG-GAA-ACA-GCT-ATG-AC-3′) and Eurofins Genomics (TDP-43 sequencing primer 1 5′-TAA-TAC-GAC-TCA-CTA-TAG-GGG-AAT-TG-3′, sequencing primer 2 5′-CGG-TGA-GGT-GCT-GAT-GGT-CC-3′, sequencing primer 3 5′-GGC-TTT-GGC-AAT-TCG-CGT-GG-3′).

Synthesis of 6-(2,4-difluorophenoxy)-8-ethyl-2-(2-isopropoxyethylamino)pyrido[2,3-*d*ay]pyrimidin-7-one (compound 1)

To a stirred solution of 2-isopropoxyethan-1-amine (406mg, 3.93mmol) was added to 6-(2,4-difluorophenoxy)-8-ethyl-2-(methylsulfonyl)pyrido[2,3-*d*ay]pyrimidin-7(8H)-one (30 mg, 0.79mmol) in DMF (3 mL). The resulting solution was stirred at 80°C for 1 h in a microwave reactor. The crude product was purified by preparative HPLC (Column: Xselect CSH OBD Column 30*150mm 5μm n; Mobile Phase A:Water (0.1% FA), Mobile Phase B: ACN; Flow rate: 60 mL/min; Gradient: 40% B to 72% B in 8 min; 254/220 nm; Rt: 7.57 min). Fractions containing the desired compound were evaporated to dryness to afford 6-(2,4-difluorophenoxy)-8-ethyl-2-((2-isopropoxyethyl)amino)pyrido[2,3-*d*ay]pyrimidin-7(8H)-one (190mg, 59.7%) as a white solid. ^{1}H NMR (400 MHz, DMSO-d_6) δ 8.56 (s, 1H), 7.76 (m, 1H), 7.52–7.41 (m, 2H), 7.26–7.18 (m, 1H), 7.06–7.02 (m, 1H), 4.42–4.32 (m, 2H), 3.65–3.45 (m,5H), 1.28–1.22 (m, 3H), 1.09–1.02 (m, 6H). m/z (ES+), [M + H]+ = 405; TFA, HPLC tR = 1.822 min. The intermediate 6-(2,4-difluorophenoxy)-8-ethyl-2-(methylsulfonyl) pyrido[2,3-*d*ay]pyrimidin-7(8H)-one was prepared as described.[168] Compound 1 (Figure 1E) was tested in a Z′-Lyte kinase assay for p38α (Thermofisher) and inhibited p38α activity with an IC_{50} of 25nM.

SH-SY5Y transfections and inhibition of p38α MAPK and methyltransferase activity

For immunocytochemical analysis, cells were grown on glass coverslips coated with 1 mg/mL poly-*L*-lysine (Sigma) in 24-well plates (Cellstar). Cells were transiently transfected using Fugene HD (Promega) following the manufacturer's instructions 24 h after seeding (Fugene HD:DNA ratio 3:1). Total transfection times were 8 h–48 h. For pharmacological inhibition of p38α MAPK, compound 1 (synthesized by AstraZeneca) or equal volume of DMSO vehicle, was added to cells for 24 or 48 h at a final concentration of 0.1μM, 1μM or 10μM. For pharmacological inhibition of arginine methyltransferase activity, adenosine-2′,3′-dialdehyde (AdOx) (Sigma) or equal volume of DMSO vehicle was added to cells for 24 h at a final concentration of 20μM. To determine the localization of TDP-43^{WT}, TDP-43^{S292E}, and TDP43^{R293F}, cells were cultured as described above and grown on uncoated glass coverslips in 6-well plates. Cells were transiently transfected using GeneX*Plus* transfection reagent (ATCC) folllowing manufacturer's protocol. Cells were harvested for immunofluorescence and western blot analysis 48 h post-transfection.

Antibodies

The following antibodies were used for immunocytochemical staining: rabbit N-terminal TDP-43 (1:500; 10782-2-AP, Proteintech), mouse anti DYKDDDDK-tag (1:500; A00187, GenScript), and mouse monoclonal anti-FLAG antibody (1:500, F1804, Sigma). Anti-rabbit and anti-mouse secondary antibodies coupled to Alexa 488, and Alexa 647 were used for detection (1:1,000 or 1:400; Thermo Fisher Scientific). For Western blot analysis, the following antibodies were used: rabbit N-terminal TDP-43 (1:7,000; 10782-2-AP, Proteintech), mouse S409/S410 phospho-TDP-43 (1:3,000; CAC-TIP-PTD-M01, Cosmo), rabbit p38 MAPK (1:1,500; 9212S, Cell Signaling Technology), rabbit COX IV (3E11) (1:1,500; 4850, Cell Signaling Technology), mouse Histone H3 (96C10) (1:1,500; 3638, Cell Signaling Technology), rabbit Mono-Methyl Arginine (R*GG) (D5A12) (1:1,500; 8711S, Cell Signaling Technology), rabbit Asymmetric Di-Methyl Arginine Motif [adme-R] MultiMab (1:1,500; 13522S, Cell Signaling Technology), rabbit Symmetric Di-Methyl Arginine Motif [sdme-RG] MultiMab (1:1,500; 13222S, Cell Signaling Technology), rabbit PRMT1 (A33) (1:1,500; 2449, Cell Signaling Technology), mouse GAPDH (1:5000 or 1:10,000; 60004-1-Ig, Proteintech), and mouse monoclonal anti-FLAG (1:1000, F1804, Sigma). Anti-mouse and anti-rabbit horseradish peroxidase-coupled secondary antibodies were purchased from Jackson Immunoresearch (1:10,000) or Cell Signaling Technology. IRDye 800CW Goat anti-Mouse IgG secondary antibody was purchased from LI-COR (1:5000).

siRNA knockdown of p38α and PRMT1

Small interfering RNAs (siRNA) were obtained from Thermo Fisher Scientific: p38α: s3585 and s3586, PRMT1: s6917, s6919, Negative control: 4390846, 4390843. Reverse transfection was performed with Lipofectamine RNAiMAX-reagent (Invitrogen) following the manufacturer's instructions. In brief, 25pmol of siRNA were mixed with 5μL of Lipofectamine RNAiMAX in 500μL of Opti-MEM medium (Invitrogen) in a 6-well plate. The mixture was incubated for 20 min at room temperature and 3–3.5 x 10^5 cells were added to mixture. Total knockdown times were 8–72 h.

Sequential extraction of insoluble protein aggregates

Extraction of insoluble proteins was performed as previously described.[53] Briefly, transfected cells were lysed in 300μL radio-immunoprecipitation assay (RIPA) buffer [50mM Tris-HCl, 150mM NaCl, 1% NP-40, 0.5% sodium deoxycholate, and 0.1% SDS] (Boston bioproducts) supplemented with 2mM EDTA, protease inhibitors (Complete, Roche), and phosphatase inhibitors (PhosStop, Roche). Lysates were sonicated 2 × 15 s with 20% maximum amplitude and centrifuged for 30 min at 100,000 × *g* and 4°C. The supernatant was collected as the RIPA-soluble fraction. The pellet was washed in RIPA buffer and centrifuged as above. The supernatant was discarded and the urea-soluble fraction was generated by resuspending the pellet in 100 μL urea buffer [7M urea, 2M thiourea, 30mM Tris-HCl pH 8.5, 4% 3-[(3-Cholamidopropyl) dimethylammonio]-1-propanesulfonate (CHAPS, Sigma)], and sonicating the samples as above followed by centrifugation at room temperature for 30 min at 100,000 × g. The supernatant was collected as the urea-soluble fraction.

Immunoblotting

Cell extracts or RIPA and urea fractions obtained from sequential extractions were diluted with NuPAGE sample buffer. Proteins were separated on 4–12% NuPAGE Bis-Tris gels (Thermo Fisher Scientific) under denaturing conditions and transferred onto polyvinylidene difluoride (PVDF) membranes (Millipore). Blots were processed for total protein stain (Thermo Scientific). All blocking and antibody incubation steps were performed either in 5% milk in Tris-buffered saline (TBS) [25mM Tris-HCl, 3mM KCl, 140 mM NaCl, pH 7.4] supplemented with 0.05% Tween 20 (TBS-T) (Thermo Fisher Scientific) or in 5% bovine serum albumin (BSA) in TBS-T. Western blots were developed with enhanced chemiluminescent substrates (ECL) or with fluorescence detection using secondary antibodies labeled with IRDye near-infrared (NIR) fluorescent dyes. Digital images were acquired with a ChemiDoc MP imaging system (BioRad) or with LI-COR. Where necessary, blots were stripped with stripping buffer for 15 min (Restore, Thermo Fisher Scientific) and re-probed with loading control antibodies.

Lactate dehydrogenase (LDH) assay to monitor cell death

NSC-34 cells grown on 96-well plates coated with poly-*L*-lysine (BioCoat multiwell plates, Corning) were transiently transfected using Lipofectamine 3000 (Thermo Fisher Scientific) following the manufacturer's instructions 24h after seeding (Lipofectamine 3000:DNA ratio 3:1). Cells were treated with DMSO or p38α MAPK inhibitor (compound 1) at final concentrations of 1 or 10μM for 4 h post-transfection. LDH activity was measured from 50μL of conditioned medium using LDH assay kit (Life Technologies) following the manufacturer's instructions.

SH-SY5Y cells were cultured and transiently transfected (using GeneX*Plus* transfection reagent (ATCC)) with 0.5μg of p38α constructs or GFP control construct according to manufacturer's protocol. After 48h, media was collected, spun down (130 x g at room temperature for 7 min), and LDH activity was measured using CyQUANT LDH Cytotoxicity Assay, following manufacturer's protocol. Corresponding cell lysates were collected for western blot analysis as described below.

To confirm expression of p38α constructs SH-SY5Y cells were lysed in RIPA buffer (Boston BioProducts) supplemented with protease inhibitors (Millipore Sigma) and phosphatase inhibitors (Millipore Sigma) and cleared by centrifugation (11,000 rpm at 4°C for 10 min). Cell lysates were diluted in NuPAGE LDS sample buffer containing NuPAGE sample reducing agent and left at room temperature for 20 min before loading onto gel. Proteins were separated on a 1.5 mm 4–12% NuPAGE Bis-Tris gel (Thermo Fisher Scientific) with NuPAGE MES SDS Running Buffer (Thermo Fisher Scientific). Proteins were transferred onto 0.2μm nitrocellulose membrane (Bio-Rad) using Trans Blot Turbo Transfer Packs (Bio-Rad) on a Trans-Blot Turbo Transfer System (Bio-Rad). Blots were processed for total protein stain (Thermo Scientific) and blocked in 5% bovine serum albumin (BSA) in TBS Tween 20 buffer (TBS-T) containing 25mM Tris, 0.15M NaCl, 0.05% Tween 20 (Thermo Scientific) for 1h at room temperature. Blots were incubated with primary antibody (1:1000) (Cell Signaling Technology) in 5% BSA in TBS-T overnight at 4°C. Blots were washed (3 × 10 min), incubated with secondary antibody (1:3000) (Cell Signaling Technology) in 5% milk in TBS-T for 1h at room temperature, and washed again (3 × 10 min). Western blots were developed with SuperSignal West Pico PLUS Chemiluminescent Substrate (Thermo Scientific) and digital images were acquired with a ChemiDoc MP imaging system (Bio-Rad).

Trypan blue viability assay

SH-SY5Y cells were cultured and transiently transfected with p38α constructs, as described. Cells were collected by trypsinization and centrifugation (300 x g, 7min) 48 h post-transfection. 10μL of the cell suspension was then mixed with 0.4% trypan blue solution (Gibco) at 1:1 ratio and then 10μL were loaded onto Countess cell counting chamber slide (Invitrogen). Live and dead cells were counted using Countess 3 FL automated cell counter (Invitrogen). The remainder of the cell suspension was spun down at 300 x g for 7 min, then cells were resuspended with sample buffer for SDS-PAGE and immunoblotting analysis, as described.

Longitudinal imaging and survival analysis of mouse primary cortical neurons

Primary cortical neurons from E17 mouse embryos were dissected and cultured in 384-well plates coated with laminin as previously described.[61] Neurons were plated at a density of 35,000/well. Neurons were co-transfected with plasmids expressing the fluorescent marker mApple and TDP-43^{M337V}-EGFP using lipofectamine 2000 in OptiMEM media (Thermo). Neurons were treated with p38a inhibitor, VX-745 (provided by AstraZeneca), at 0.3, 1, 3, or 9 μM, with a final DMSO concentration of 0.09%, and imaged daily for 7 days on a custom-built highthroughput robotic microscopy system (Robo3).[61,161] Each well was imaged with a 10× objective four times daily. Images were montaged for each well and fluorescently labeled neurons were segemented and tracked using custom-built algorithms. Drug-treated neurons from 2 replicates were combined for tracking and analysis. Cox proportional hazard analysis was used to determine hazard ratios. DMSO treatment of TDP43^{M337V} was used as a negative control, and GFP-expressing DMSO-treated neurons were used as a positive "healthy" control.

MG-132 stress model in iPSC-derived motor neurons (iMNs)

On Day 34 of differentiation iMNs derived from human male XCL-1 iPSCs (XCell Science) were subjected to proteotoxic stress by treatment with 0.5μM MG-132 (Millipore Sigma) plus 0.1% DMSO or 1μM VX-745 for 24 h. On day 35 cells were harvested and subjecyed to Sequential extraction of insoluble protein aggregates.

Rate of death analysis of human iMNs TDP-43^{A382T} variant using the GEDI biosensor

One day before thawing, 12-well plates (Corning) were coated with 1:4 dilution of poly-/-ornithine solution and left at room temperature overnight. The next day, the plates were rinsed three times with cell culture water and 500μL of a 1:50 dilution of 1 mg/ml mouse laminin (Sigma) in cell culture water was added and incubated at 37°C for a minimum of 30 min. The Day 13 NINDS MNPCs were thawed into the precoated 12-well plates into Stage 3 media[164,165] with the addition of ROCKI at a density of 2.5E6 cells per well. The media was changed the next day to only Stage 3, and the MNPCs were fed every other day. The MNPCs were transduced with lentivirus on Day 15 with the RGEDI[169] biosensor at an MOI of 2.5 and washed the next day. On Day 18, PhenoPlate 384-well microplates (PerkinElmer) were coated with a 1:4 dilution of poly-/-ornithine solution. The next day, plates were washed and coated with 30μL of a solution of 1:50 dilution of 1 mg/ml mouse laminin (Sigma) and 5 μg/mL of fibronectin (Corning) in cell culture water and incubated overnight at 37°C. On Day 20, MNPCs are dissociated using Accutase and plated at a density of 30,000 cells per well of a 384 well dish in Stage 3 media and ROCKI. On Day 21, media was completely replaced and cells were treated with compound VX-745 (Selleck Chem) at a working concentration of 3μM or DMSO control and continuously treated with fresh compound every other day until experimental end at D37. After Day 25 the cells were considered iMNs. iMNs were subjected to robotic microscopy (RM) from day 27–37.

Longitudinal imaging

iMNs that contained RGEDI were imaged on an ImageXpress Micro Confocal High-Content Imaging System from Molecular Devices for 7–10 days starting on differentiation day 27. Montages of 9 tiles were imaged in RFP (200ms) and GFP (100ms) channels at 20× magnification per well. Images were processed using a custom workflow in Galaxy.[170]

Odds ratio of cell death

Cells from each line were assessed as alive or dead by the GEDI biosensor[169] on different plates at multiple points in time. The change in odds of cell death (OR-CD) at any point in time was modeled using a generalized linear model[171] using the glm function in R,[172] between the cell line and time using the binomial probability distribution as the family argument to this function. The modeled changes included the plate on which the cell was assayed, the time (as a continuous variable) at which the cell status was ascertained, the cell line from which the cell was derived and the interaction between the cell line and time. These changes, as odds ratios, were derived from the model fits to the data. Custom-built scripts in R were developed to model the data.

Determining Nuclear-Cytoplasmic distribution of TDP-43 in control iMNs or iMNs bearing a G_4C_2-repeat expansion in the C9ORF72 gene

When iMN differentiation was on Day 13, 96-well plates (for viability assays) and 24-well plates with coverslips (for imaging) were coated overnight at 37°C in Matrigel (Corning). On Day 14 of differentiation iMNs were plated at a density of 30,000 cells/well for 96-well plates and 150,000 cells/well for 24-well plates in Neurobasal media + NEAA, Glutamax, N2, B27 (Gibco), plus 10 ng/mL BDNF, GDNF, CNTF (PeproTech) and 0.2 μg/ml Ascorbic acid (Sigma-Aldrich). iMNs were fed every 2 days and maintained for 13 additional days in the same media. Treatments started on day 13 after plating (DIV27) and were kept on for 24 h.

For viability studies, a VX-745 dose-response analysis was performed to determine a concentration that would not reduce viability significantly in both control and C9 neurons. VX-745 (Tocris) was dissolved in DMSO (Sigma-Aldrich), serial dilutions were made in OptiMEM (Gibco), added dropwise to each well and incubated at 37°C for 24 h iMN viability was measured using the CellTiter-Glo kit (Promega) on 3 separate experiments (n = 3 per run, n = 9 final). Using this approach, we established that 1μM VX-745 exhibited no toxicity.

For imaging and Nuclear-Cytoplasmic distribution of TDP-43 (Nuc/Cyt ratio), VX-745 was used at a concentration of 1μM. Immediately after the 24 h were completed, iMNs were washed once in PBS (Gibco) and fixed in 4% PFA for 20 min (Electron Microscopy Sciences). iMNs were then washed 3 times in PBS and blocked with 5% Donkey Serum (Jackson ImmunoResearch) + 0.3% TX-100 (Sigma-Aldrich) in PBS for 30 min at room temperature. Primary antibodies (goat MAP2 1:1000, Phosphosolutions; rabbit TDP-43 N-terminal 1:300, Proteintech) were diluted in blocking solution and incubated overnight at 4°C. Secondary antibodies (donkey Alexa Fluor, Jackson ImmunoResearch) were used at 1:1000 dilution in blocking solution and incubated for 60 min at room temperature. All treatments/iMN lines were treated and probed simultaneously to decrease variability. Coverslips were mounted in Prolong Glass (Invitrogen) and were left to air dry at room temperature for at least overnight before imaging.

Images were acquired (10/group) using an A1R Nikon Confocal Microscope and fields of view (FOV) were processed for analyses using Nikon NIS Elements Software. Briefly, images were batch processed for Max intensity projection using the GA3 tool. Then, nuclei were selected using the autodetect tool in the ROI editor. Cell bodies (cytoplasm) were hand drawn using the Bezier tool. Data was exported to Excel and nuclear-cytosolic ratios were calculated using the mean intensity values for the 488 channel (TDP-43 signal) for matched nuclear and cytoplasmic selections. Data were analyzed by two-way ANOVA using genotype and treatment as variables using Prism.

Cytoplasmic and nuclear protein extraction

Cytoplasmic and nuclear protein extraction was performed using a commercial subcellular protein fractionation kit (Thermo Fisher Scientific). Briefly, ~80% confluent SH-SY5Y cells plated in a 100 -mm dish were transfected as indicated for 24 h. Cells were

trypsinized and rinsed with cold PBS, and cell suspensions were transferred to pre-chilled 1.5mL microcentrifuge tubes. Cells were lysed in cytoplasmic extraction buffer at 4°C for 10 min with gentle mixing. After centrifugation at 500 x g at 4 °C for 5 min, the supernatant was collected and stored as the cytoplasmic fraction. After addition of appropriate amounts of membrane extraction buffer to the pellet, the tube was vortexed vigorously for 5 s and incubated at 4°C for 10 min with gentle mixing. After centrifugation at 3,000 x g at 4 °C for 5 min, the supernatant was collected and stored as the membrane fraction. The pellet was resuspended in appropriate amounts of nuclear extraction buffer followed by vigorous vortexing for 15 s and incubation at 4°C for 30 min with gentle mixing. After centrifugation at 5,000 x g at 4 °C for 5 min, the supernatant was collected and stored as the soluble nuclear fraction. The pellet was resuspended in appropriate amounts of chromatin-bound extraction buffer followed by vigorous vortexing for 15 s and incubation at room temperature for 15s. The vortexing and incubation steps were repeated twice. After centrifugation at 16,000 x g at 4 °C for 5 min, the supernatant was collected and stored as the chromatin-bound nuclear fraction. Bicinchoninic acid (BCA) assay was used to measure protein concentrations.

Immunocytochemistry

Cells grown on poly-*L*-lysine-coated glass coverslips were washed in phosphate-buffered saline (PBS) and fixed in 4% paraformaldehyde (in PBS) for 15 min followed by permeabilization in 0.25% Triton X-(in PBS) for 10 min. Cells were blocked with 10% normal goat serum (in PBS, Abcam) for 1h at room temperature and incubated overnight at 4°C in primary antibody diluted in blocking solution. The next day, cells were washed with PBS and incubated for 1h in secondary antibody diluted in blocking solution. Coverslips were mounted with Prolong Gold Antifade Mountant with DAPI (Thermo Fisher Scientific). Image acquisition was performed using a Nikon A1 confocal/Eclipse Ti inverted microscope system and NIS Elements software (Nikon). To determine the localization of TDP-43^{WT}, TDP-43^{S292E}, and $TDP43^{R293F}$, cells were washed in PBS and fixed in 2% formaldehyde (in PBS) for 30 min followed by permeabilization in 0.2% Triton X-(in PBS) for 6 min. Cells were incubated for 1 h in primary antibody diluted in blocking solution. Cells were then washed with PBS and incubated for 30 min in secondary antibody diluted in blocking solution. Coverslips were mounted as described above and image acquisition was performed using EVOS M5000 imaging system.

Protein kinase assays with recombinant proteins

5μL of 10 x kinase assay buffer [25mM Tris-HCl (pH 7.5), 5 mM β-glycerophosphate, 2 mM DTT, 0.1mM Na_2VO_4, 10mM $MgCl_2$] (Cell Signaling Technology), 200μM ATP (Cell Signaling Technology), 750ng of recombinant human TDP-43 protein (Proteintech) and 300ng of recombinant active p38α kinase (SignalChem) were mixed in pre-chilled 1.5mL tubes. Reactions were made up to a total volume of 50μL with ddH_2O. Samples were mixed by flicking the tubes followed by brief centrifugation at 4°C and incubation at 30°C for 30 min. When indicated, kinase reactions were treated with 10μM of the p38α inhibitor compound 1. Reactions were stopped by adding 18μL of 4× NuPAGE sample buffer and boiling samples at 95°C for 5 min. Samples were subjected to immunoblotting or Coomassie staining followed by phosphorylation analysis by LC-MS/MS.

Phosphorylation analysis by LC-MS/MS

In vitro kinase reactions were separated on 4–12% NuPAGE Bis-Tris gels (Thermo Fisher Scientific) and gel bands were visualized with SimplyBlue SafeStain (Thermo Fisher Scientific). Gel bands were excised and cut into ∼$1mm^3$ pieces. The samples were reduced with 1mM dithiothreitol (DTT) for 30 min at 60°C and then alkylated with 5 mM iodoacetamide for 15 min at room temperature. Gel pieces were then subjected to a modified in-gel trypsin digestion procedure.[173] Briefly, gel pieces were washed and dehydrated with acetonitrile for 10 min followed by removal of acetonitrile. Pieces were then completely dried using a speed-vac. Gel pieces were rehydrated in 50mM ammonium bicarbonate solution containing 12.5 ng/μL modified sequencing-grade trypsin (Promega) at 4°C before incubation overnight at 37°C. Peptides were later extracted by removing the ammonium bicarbonate solution, followed by one wash with a solution containing 50% acetonitrile and 1% formic acid. The extracts were then dried in a speed-vac for 1 h and stored at 4°C until analysis. On the day of analysis, samples were reconstituted in 5–10 μL of High-Performance Liquid Chromatography (HPLC) solvent A (2.5% acetonitrile, 0.1% formic acid). A nano-scale reverse-phase HPLC capillary column was created by packing 2.6μm C18 spherical silica beads into a fused silica capillary (100 μm inner diameter, ∼30 cm length) with a flame-drawn tip.[174] After equilibrating the column, each sample was loaded onto the column via a Famos auto sampler (LC Packings). A gradient was formed, and peptides were eluted with increasing concentrations of solvent B (97.5% acetonitrile, 0.1% formic acid). As each peptide was eluted it was subjected to electrospray ionization before entering an LTQ Orbitrap Velos Pro ion-trap mass spectrometer (Thermo Fisher Scientific). Eluting peptides were detected, isolated, and fragmented to produce a tandem mass spectrum of specific fragment ions for each peptide. Peptide sequences were determined by matching protein or translated nucleotide databases with the acquired fragmentation pattern using the software program Sequest (ThermoFinnigan).[175] The modification of 79.9663 mass units to serine, threonine, and tyrosine was included in the database searches to determine phosphopeptides. Phosphorylation assignments were determined using the A-Score algorithm.[176] All databases include a reversed version of all sequences and the data was filtered to 1–2% peptide false discovery rate.

Proteomic data analysis was carried out as previously described.[177,178] Briefly, peptide sequences were determined following spectral searches using the UniProt TARDBP human protein sequence along with the acquired fragmentation pattern using MSGF+.[179] The search was carried out using settings for high-resolution Orbitrap mass spectrometers, tryptic digestion, no limit to enzyme missed cleavages, 20 ppm precursor mass tolerance, charge states of +2 to +5, minimum and maximum peptide lengths

of 6–40 amino acids in length, respectively, and a fixed modification of standard amino acids with C + 57. For phosphopeptide detection a variable modification of 79.9663 mass units to serine, threonine, and tyrosine was included in the database searches. The resulting.mzID files from the spectral searches were combined with mzXML files using the MSnbase package in R[162,163] (accessed November 15th 2022), and used to calculate spectral counts for total and phosphorylated-TARDBP peptides. Phosphorylation assignments were determined by the A score algorithm.[176]

Co-immunoprecipitation (Co-IP)

Approximately 80% confluent SH-SY5Y cells plated in 6-well plates or 100-mm dishes were transfected as indicated. Cells were rinsed with cold PBS, and then lysed in cold lysis buffer [20mM Tris-HCl (pH 7.5), 150mM NaCl, 1mM Na_2EDTA, 1mM EGTA, 1% Triton, 2.5mM sodium pyrophosphate, 1mM beta-glycerophosphate, 1mM Na_3VO_4, 1 μg/mL leupeptin] (Cell Signaling Technology), supplemented with protease inhibitors (Complete, Roche). Cells were incubated on ice for 5 min, collected in pre-chilled 1.5 mL tubes, sonicated briefly and cleared by centrifugation (14,000 x g at 4°C for 10 min). Lysate aliquots were stored as the input samples. Cell lysates were either incubated with Anti-FLAG M2 Magnetic Beads (Millipore Sigma) overnight with continuous rotation at 4°C, or were subjected to pre-cleaning with protein A Dynabeads (Thermo Fisher Scientific) for 1 h at 4°C followed by incubation with indicated primary antibodies overnight with continuous rotation at 4°C. Protein A Dynabeads were then added to pre-cleared antibody-containing samples, and the incubation was continued for an additional 2 h at room temperature. Beads with immunoprecipitated proteins were washed 5x with either TBS [50mM Tris-HCl, 150mM NaCl, pH 7.4] (Anti-FLAG M2 Magnetic Beads) or lysis buffer (Protein A Dynabeads). Immunoprecipitated proteins were eluted with 2x NuPAGE sample buffer by boiling for 3 min. Both input samples and immunoprecipitated proteins were analyzed by immunoblotting.

Purification of recombinant TDP-43-MBP

Wild-type TDP-43-MBP-6xHis and TDP-43 mutants S292E, S409:S410E, S292:S409:S410E, and R293F were expressed and purified as previously described.[180] Briefly, TDP-43 variants were expressed in *E. coli* BL21-CodonPlus (DE3)-RIL cells (Agilent). Cell cultures were grown to an OD_{600} of ~0.5–0.7 and then cooled down to 16°C. Protein expression was induced with 1mM IPTG overnight. Cells were harvested and resuspended in purification buffer (20mM Tris-HCl, pH 8.0, 1M NaCl, 10mM imidazole, 10% (v/v) glycerol, 2mM β-mercaptoethanol supplemented with complete EDTA-free protease inhibitor cocktail) and lysed using 1 mg/ml lysozyme and sonication. Proteins were purified using Ni-NTA agarose (Qiagen) and eluted using 300mM imidazole in purification buffer. Proteins were then further purified over amylose resin (NEB) and eluted with elution buffer (20mM Tris-HCl, pH 8.0, 1M NaCl, 10mM imidazole, 10mM maltose, 10% (v/v) glycerol, and 1mM DTT). Purified proteins were concentrated, flash frozen and stored at −80°C.

Protein methylation assays with recombinant proteins

Recombinant TDP-43-MBP-6xHis (20μM) was incubated with *S*-Adenosyl methionine (100μM) in the presence or absence of PRMT1 (0.5μM) (Abcam) in TDP-43 buffer (20mM Tris-HCl pH 8, 300mM NaCl, 1mM DTT) for 16 h at 37°C. Reactions were halted by the addition of formic acid and analyzed by bottom up LC-MS/MS as described below. R293Me peptides were only observed in the PRMT1 treated samples, ruling out non-enzymatic methylation.

Equal amounts of protein were taken from both reactions for digestion. The protein samples were reduced and alkylated using 5mM dithiothreitol (DTT) and 10mM iodoacetamide (IAA), respectively. Trypsin digestion was carried out using modified sequence-grade trypsin (Promega, Madison, WI) in 1:50 enzyme:protein ratio and reactions were left shaking at 37°C overnight. Digested peptides were cleaned using C18 StageTip, vacuum dried, and stored at −20°C before data acquisition.

Methylation analysis by LC-MS/MS

Thermo Scientific Orbitrap Exploris 240 mass spectrometer (ThermoFisher Scientific, Bremen, Germany) connected to the Thermo Scientific UltiMate 3000 HPLC nanoflow liquid chromatography system (ThermoFisher Scientific) was used for data acquisition. Peptide digests were reconstituted in 0.1% formic acid in water (solvent A) to a final peptide concentration of 500 ng/μL and separated on an analytical column (75μm × 15cm) at a flow rate of 300 nL/min using a step gradient of 1–25% solvent B (0.1% formic acid in acetonitrile) for the first 100 min, 25–30% for 5 min, 30–70% for 5 min, 70–1% for 5 min and 1% for 5 min for a total run time of 120 min. The mass spectrometer was operated in data-dependent acquisition mode. A survey full scan MS (from m/z 400–1600) was acquired in the Orbitrap with a resolution of 6000 Normalized AGC target 300. Data was acquired in topN with 20 dependent scans. Peptides were fragmented using normalized collision energy with 37% and detected at a mass resolution of 30,000. Dynamic exclusion was set for 8s with a 10 ppm mass window.

The raw files obtained after data acquisition were searched using Proteome Discoverer software suite version 3.0 (ThermoFisher Scientific). Data was searched against the sequence of TDP-43-MBP-6xHis using SEQUEST. Search parameters included carbamidomethylation of cysteine as a static modification. Dynamic modifications included oxidation of methionine, mono- and di-methylation at arginine and acetylation at protein N terminus. The minimum peptide length was set as seven amino acids with one missed cleavage allowed. Mass tolerance was set to 10 ppm at the MS level and 0.05Da for the MS/MS level, and the false discovery rate was set to 1% at the PSM level.

In vitro TDP-43 aggregation assay

Purified recombinant TDP-43-MBP-6xHis wild-type and TDP-43 mutants were first thawed and buffer exchanged into 20mM HEPES-NaOH, pH 7.4, 150mM NaCl and 1mM DTT using Micro Bio-Spin P-6 Gel Columns (Bio-Rad). Protein concentration was determined by nanodrop, and the final concentration of TDP-43 was then adjusted to 5μM in the same buffer. To measure aggregation kinetics, aggregation was initiated by cleavage of the MBP-6xHis tag using 1 μg/ml TEV protease at t = 0, and turbidity was measured over 16 h at an absorbance of 395nm using a TECAN M1000 plate reader. Values were normalized to wild-type TDP-43 + TEV protease to determine the extent of aggregation of TDP-43 mutants.

In vitro TDP-43 LLPS assay

Purified recombinant TDP-43-MBP-6xHis wild-type and TDP-43 mutants were thawed and buffer exchanged as described above for the aggregation assay. Protein concentration was determined by nanodrop, and reactions were prepared in phase separation buffer (20mM HEPES-NaOH, pH 7.4, 150mM NaCl, 1mM DTT, 100 mg/mL dextran from *Leuconostoc* spp. (Sigma)). Protein was always added last to each phase separation reaction, at a final concentration of 10μM. Reactions were incubated for 30 min at room temperature, and then 7.5μL of each reaction was mounted onto a glass slide and imaged by differential interference contrast (DIC) microscopy.

Droplet image analysis

DIC images of TDP-43 wild-type and its variants were analyzed using custom-written code in MATLAB. Each image was first converted into grayscale for processing. Then, Robert's gradient was used to filter out the noise. The pixel weight for each pixel in the image was determined based on the grayscale intensity differences before segmenting the images. The threshold for image segmentation was adjusted manually to ensure complete and accurate conversion to logical array. Droplets in the images were identified using circular Hough transform. The sensitivity was toggled either to detect missed droplets or to reduce the number of false positives. The detected circles were visualized on the original images. Various quantitative parameters, including the average area, total area, number of droplets and the lists of areas, were given as outputs to the code and were analyzed further through Prism. The accuracy of the circular Hough transform was limited for droplets that were smaller than 5 pixels, where 10.8 pixels are equivalent to 1μm.

QUANTIFICATION AND STATISTICAL ANALYSIS

Western blot band densities and immunocytochemical staining were quantified with ImageJ-Win64 software.[160] For statistical analysis, we used GraphPad Prism 7 and 8, and used unpaired t test or one-way ANOVA followed by Sidak's or Dunnett's multiple comparison test, as indicated for each experiment. All assays were repeated at least three times. A p-value less than 0.05 was considered statistically significant.

Cell Reports, Volume *44*

Supplemental information

Opposing roles of p38α-mediated phosphorylation and PRMT1-mediated arginine methylation in driving TDP-43 proteinopathy

Mari Aikio, Hana M. Odeh, Heike J. Wobst, Bo Lim Lee, Úna Chan, Jocelyn C. Mauna, Korrie L. Mack, Bradley Class, Thomas A. Ollerhead, Alice F. Ford, Edward M. Barbieri, Ryan R. Cupo, Lauren E. Drake, Joshua L. Smalley, Yuan-Ta Lin, Stephanie Lam, Reuben Thomas, Nicholas Castello, Ashmita Baral, Jenna N. Beyer, Mohd A. Najar, John Dunlop, Aaron D. Gitler, Ashkan Javaherian, Julia A. Kaye, George M. Burslem, Dean G. Brown, Christopher J. Donnelly, Steven Finkbeiner, Stephen J. Moss, Nicholas J. Brandon, and James Shorter

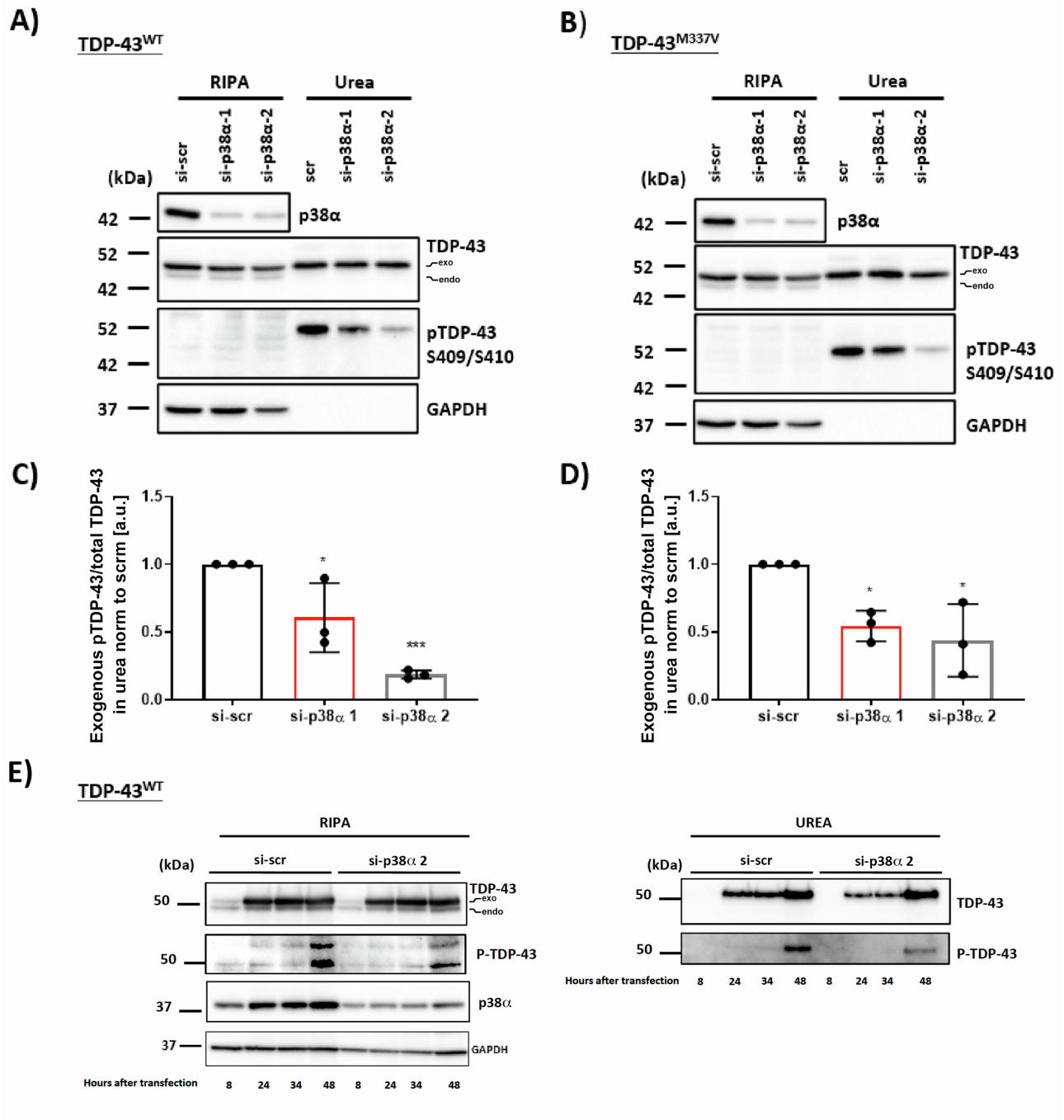

Figure S1. Genetic ablation of p38α MAPK reduces aggregation and S409/S410 phosphorylation of TDP-43^{WT} and TDP-43^{M337V}. (A) Western blot of total and pTDP-43^{WT} in RIPA and urea fractions of SH-SY5Y cells with siRNA-induced p38α knockdown after 48h. GAPDH was used as a loading control. The position of myc-tagged TDP-43 (exo) and endogenous TDP-43 (endo) is indicated. **(B)** Western blot of total and pTDP-43^{M337V} in RIPA and urea fractions of SH-SY5Y cells with siRNA-induced p38α knockdown after 48h. GAPDH was used as a loading control. The position of myc-tagged TDP-43^{M337V} (exo) and endogenous TDP-43 (endo) is indicated. **(C)** Quantification of pTDP-43^{WT}/total TDP-43^{WT} (exogenously expressed) ratio in urea fraction normalized to levels in scrambled siRNA (si-scr). (mean band signal ± SD,

one-way ANOVA with Sidak's multiple comparison test, n =3). $^{*}p < 0.05$, $^{***}p < 0.001$. **(D)** Quantification of pTDP-43^{M337V}/total TDP-43^{M337V} (exogenously expressed) ratio in urea fraction normalized to levels in si-scr (mean band signal ± SD, one-way ANOVA with Sidak's multiple comparison test, n = 3). $^{*}p < 0.05$. **(E)** Western blot of total and phosphorylated TDP-43 in RIPA and urea fractions of SH-SY5Y cells with siRNA-induced p38α knockdown. SH-SY5Y cells were treated with siRNA for 24h and then transfected with TDP-43 (myc-tagged). The position of myc-tagged TDP-43 (exo) and endogenous TDP-43 (endo) is indicated.

Related to Figure 1.

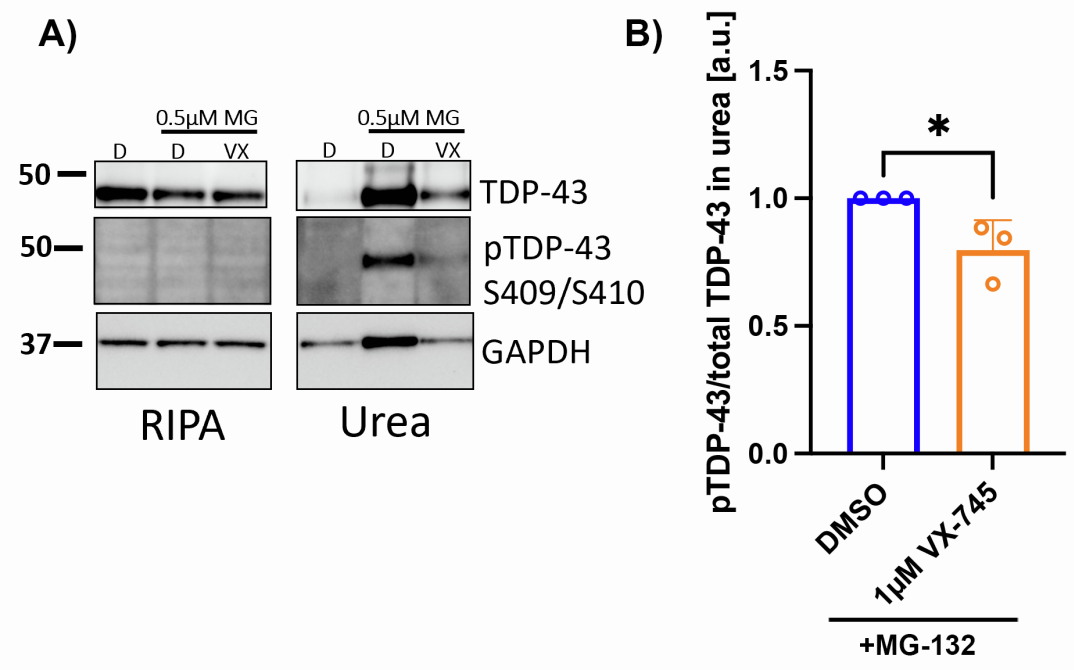

Figure S2. Pharmacological inhibition of p38α MAPK reduces accumulation of insoluble TDP-43 phosphorylated at S409/S410 in iMNs subjected to MG-132-induced stress. (A) Western blot of total and phosphorylated TDP-43 in RIPA and urea fractions of iMNs treated without MG-132 (left), with 0.5µM MG-132 (middle) to induce proteosomal stress, or with MG-132 (0.5µM) and VX-745 (right). **(B)** Quantification of pTDP-43/total TDP-43 ratio in urea fraction normalized to levels in DMSO+MG-132-treated cells (mean band signal±SD, Unpaired t-test, n=3). *p <0.05.

Related to Figure 1.

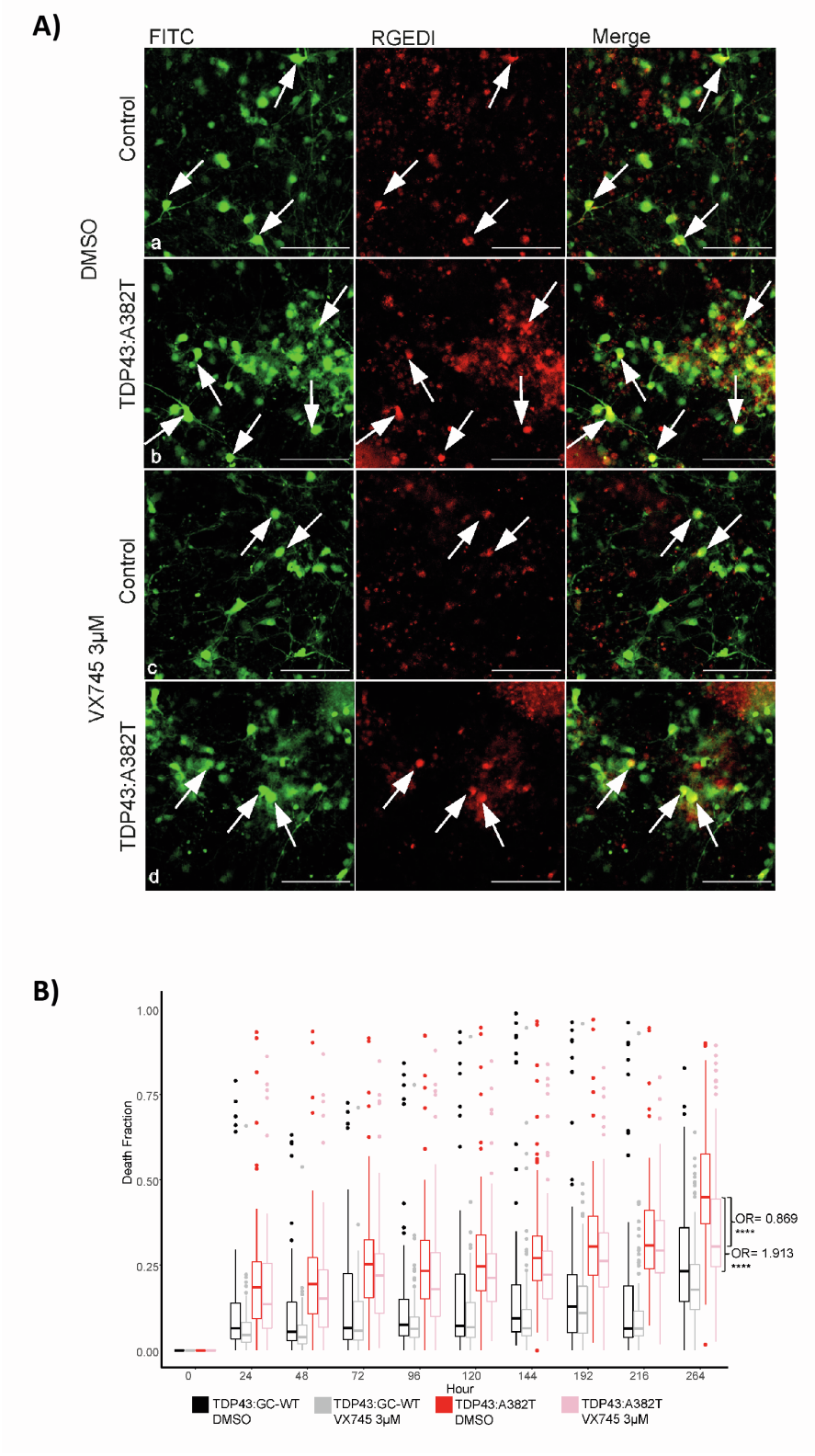

Figure S3. Inhibition of p38α reduces TDP-43^{A382T} toxicity in patient-derived iMNs. (A) Representative images of differentiated iMNs[152,153] at D34 transduced with the cell death

biomarker. iMNs were treated with VX-745 or DMSO control beginning on Day 20. Left panels show the GFP channel, highlighting neurons that express the EGFP morphology marker, middle panels the same neurons imaged in the RFP channel to capture the RGEDI signal that labels dead or dying cells, and on the right are merged images. Arrows point to dying or dead cells (scale bar=100µm): a) Control iMNs treated with DMSO control; b) $TDP43^{A382T}$ iMNs treated with DMSO control; c) Control iMNs treated with 3µM VX-745 ; and d) $TDP43^{A382T}$ iMNs treated with 3µM VX-745. **(B)** Plotted rate of cell death between iMNs treated with DMSO or 3µM VX-745. (n=4 independent experiments, live neurons=597,727 and dead neurons=113,993). $TDP43^{A382T}$ iMNs display a higher death rate than gene-corrected (GC) control iMNs OR=1.913, $p<0.00001$. VX-745 reduces the death rate of $TDP43^{A382T}$ iMNs significantly, OR=0.869, p-value=5.9e-06. VX-745 also improves survival of GC control iMNs OR= 0.671, $p<0.00001$.

Related to Figure 1.

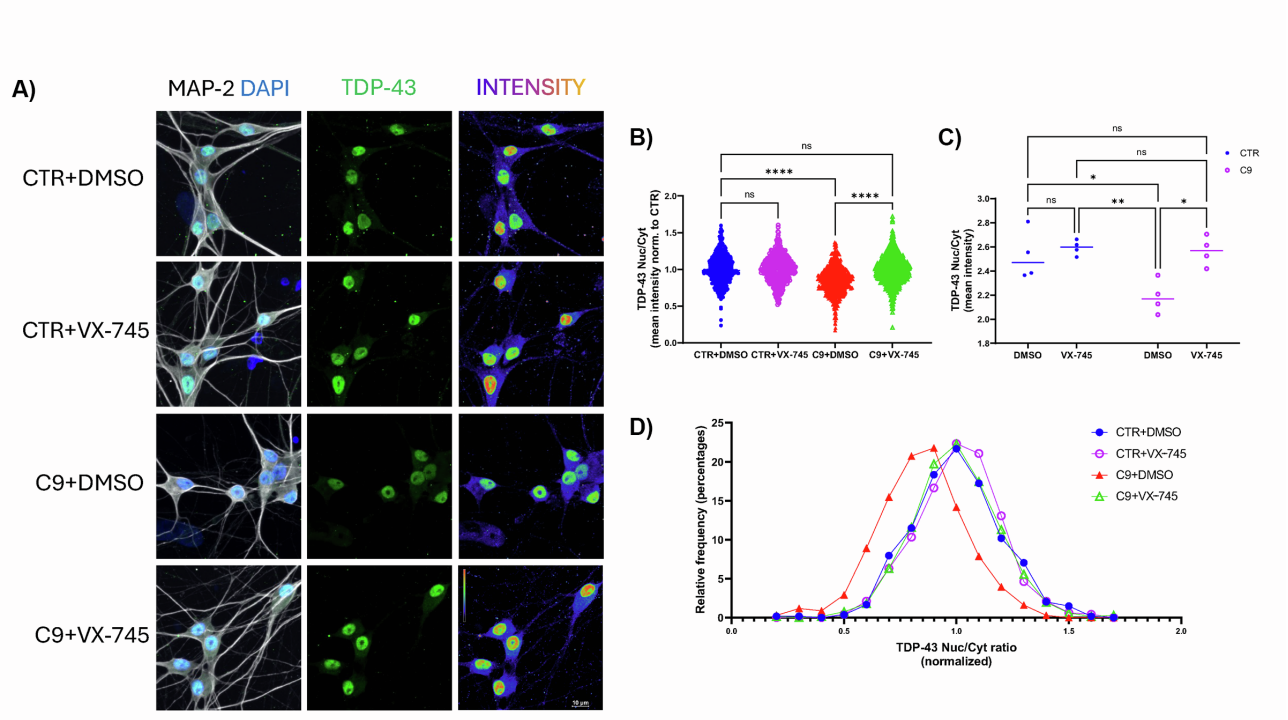

Figure S4. Inhibition of p38α restores nuclear TDP-43 in patient-derived iMNs that harbor a hexanucleotide repeat expansion in the *C9ORF72* gene. (A) Control or c9 iMNs were treated with DMSO control or VX-745 (1μM) for 24h. iMNs were then processed for confocal imaging and immunofluorescence for a neuronal marker, MAP2 (left, white), DAPI staining to mark the nucleus (left, blue), and immunofluorescence for TDP-43 (middle, green). An intensity gradient of TDP-43 signal was determined (right). Nuclear TDP-43 signal in c9 iMNs treated with DMSO (3rd row) is lower than control iMNs (1st row) and c9 iMNs that have been treated with VX-745 (4th row). Scale bar, 10μm. **(B)** The ratio of nuclear to cytoplasmic TDP-43 was determined for iMNs treated as in (A). Each data point represents a single neuron. All data points for each group normalized to CTR+DMSO (CTR-DMSO N= 540 [blue]; CTR-VX-745 N=475 [purple]; C9-DMSO N= 685 [red] and C9-VX-745 N=665 [green]). A two-way ANOVA with Tukey's multiple comparisons test was performed. Ns=not significant; ****p<0.0001. **(C)** The ratio of nuclear to cytoplasmic TDP-43 was determined for iMNs treated as in (A). The means for each individual experiment (n=4) in each treatment group is plotted (2 different iMN lines with 2 iMN differentiations each). A two-way ANOVA with Tukey's multiple comparisons test was performed. Ns=not significant; *p<0.05; **p<0.01. **(D)** Frequency distribution for the nuclear to cytoplasmic TDP-43 ratios for iMNs treated as in (A). All groups present a normal distribution of nuclear to cytoplasmic TDP-43 ratios but the distribution for c9 IMNs treated with DMSO (red) is left shifted (i.e., lower nuclear to cytoplasmic TDP-43 ratios). By contrast, the distribution of nuclear to cytoplasmic TDP-43 ratios for c9 iMNs treated with VX-745 (green) are very similar to control iMNs (blue and purple).

Related to Figure 1.

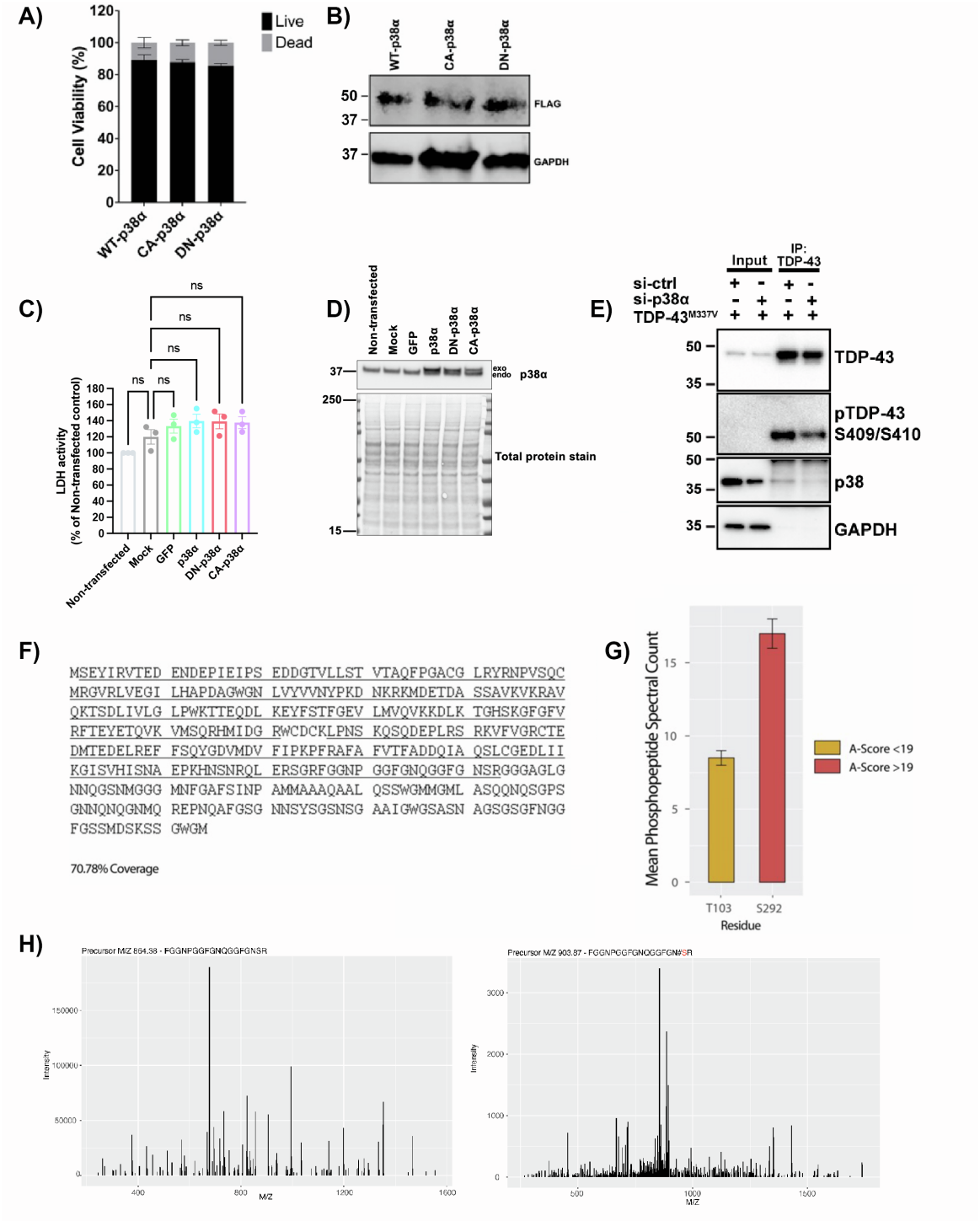

Figure S5. p38α interacts with TDP-43 and directly phosphorylates TDP-43 at S292, S409, and S410. (A) Expression of CA-p38α, DN-p38α, or p38α alone for 48h in SH-SY5Y cells did not elicit cell death as determined by trypan blue staining. Bars represent means±SEM (n=2), two-way ANOVA with Tukey's multiple comparisons test revealed no significant differences. **(B)** Western blot showing the expression levels of each p38α construct are similar. GAPDH serves as a loading control. **(C)** LDH release assay following transfection of SH-SY5Y cells for 48h with

p38α, DN-p38α, CA-p38α, or GFP control. Values are shown as percent of non-transfected control. Bar represents means±SEM (n=3). Each condition was compared to buffer the mock-transfected control using a one-way ANOVA and a Dunnett's multiple comparisons test; ns=not significant. **(D)** Representative western blot from SH-SY5Y cell lysates harvested after 48 h transfection with p38α, DN-p38α, CA-p38α, or GFP control. Top panel: upper band (exo) indicates exogenous p38, and lower band (endo) indicates endogenous p38. Bottom panel: corresponding colorimetric total protein stain. **(E)** Western blot of immunoprecipitated TDP-43^{M337V} and co-immunoprecipitated endogenous p38α from the SH-SY5Y cells with and without siRNA-induced p38α knockdown. GAPDH serves as a loading control. **(F)** LC-MS/MS analysis of TDP-43. The gel purification yielded highly enriched TDP-43 protein that facilitated the detection of 70.78% coverage of the total sequence. **(G)** Spectral counts were calculated for the phosphorylated peptides identifying modifications to the T103 and S292 residues, the only two phosphorylated sites detected. Values represent means±SEM (n=3). A-Scores were calculated for both sites, where a score >19 represents 99% confidence in assignment. The A-Score for the S292 site was greater than 19, which indicates ~99% certainty in the assignment. Our LC-MS/MS data also suggested that T103 might be phosphorylated directly by p38α, but here the A-Score was less than 19 and thus we do not have high confidence in this assignment. **(H)** Representative spectral plots showing the most abundant peptide that contained the S292 phosphorylation site in its unphosphorylated form (left) and phosphorylated form (right).

Related to Figure 1, 2, and 3.

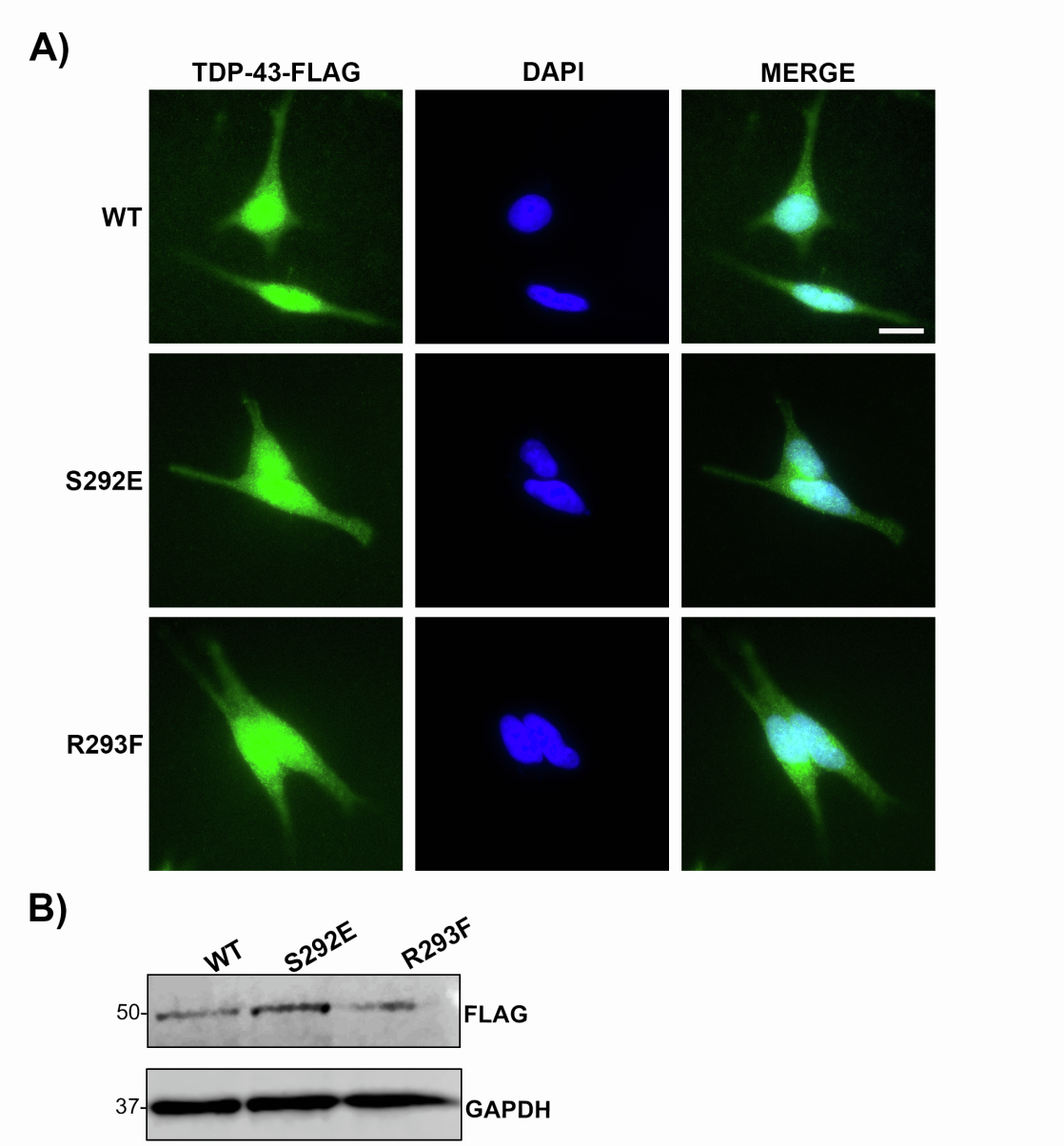

Figure S6. Expression and localization of TDP-43 variants in SH-SY5Y cells. (A) Immunofluorescence microscopy images showing the localization of FLAG-tagged TDP-43^{WT}, TDP-43^{S292E}, and TDP-43^{R293F}, using anti-FLAG antibody (scale bar=10µm; n=3). **(B)** Western blot showing the expression levels of each TDP-43 construct. GAPDH serves as a loading control.

Related to Figure 3, 4, and 5.

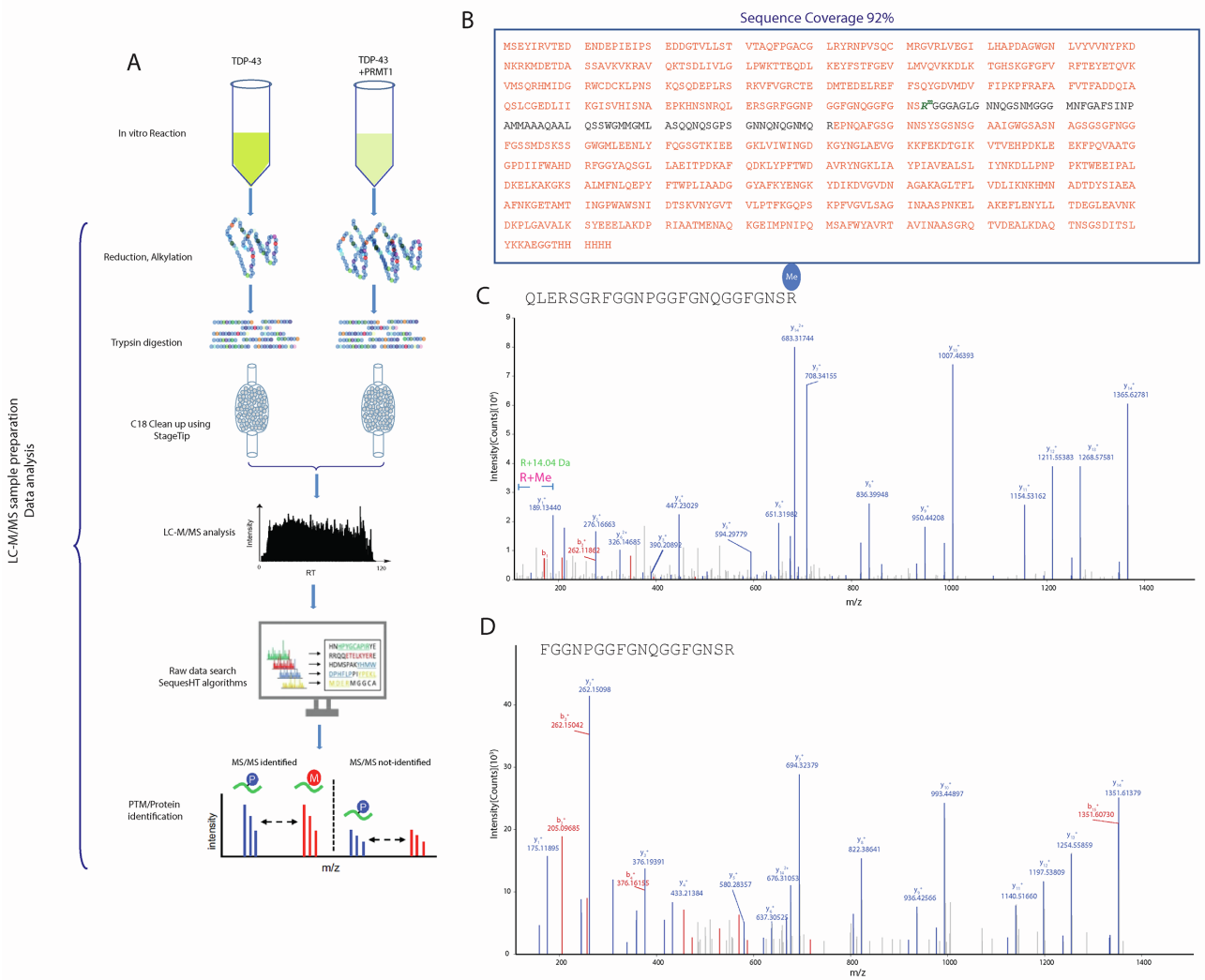

Figure S7. PRMT1 directly monomethylates TDP-43 at R293. (A) Workflow of *in-vitro* reaction followed by bottom-up LC-MS/MS analysis of TDP-43. **(B)** Sequence coverage of TDP-43-MBP-6xHis by LC-MS/MS. Orange detected. Black not detected. R293 can be detected and is denoted in green. **(C)** MS/MS spectra of R293Me modified peptide from TDP-43 only detected in the presence of PRMT1. **(D)** MS/MS spectra of unmodified peptide of TDP-43 in absence of PRMT1.

Related to Figure 4, 5, 6, and 7.